YEARBOOK OF PHYSICAL ANTHROPOLOGY 49:2–48 (2006)

Direct Dating of Human Fossils

Rainer Grün*

Research School of Earth Sciences, Research School of Pacific and Asian Studies, The Australian National University, Canberra ACT 0200, Australia

KEY WORDS 14C; U-series; ESR; Border Cave; Tabun; Skhul; Qafzeh; Vindija; Banyoles; Mungo

ABSTRACT The methods that can be used for the direct dating of human remains comprise of radiocarbon, U-series, electron spin resonance (ESR), and amino acid racemization (AAR). This review gives an introduction to these methods in the context of dating human bones and teeth. Recent advances in ultrafiltration techniques have expanded the dating range of radiocarbon. It now seems feasible to reliably date bones up to 55,000 years. New developments in laser ablation mass spectrometry permit the in situ analysis of U-series isotopes, thus providing a rapid and virtually non-destructive dating method back to about 300,000 years. This is of particular importance when used in conjunction with non-destructive ESR analysis. New approaches in AAR analysis may lead to a renaissance of this method. The potential and present limitations of these direct dating techniques are discussed for sites relevant to the reconstruction of modern human evolution, including Florisbad, Border Cave, Tabun, Skhul, Qafzeh, Vindija, Banyoles, and Lake Mungo. Yrbk Phys Anthropol 49:2–48, 2006.

When reconstructing human evolution, it is necessary to know how old the human fossils are. This information is usually extracted from a variety of sources, including the general chronological frameworks of the local geology, the flora, fauna, and artifacts found in association with the human fossils as well as numerical dating studies on these associated materials. This indirect dating approach, with respect to the human fossils, is in many cases not satisfactory, because:

i. the human remains are often buried into the sediments and the association with other materials is uncertain (e.g. Skhul, Qafzeh, etc.);
ii. faunal remains or minerals from the sediment are reworked from older deposits (see e.g. present discussion of the age of the *Homo erectus* remains in Indonesia);
iii. the hominid specimens were discovered at a time when no careful excavations were carried out and it has become impossible to correlate the human remains with other datable material (nearly 90% of all paleoanthropological specimens).

Direct dating of human remains would, of course, alleviate many of these problems (see also Trinkaus, 2005). Until recently, human fossils could only be directly dated by radiocarbon. This method reaches back to about 50,000 years. As a consequence, all older fossils did not yield meaningful chronological results and many important questions in our understanding of human evolution could not be addressed. Furthermore, most dating techniques are destructive. Human remains are scarce and extremely valuable, therefore any sort of destruction has to be kept to an absolute minimum. This is of particular importance in Australia, where any human fossils are sacred to the Aboriginal communities. This, of course, also applies to other areas, such as parts of North America. It is therefore necessary to develop and apply more or less non-destructive techniques for the analysis of human material. New technical developments, particularly in U-series and electron spin resonance (ESR), now allow the virtually non-destructive analysis of human remains.

The dating methods that can be used for dating fossil bones and teeth consist of radiocarbon, U-series, ESR, and amino acid racemization (AAR). These methods can generally be applied on a wide range of materials, but in this paper only their application for dating human remains is critically appraised (for general reviews on dating techniques, see e.g. Noller et al., 2000 and references therein).

Because of analytical and technical limitations, each dating technique has a certain age range, to which it can be applied (Fig. 1). It is obvious that radiocarbon, including the most advanced pretreatment techniques (Bird et al., 1999; Bronk Ramsey et al., 2004b) can only address chronological issues relating to relatively recent fossils, mainly *Homo sapiens*, and perhaps the youngest Neanderthal and *Homo erectus* specimens as well as *Homo floresiensis* (Brown et al., 2004; Morwood et al., 2004, 2005). On the other hand, U-series and AAR can cover, in principle, all chronological aspects of modern human evolution; ESR could be used to explore chronological relationships of earlier human groups. However, for the age estimation of older fossils, including most *Australopithecus* and *Paranthropus* species, there is presently no direct dating technique available.

METHODS

The underlying principles of scientific methods do not rapidly change. Thus, the following introductions to and descriptions of the dating methods are updated versions of Grün (in press; submitted-a,b) and Grün et al. (in preparation), tailored to the topic and audience of this review.

*Correspondence to: Rainer Grün, Research School of Earth Sciences, Research School of Pacific and Asian Studies, The Australian National University, Canberra ACT 0200, Australia.
E-mail: Rainer.Grun@anu.edu.au

DOI 10.1002/ajpa.20516
Published online in Wiley InterScience (www.interscience.wiley.com).

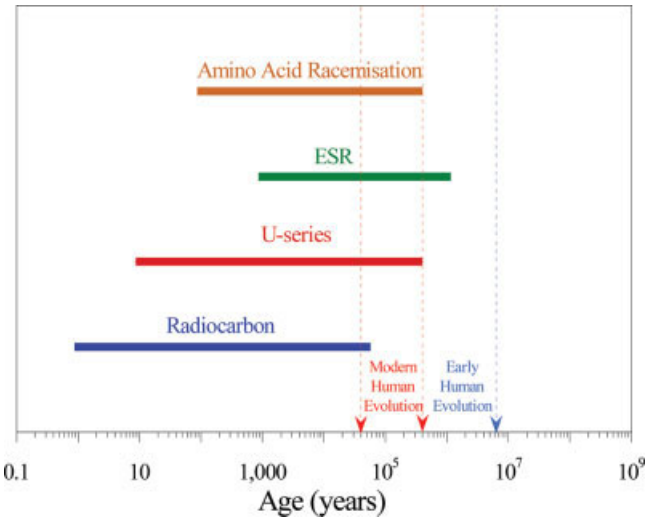

Fig. 1. Approximate dating ranges of the methods that can be used for the direct dating of human remains. [Color figure can be viewed in the online issue, which is available at www.interscience.wiley.com.]

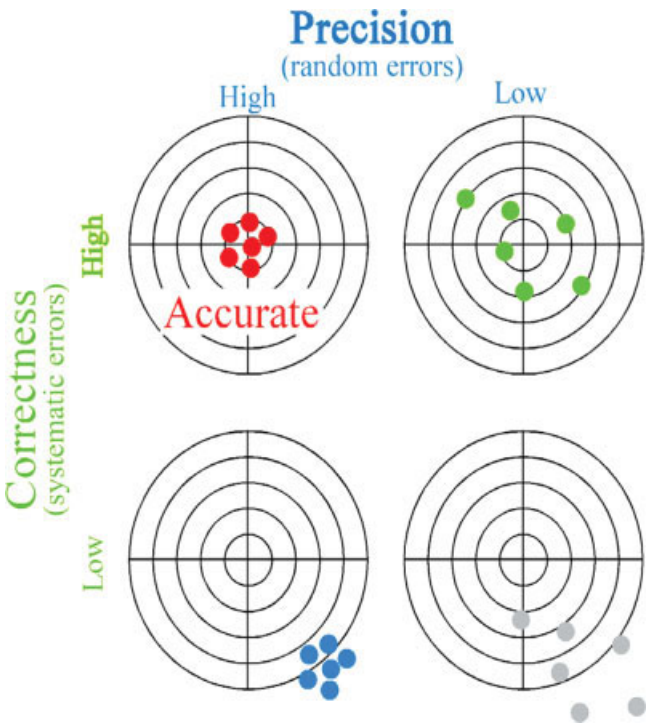

Fig. 2. Relationship between random and systematic errors. Random errors govern the precision, systematic errors the correctness. Accurate results can only be obtained if both error sources are small (after Wagner, 1998). [Color figure can be viewed in the online issue, which is available at www.interscience.wiley.com.]

Before describing the dating techniques, it is necessary to delve ever so slightly into the tedious subject of error calculations, and their meaning in the assessment and interpretation of dating results. It is the aim of every dating method to produce highly precise, highly correct, and therefore accurate results (see Fig. 2 (after Wagner, 1998), which is based on German phraseology and has the advantage of distinguishing more clearly between precision and accuracy). Note that in some statistics books, accuracy is used for overall systematic error, (correctness in Fig. 2, e.g., Saunders and Fleming, 1957), in others for the combination of random and systematic errors (as used in Fig. 2, e.g., Lyon, 1970).

Each measurement that is carried out for a quantitative analysis has a degree of uncertainty. There are two sources of error: random errors (determining the precision) and systematic errors (responsible for the correctness of the result, see Fig. 2). Only if both error sources are small, can accurate results be obtained.

Random errors

These are introduced by the degree of inability to measure the same quantity exactly in repeated measurements. When carrying out an experiment, e.g. weighing with a high precision balance, one will notice that there are slight differences in the measured weights. The best estimate of the result is provided by the mean value, which is obtained by adding up all individual measurements, and dividing them by the number of measurements. When a large number of these measurements are plotted on a frequency diagram, they follow a normal, or Gaussian distribution. The Gaussian curve is bell shaped and is defined by two parameters, the mean value and the standard deviation, σ_r.

The standard deviation (SD) means that there is a 68.3% probability that a single measurement falls within the range of mean value $\pm$ σ_r. However, about one-third of all measurements will fall outside this range. The $2\sigma_r$ range contains 95.4% of all measurements (one in twenty results will still fall outside this range!) and the $3\sigma_r$ range contains 99.7%. To be explicit, if the dating result of a single sample of human material is 10,000 $\pm$ 1,000 years, its age has about a two-third chance to be *anywhere* within 9,000–11,000 years, and a one-third chance to either be younger than 9,000 years or older than 11,000 years. No one betting on horses would ignore such odds. Also, when analyzing larger sample sets, it lies in the nature of statistics that some samples lie outside the 2-σ range (here 8,000–12,000 years). These are not necessarily outliers and should not be ignored when assessing and interpreting analytical results. Data sets can be analyzed with appropriate tests to check whether certain results are outliers or not (using t or χ^2 tests, for more details, see e.g., Lyon, 1970).

The standard error, S_r, defines the confidence interval for the mean and is the standard deviation divided by the square root of the number of measurements. This means that the confidence interval of a mean value is critically dependent on the number of measurements that have been carried out, i.e., the uncertainty in the mean can be reduced by increasing the number of measurements. This relationship can be used to improve the age determination of an object or a stratigraphic unit (provided the samples have the same age). Compared to a single measurement, the age uncertainly is halved, when measuring four samples.

Systematic errors

The difference between random and systematic errors are shown in Figure 2. The systematic error may have

been caused by incorrect calibration. For example, if the balance was calibrated with a weight of 105 mg instead of 100 mg, we can determine a weight of a sample very precisely with a large number of repeated measurements, but the mean of our measurements will be 5% off the correct weight. Here, the systematic error, σ_s, is 5%. There are two main sources for systematic errors. The first source is method specific and derives from the fact that nearly all dating techniques are based on certain assumptions (e.g. for radiocarbon dating that the production of radiocarbon in the atmosphere was constant in the past, or for ESR that the few measured α efficiency values apply to all samples). The second source is laboratory specific and derives from the specific analytical techniques and data evaluation procedures carried out in different laboratories. In some cases, the method specific systematic errors can be easily evaluated (see radiocarbon calibration, below), in other cases they are virtually unknown and cannot be determined. Laboratory specific systematic errors can be assessed in laboratory intercomparison projects and are usually reasonably small for simple isotopic methods (such as radiocarbon, U-series, or K/Ar dating), but can be surprisingly large for other techniques (for ESR, see Wieser et al., 2000, 2005).

Error propagation

As we have seen above, each individual measurement has, in the ideal case, a Gaussian distribution, which can be calculated from counting statistics. Roddick (1987) provided the strategy for propagating errors for a function, e.g. an age equation, which contains several independent variables, each associated with an individual error. The age errors can be calculated in this way for the age functions of radiocarbon or $^{40}Ar/^{39}Ar$ dating (see e.g. Renne, 2000). Some age functions are derived from complicated formulae, where analytical error propagation may provide unrealistic estimates, as, for example, for U-series data close to the limit of the method (Ludwig, 2001). Other age results are derived from nonsolvable equations and estimated by iteration processes. As a consequence, it is sometimes not possible to analytically calculate the influence of each error source on the final result. In these cases, Monte Carlo strategies can be used to estimate the overall errors. The age calculation is repeatedly carried out (at least 1,000 times) and each parameter is randomly varied within the measured uncertainty. The age simulation results are then statistically evaluated. Because of the nonlinear nature of many dating equations, the dating results may have nonsymmetrical errors (i.e. the plus error differs from the minus error, see e.g. Fig. 13, below).

The details of error calculation are the subject of ongoing discussions in the scientific communities of the various dating techniques. For the user of dating laboratories, it is important to know that the errors given with a result are meaningful. The errors for stratigraphic units can be deduced from the error of the mean, provided that samples are not of mixed ages. The chronology for a given site can be refined with the application of Bayesian analysis (for more details, see Buck et al., 1996). In the case of human remains, where only one or two samples are available for measurement, it is not possible to improve the precision of the dating result by measuring more samples. As we will see below, some of the results on human remains are associated with such large errors that any chronological interpretation would be fatuitous.

RADIOCARBON DATING

In archaeological research, radiocarbon is the most widely applied and best established dating technique. There are numerous books and reviews on radiocarbon dating, some were recently published by Taylor 1997, 2001; Hedges (2000); Higham and Petchey (2000); Trumbore (2000).

Basic principles

The element carbon occurs in nature in three isotopic forms: the stable isotopes ^{12}C (with a natural abundance of 98.9%) and ^{13}C (1.1%) as well as the radioactive isotope ^{14}C, radiocarbon. In the atmosphere, only about one in one billion (10^{12}) carbon atoms is ^{14}C. The basic principles of radiocarbon dating are shown in Figure 3. When cosmic high energy particles collide with atoms in the upper atmosphere, some of the atoms break up. Amongst the spallation products are slow, thermal neutrons, which may interact with nitrogen, oxygen, and carbon to produce ^{14}C. By far the most abundant reaction is that of the stable isotope ^{14}N converting into ^{14}C by absorbing a neutron and emitting a proton. The newly formed radiocarbon atoms oxidize to $^{14}CO_2$ molecules, which are rapidly mixed throughout the atmosphere and hydrosphere. Within about 8 years, any local radiocarbon spike is completely mixed with the global atmosphere (Nydahl and Lövseth, 1983).

Once ^{14}C is formed, it starts to decay. One of its neutrons transforms into a proton through the emission of a negatively charged β particle. In that way, ^{14}C turns into the stable isotope ^{14}N. The rate of decay is controlled by the isotope's half-life, which is defined as the time required for half of the number of initial radioactive atoms to decay. After another half-life the number of atoms have halved again and so on. The atmosphere has constant ^{14}C levels, which are maintained by the production of new ^{14}C in the atmosphere on the one hand and decay of ^{14}C on the other (steady state equilibrium).

From the atmosphere, $^{14}CO_2$ is incorporated into plants by photosynthesis and, to a lesser extent, absorption through the roots. The ^{14}C-concentration of the living tissue of a plant is in equilibrium with the atmosphere due to constant absorption of ^{14}C from the atmosphere and its subsequent decay. Animals feeding on plants and drinking water also introduce ^{14}C into their system, where it remains in equilibrium with the atmosphere. When the tissue dies (which may be associated with the death of the organism or conversion of sapwood into hardwood), absorption of ^{14}C from the atmosphere or hydrosphere stops and the number of ^{14}C atoms continuously decreases through radioactive decay. If the amount of radiocarbon in the living tissue is known, then the amount of radiocarbon left in the dead plant or animal can be used to assess the time that has passed since its death. This is the radiocarbon age of the sample.

Radiocarbon dating was introduced to archaeology in the late 1940s by W.F. Libby (e.g. Arnold and Libby, 1949, 1951a). At the time, the best estimate for the half-life of radiocarbon was 5,568 $\pm$ 30 years (Arnold and Libby, 1951b). This was revised in the early 1960s and the accepted estimate of the half-life is now 5730 $\pm$ 40 years (Mann et al., 1961).

Because isotopes have different weights, fractionation may occur in physical processes, such as evaporation or diffusion. During photosynthesis, plants preferentially

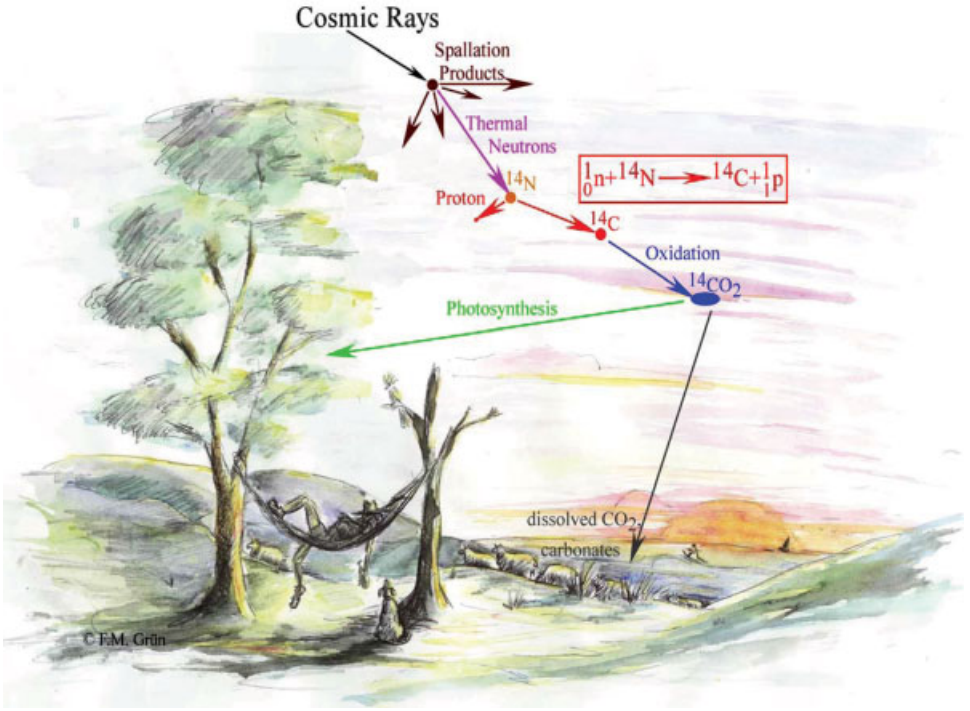

Fig. 3. The basic principles of radiocarbon dating. When cosmic rays interact with atoms in the upper atmosphere, some of the spallation products are slow, thermal neutrons. These may interact with ^{14}N to form the radioactive isotope ^{14}C. The newly formed radiocarbon atoms oxidize to $^{14}CO_2$, which is rapidly mixed with the rest of the global atmosphere. Mainly through photosynthesis ^{14}C is incorporated into living plants. The whole faunal food chain incorporates radiocarbon, which is ultimately derived from plants and drinking water. As a result, the radiocarbon activity of living tissues is in equilibrium with the atmosphere (there is a steady state between newly incorporated radiocarbon and its decay to ^{14}N). After the living tissue of the plant or animal dies, no radiocarbon is exchanged with air, and the previously incorporated radiocarbon decays. A radiocarbon age can be calculated by comparing the amount of radiocarbon left in the sample with the present day amount in living tissue. Atmospheric radiocarbon is also incorporated into carbonates such as mollusk shells, corals, or speleothems, which can also be dated by radiocarbon (background drawing with kind permission of F.M. Grün). [Color figure can be viewed in the online issue, which is available at www.interscience.wiley.com.]

incorporate the lighter isotopes, i.e. plant tissue is relatively depleted in ^{14}C, by between 2 and 6%. This would correspond to apparent ages of between 160 and 480 years (a 1% decreased radiocarbon concentration corresponds to an apparent radiocarbon age of ~80 years). The fractionation that has occurred during the incorporation of ^{14}C can be assessed by measuring the $^{13}C/^{12}C$ ratio in the sample. The fractionation of a sample is measured against a standard and expressed in delta (δ) units (permil difference between the sample and a standard). The $^{14}C/^{12}C$ fractionation is then assumed to be twice the $^{13}C/^{12}C$ fractionation. For example, if the sample has a ^{13}C value of −10‰ (relative to atmosphere), its ^{14}C is depleted by 20‰. The physiological processes in herbivores lead to an enrichment of ^{13}C over their diet (about 4‰ in collagen and 9‰ in apatite), carnivores show significantly less fractionation relatively to their diet. The collagen extracts from most human bones have ^{13}C values in the range of about −10 to −22‰ (e.g. Bronk Ramsey et al., 2000a,b).

Radiocarbon measurement

The activities of the sample and modern standard can be measured by either observing the rate of decay of ^{14}C atoms or by measuring the amount of ^{14}C atoms present in the sample. Because of the scarcity of human material, decay counting techniques are not appropriate, because they require large amounts of sample (e.g. Loosli et al., 1980; Schotterer and Oeschger, 1980). Until recently, the direct measurement of radiocarbon atoms required large tandem accelerator mass spectrometers (AMS) (e.g., Finkel and Suter, 1993; Theodorsson, 1996; Tuniz et al., 1998). New technical developments have resulted in low-energy, single stage accelerators, which are significantly smaller and less expensive, plus they can be maintained by fewer people (e.g. Schroeder et al., 2004). The dating range of radiocarbon is limited to an apparent age that is obtained on a sample that does not contain any radiocarbon (for example, geological coal or oil). This apparent age arises from CO_2 contamination during sample preparation, memory effects in the equipment and electrical noise in the detectors. The total procedural background levels for AMS are in the range of 50–55 ka for geological, radiocarbon free anthracite (Bronk Ramsey et al., 2004b).

Conventional radiocarbon ages

As mentioned above, the best estimate of the half-life is 5730 ± 40 years, a significantly smaller value than was originally used. In order to maintain continuity, it was decided that all radiocarbon ages reported in the journal "Radiocarbon" are based on the old half-life. Furthermore, the term "before present" (BP) was introduced, which takes reference to the year 1950. A conventional radiocarbon date, expressed in years BP, is calculated by (Stuiver and Polach, 1977):

1. the use of the 5,568 year half-life;
2. the assumption that the specific atmospheric ^{14}C activity was constant;
3. the use of oxalic acid as standard for the amount of initial radiocarbon;
4. normalization for isotopic fractionation on a value of $\delta^{13}C = -25‰$ (the value of wood relative to the PDB standard, a belemnite from the Pee Dee formation);
5. the base year of 1950, with ages given in years BP.

Because of this specific definition, the term BP should not be used for reporting the age estimates of any other method. The radiocarbon timescale, as defined by Stuiver and Polach (1977), differs from the real (calendar) timescale. The two time scales are connected by calibration (see below).

Changes in the past atmospheric specific radiocarbon activity

A few years after the conception of radiocarbon dating, it turned out that the production of radiocarbon in the atmosphere had not been constant over time. This was shown by measuring tree rings and comparing their known age with the radiocarbon results. Subsequently, dendrochronological samples were used to establish radiocarbon calibration curves. It has proved difficult to find deciduous trees that can extend the continuous chronology beyond about 12,000 years ago (because of the severe climatic changes related to the last ice age). Prior to this time, radiocarbon calibration is based on U-series dated corals (e.g. Bard et al., 1998; Burr et al., 1998) and speleothems (Vogel and Kronfeld, 1997; Goslar et al., 2000; Beck et al., 2001), radiocarbon results on laminated lake sediments (Kitagawa and van der Plicht, 1998a, b, 2000), as well as radiocarbon data on planktonic foraminifera, which were correlated to the annual-layer chronology of the GISP2 (Greenland Ice Sheet Project Two) ice core (Voelker et al., 1998, 2000). Recent effects on the ^{14}C concentration have been introduced by humans, such as the combustion of fossil fuels since the industrial revolution (Suess, 1955), or nuclear testing (see Manning and Melhuish, 1994; Levin et al., 1996). Over most of the past 45 ka, the Earth's magnetic field was weaker than today, causing an increased ^{14}C production and apparently younger radiocarbon ages (e.g. Bard, 1997, 1998). This general trend is overprinted by changes in atmospheric CO_2 concentration, which are particularly well documented in the Antarctic ice cores. The Vostok core shows strong increases of atmospheric CO_2 at onsets of interglacial periods (e.g. Barnola et al., 1987; Petit et al., 1999). These increases, because of variations in the CO_2 exchange between atmosphere and oceans, have a similar effect as the burning of fossil fuels: the calibration curve becomes flat and radiocarbon dating becomes problematic. Figure 4 shows a summary of calibration data for the time span of 10–50 ka (from Hughen et al., 2004a, see also Shackleton et al., 2004). It can be seen that between 10 and 44 ka ago, the conventional radiocarbon results are significantly younger than the independent age estimates, prior to that time both time scales are closely similar. Up to about 30 ka, the offset of up to 5 ka between radiocarbon ages and those of independent dating techniques lies within a relatively narrow error range. For samples older than 30 ka, the different calibration approaches yielded significantly different results. For example, the study based on the Bahama speleothem (Beck et al., 2001) yielded significantly younger radiocarbon dates than the marine material, and furthermore shows very strong fluctuations in the radiocarbon dates between 44 and 40 ka. These fluctuations, which could have serious implications for past ocean circulations, are not replicated in the other data sets. The data obtained from Lake Suigetsu are older (Kitagawa and van der Plicht, 1998a, b, 2000) than those from the marine environment.

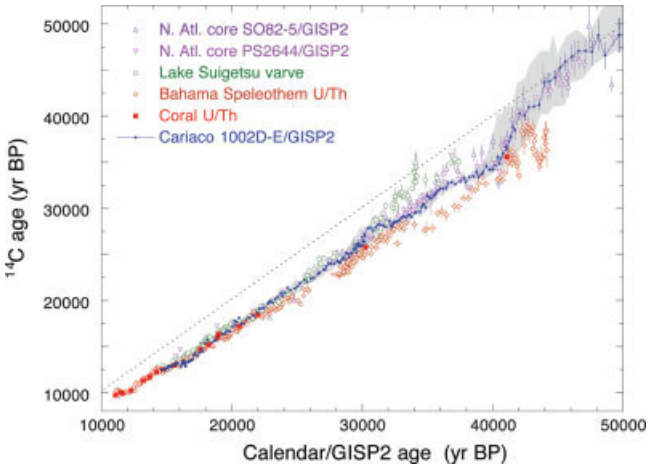

Fig. 4. Compilation of radiocarbon calibration data for the time range of 10–50 ka (after Hughen et al., 2004a, modified and kindly provided by Konrad Hughen). It is obvious that any calibration beyond 30 ka is associated with substantial uncertainty (Reproduced with permission from Hughen et al., Science, 2004a, 303, 202–207). [Color figure can be viewed in the online issue, which is available at www.interscience.wiley.com.]

Calibration of conventional radiocarbon dates

For younger radiocarbon dates (<26 ka), conventional radiocarbon ages (BP) can be easily converted into a calibrated ages (cal BP). The calibration curve is plotted with one and two-sigma error envelopes (see Fig. 5). Depending on the shape of the curve, three qualitatively different results may be obtained:

1. if the calibration curve is steep, the calibrated radiocarbon age may have smaller errors than the conventional age (Fig. 5A, lower calibration);
2. if the calibration curve is shallow, the calibrated radiocarbon age may have larger errors than the conventional age (Fig. 5A, upper calibration);
3. if the calibration curve has pronounced peaks or troughs, several age ranges may be possible (Fig. 5B).

Because of the shape of the calibration curve, the original (Gaussian) error distribution of the conventional ^{14}C date does not produce a similar distribution in the calibrated ^{14}C age. Instead of giving a mean age with one or two sigma errors, the projections give probability distributions for the calibrated age, which are not normal probability distributions. Thus, calibrated ages are usually given as age ranges, representing the one or two sigma error of the conventional radiocarbon age estimate and the corresponding error envelope of the calibration curve. Calibrated radiocarbon age estimates are denoted with "cal BP," i.e. calibrated (or calendar) ages before 1950 AD (Van der Plicht, 2000). The presently recommended calibration curve is IntCal04 (Reimer et al., 2004), for the ma-

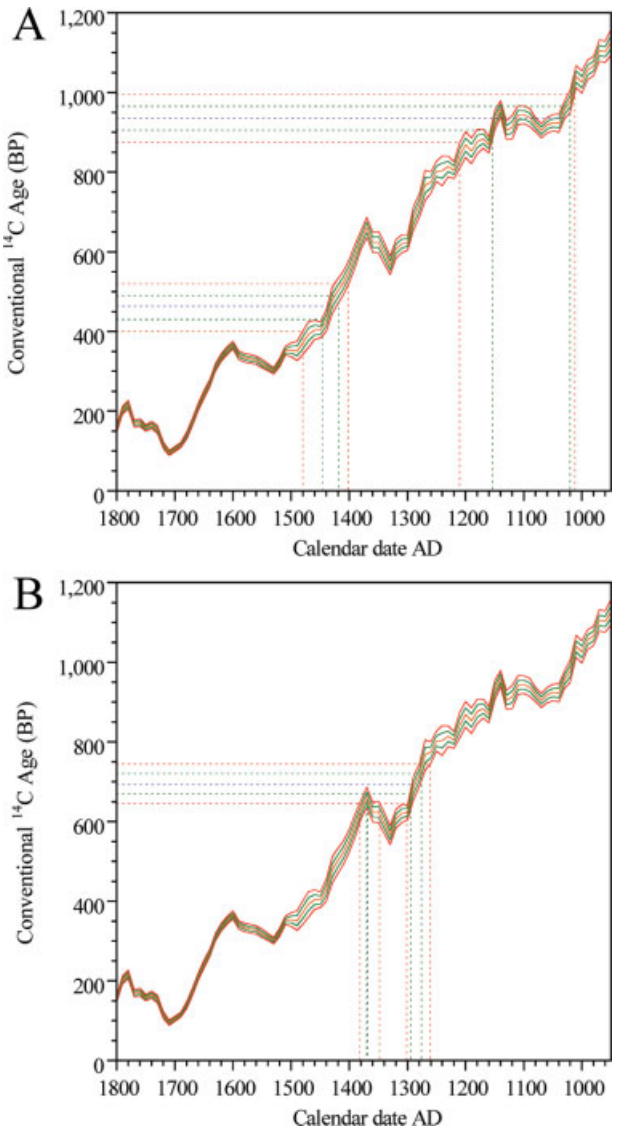

Fig. 5. Calibration of conventional radiocarbon ages. Depending on the shape of the calibration curve, the calibrated ages may have smaller or larger errors than the conventional radiocarbon age (**A**), or may result in two separate age ranges (**B**). Calibration data from INTCAL98 (Stuiver et al., 1998; http://depts.washington.edu/qil/). Central line: mean age value; next pair of dotted lines: 1-σ error in age and projection of the 1-σ error envelope of the calibration curve; outer dotted lines: the same for a 2-σ age error. [Color figure can be viewed in the online issue, which is available at www.interscience.wiley.com.]

rine environment see Hughen et al., 2004b. Calibration programs are used calibrated age ranges from measured ^{14}C dates, for example OxCal (Bronk Ramsey, 2001, 2005; http://c14.arch.ox.ac.uk/oxcal.php).

For the dating of the disappearance of recent human groups such as the Neanderthals of Europe or *Homo erectus* in Asia, the age range of 60,000–30,000 cal BP is of particular interest. Van der Plicht (2000) reviewed the state of the art of radiocarbon calibration and pointed out that the data sets relating to the calibration of radiocarbon ages before 24 ka are at present not unambiguous enough to be regarded as calibration curves. He prefers the term "reference datasets." This still seems to apply after the publication of the newer data sets. As a rule of thumb, it can be assumed that the calendar ages of radiocarbon results between 30 and 40 ka BP are ~5 ka older (for noncontaminated samples, see below). However, the use of calibration programs such as Calpal (Weninger et al., 2002; http://www.calpal.de/calpal/index.htm) in the time range of >30,000 years seems at present premature (Van der Plicht et al., 2004; Reimer et al., 2006).

Postdepositional carbon exchange

The main problem in attaining reliable radiocarbon ages of older samples lies in the fact that nearly all samples, particularly bones, exchange CO_2 with their environment. For young samples, any exchange has little effect on the calculated age. Figure 6A shows the effect of carbon exchange (expressed in percent modern carbon, pMC). If samples experience a carbon exchange corresponding to 0.02 pMC, it is not possible to exceed an age of about 70,000 years, 0.5 pMC corresponds to about 44,000 years and 5 pMC to 25,000 years. Figure 6B shows how much contamination is required to lower the radiocarbon age of a sample by between 1 and 5 half-lives. For example, the human remains of Vogelherd, originally associated with the early Aurignacian, were dated to about 5,000 BP (Conard et al., 2004). Other material, also associated with the Aurignacian, yielded radiocarbon results of around 32,000 BP (Conard and Bolus, 2003). If the young ages of the human material were due to contamination, the 27,000 age underestimation in a 32,000 BP old sample would require a contamination with modern carbon of 60% (which is extremely unlikely). The incorporation of "dead" carbon is not a significant problem. Regardless of the age of the sample, incorporation of 5% dead carbon will increase the age of a sample by 412 BP.

Radiocarbon dating of bones and teeth

Bones are notoriously difficult to date because with time, their original organic matter decomposes, and the mineralogic compounds change. Besides the formation of new minerals (Piepenbrink, 1989), disintegration of the mineral phase and conversion of the amorphous phase into hydroxyapatite is observed (Newesely, 1989) as well as growth of the crystal size of hydroxyapatite (Hassan et al., 1977) even under subaerial conditions (Tuross et al., 1989). Furthermore, bones may exchange a large amount of ions with their environment. To obtain original, unaltered bone material, radiocarbon dating is usually carried out on bone collagen. Collagen is a group of proteins that are part of whitish fibers found in tendons, ligaments, cartilage, etc. The collagen extracted from fossil bones can be checked for contamination by analyzing its amino acid composition (e.g. Van Klinken and Mook, 1990) and/or the carbon/nitrogen ratio. Routine extraction techniques are usually associated with contaminations in the range of 0.2–2 pMC (particularly for small collagen yields, see Fig. 2 in Bronk Ramsey et al., 2004a). Some of this contamination can be removed using ultrafiltration techniques (Bronk Ramsey et al., 2004a). Where bones do not contain sufficient, uncontaminated collagen, any radiocarbon results are questionable. Tooth enamel (viz-a-viz dentine) is not routinely dated by radiocarbon because it is difficult to extract unaltered chemical components and older tooth enamel has a tendency to exchange secondary carbonates (Hedges et al., 1996b; Grün et al., 1997).

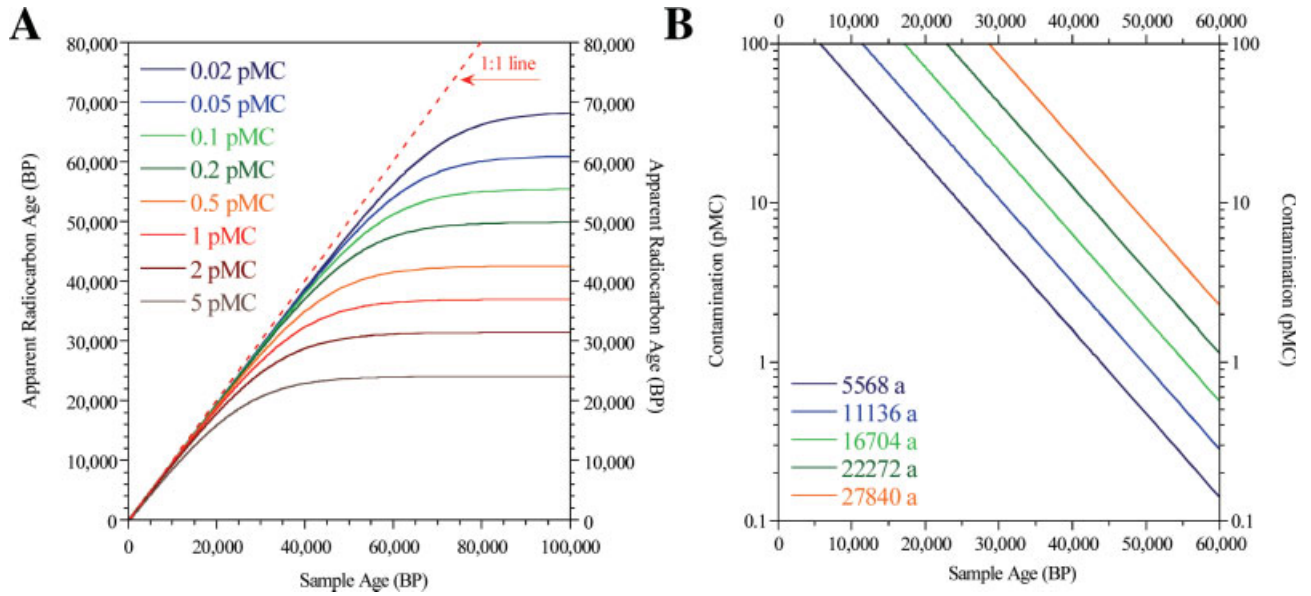

Fig. 6. The effect of postdepositional radiocarbon exchange (expressed in percent modern carbon, pMC). (**A**) If a sample experiences a minute exchange of CO_2 corresponding to 0.2 pMC it is not possible to exceed a radiocarbon age of 50 ka BP. Bottom line is 5pMC. (**B**) Amount of contamination required for an age underestimation of a given radiocarbon result by between one and five half-lives (remember BP results are obtained using the old half-life, also note the logarithmic Y-axis). Lefthand line is 5568a. [Color figure can be viewed in the online issue, which is available at www.interscience.wiley.com.]

Chappell et al. (1996) analyzed a large number of radiocarbon age estimates and showed that the vast majority of shell samples with radiocarbon age estimates in the range of 22–40 ka BP were most likely of last interglacial (or older) age, i.e. older than 125,000 years. This implied that the shells had exchanged carbon equivalent to between about 1 and 5 pMC (the real amount of carbon exchanged is higher because carbon that was taken up at some time in the past has already partly decayed). One can reasonably assume that the same applies to bones, where apparent age results of >30 ka BP are, more often than not, minimum age estimates. In the context of an archaeological site, this can be alleviated to some extent by analyzing a large number of samples and select the results of those bones, which gave the highest collagen yield and where other contaminants were negligible. At an archaeological site, one can usually observe a significant scatter in the radiocarbon results for a particular archaeological layer (see e.g. Devil's Lair, Western Australia: Turney et al., 2001). Provided reworking can be excluded, it is usually thought that the oldest results are the most reliable ones, because of incremental contamination of the samples leading to younger ages. Such multisample approaches are usually not feasible on human remains. If associations of the human specimen with other datable material cannot be established, any possible contamination is difficult to assess.

The radiocarbon dating attempts of the Vindija Neanderthal may serve as an example (see below). The radiocarbon results on the Neanderthal remains were unexpectedly young (Smith et al., 1999). It was thought that the reasonable reproducibility of the radiocarbon analyses of two subsamples was an indication that the sample was not contaminated. Unfortunately, besides being random and otherwise opposed to any dating attempts, nature seems also capable of providing constant contamination levels in the subsamples of a Neanderthal skeleton. Indeed, a subsequent radiocarbon study using ultrafiltration techniques yielded significantly older ages (Higham et al., 2006a). In other words, if one cannot check the reliability of an old ($\sim$ > 30 ka) radiocarbon date on bones by independent or systematic means, it is difficult to assess whether such a radiocarbon date is reliable. Although this sound rather discouraging, the same applies to all samples where only one or two analyses are available, and indeed to single stand-alone results of most dating techniques.

Dating range

Radiocarbon dating of bones exceeds 45 ka only in exceptional circumstances, because of the problems of contamination as well as the limitations of accelerators. The application of ultrafiltration pretreatment techniques seem to overcome some contamination problems and radiocarbon ages of up to 55 ka are obtainable on bones (e.g. Higham et al., 2006a,b; Jacobi et al., 2006). This is, however, on the proviso that the samples actually contain unaltered, original organic matter.

U-SERIES DATING

U-series is a family of dating methods based on measuring disequilibrium in the two naturally occurring decay chains of the element uranium, ^{238}U and ^{235}U. In recent years, U-series (Th/U) has become one of the most widely applied and accurate dating technique in Quaternary sciences. The most comprehensive reviews of the application of U-series measurements in earth sciences are the books edited by Ivanovich and Harmon (1992) and more recently by Bourdon et al. (2003). Reviews on U-series dating in Quaternary and archaeological sciences have been published by Schwarcz (1993, 1997), Ku (2000), Latham (2001), and Pike and Pettitt (2003).

Basic principles

The element U has two naturally occurring decay chains, the parent isotopes being ^{238}U (99.28% natural

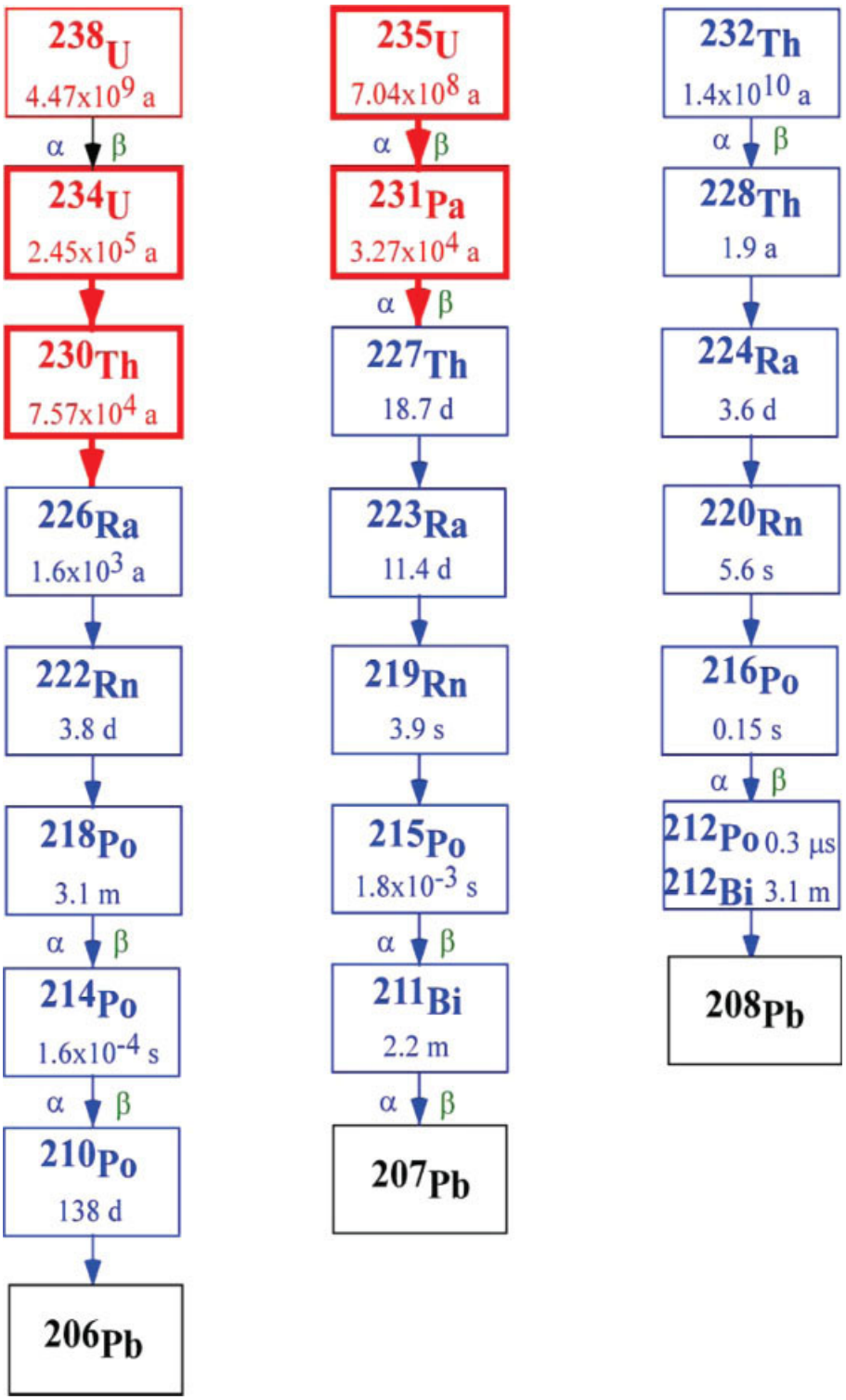

Fig. 7. The main α emitters of the natural U and Th decay chains. A series of α and β decays are indicated by the α and β symbols. The bold boxes indicate the isotopes used for U-series dating. The lowest boxes in the chains are the stable end members. The remaining boxes are the main α emitters. [Color figure can be viewed in the online issue, which is available at www.interscience.wiley.com.]

abundance) and ^{235}U (0.72%). ^{238}U decays via eight α and a number of β decays to the stable isotope ^{206}Pb, ^{235}U via seven α and several β decays to ^{207}Pb (see Fig. 7). When the decay chains are in equilibrium, the activity (decays per time unit) of all isotopes within the decay chain is the same, i.e., the number of atoms of a parent isotope (^{238}U or ^{235}U) decaying within a given time period is the same as for all intermediate isotopes as well as the number of stable end members produced (^{206}Pb and ^{207}Pb, respectively). U-series dating is based on the different geochemical behavior of uranium (U), thorium (Th), and protactinium (Pa). Uranium in the U^{6+} oxidation state is water-soluble, whereas Th and Pa are in practical terms water-insoluble. Natural waters therefore contain traces of U, but are virtually free of Th and Pa. Minerals precipitated from water, such as secondary carbonates (e.g., speleothems, travertines, shells, corals etc.), contain uranium, but no Th and Pa. Therefore, the ^{230}Th/^{234}U activity ratio

in the ^{238}U decay chain as well as the ^{231}Pa/^{235}U activity ratio of the ^{235}U decay chain are zero at the time of formation of these minerals ($t = 0$). As soon as the parent isotopes are incorporated into a mineral, they start to decay and isotopes of the decay chains grow towards secular equilibrium, where all activity ratios are indistinguishable from 1. A U-series ages can be calculated from the measured Th/U or Pa/U activity ratios and the mathematical function behind U-series disequilibrium. For practical purposes, after about seven half-lives of the daughter isotope, equilibrium is restored. The half-lives of ^{230}Th and ^{231}Pa are 75,690 ± 230 a and 32,713 ± 110 a, respectively (Robert et al., 1969; Cheng et al., 2000), thus allowing Th/U and Pa/U dating to about 500 ka and 200 ka, respectively. Other U-series dating approaches are based on isotopes with much shorter half-lives, such as ^{226}Ra ($T_{1/2}$ = 1,300 a) and ^{210}Pb ($T_{1/2}$ = 22.3 a), see Schwarcz (1989) and Noller (2000), respectively. In tune with their short half-lives, the dating ranges of these methods are limited to very recent times.

The other naturally occurring decay chain that of ^{232}Th, which decays via six α decays to the stable isotope ^{208}Pb, has not been used for dating of Quaternary materials, because all isotopes of this decay chain have such short half-lives, which makes them unsuitable for dating via disequilibrium (see Fig. 7). However, the presence of ^{232}Th can be used to identify contamination of the samples.

^{230}Th/^{234}U (Th/U for short) dating is slightly complicated because most natural waters have an excess of ^{234}U over ^{238}U (e.g. chapter V in Cherdyntsev, 1971). This is due to the fact that ^{234}U is produced by α-decay of ^{238}U: when an α particle is emitted, the decaying atom recoils, which in turn leads to a weakening of its lattice position. Dissolution of minerals starts preferentially at weakened lattice sites, as a consequence, these solutions are enriched with ^{234}U. Alternatively, the recoiled atom can be directly ejected from the mineral surface into the solution. Because of its long half-life 245,250 ± 490 a (Cheng et al., 2000), the excess ^{234}U activity has to be taken into account.

U-series measurement

The measurement techniques for U-series dating were recently reviewed by Goldstein and Stirling (2003). Until the late 1980s, U-series isotopes had been measured by α spectrometry. An alternative is γ spectrometry (Yokoyama and Nguyen, 1980). The latter method has the disadvantage that only a small percentage of the total number of radioactive decays is associated with γ-ray emissions. Therefore, the analytical errors of γ spectrometry are considerably larger than of α spectrometry. The advantages of γ spectrometry are that important paleoanthropological samples can be measured without any sample preparation or destruction and that the isotopes of both U-decay chains can be measured simultaneously (e.g. Yokoyama and Nguyen, 1981; Yokoyama et al., 1988, 1997).

Edwards et al. (1987a,b) were the first to use thermal ionization mass spectrometry (TIMS) for the combined measurement of ^{238}U, ^{234}U, and ^{230}Th. Similar to AMS measurements of radiocarbon, mass spectrometric measurements of isotopes are far more precise than decay counting techniques. As a consequence, the dating range was expanded from about 350 ka to about 500 ka, and much smaller samples can now be analyzed. Edwards et al. (1997) demonstrated that ^{231}Pa could also be measured by mass spectrometry. Recent developments in laser ablation ICP-MS (inductively coupled plasma mass spectrometry) have demonstrated that in situ analysis of U-series isotopes (^{238}U, ^{234}U, and ^{230}Th, but not ^{231}Pa) in bones and teeth is feasible (Eggins et al., 2003, 2005).

U-series dating of bones and teeth

U-series dating has been applied with great success to corals (e.g. Edwards et al., 1987a, b; Bard et al., 1990, 1998), as well as speleothems (e.g. Beck et al., 2001). For these materials, U-series provides highly precise and accurate age estimations. Unfortunately, these materials are nearly never (corals) or only rarely directly associated with paleoanthropological specimens, e.g. calcite or calcrete incrustations were found on the human fossils at Petralona (Liritzis, 1980, 1982; Shen and Yokoyama, 1984), Guattari (Blanc, 1939; Schwarcz et al., 1991), Singa (McDermott et al., 1996), and Liujiang (Shen et al., 2002).

It is well known that bones and teeth are open systems for uranium. Under normal circumstances geochronologists try to identify samples that show open system behavior to avoid their analysis. Nevertheless, there have been numerous attempts to apply U-series dating to bones and teeth, because of the lack of other suitable dating material and the age restrictions of radiocarbon dating at paleoanthropological sites (see above). Modern bones and teeth contain only very small amounts of U (<1–50 ppb, Tandon et al., 1998), whereas archaeological specimens may contain several hundreds of ppm U. For dating, the temporal uptake of uranium has to be reconstructed. If U-uptake is the dominating geochemical process (as observed by the simple fact that archaeological bones have higher U-concentrations than modern bones), an apparent U-series age (based on a closed system assumption) would underestimate the correct age of the bone. The same would apply, if Th was leached from the bone. There are, however, no observations implying that Th-loss takes place in nature. If uranium is leached from the bone (after an initial uptake phase), the apparent U-series age may overestimate the correct age, the same applies if the bone contains detrital Th. This can be detected by the presence of ^{232}Th.

The mechanism of uranium uptake in bones and teeth is governed by diffusion of uranyl (UO_2^{2+}), followed by adsorption onto the large surface area of the bone mineral hydroxyapatite (Millard, 1993; Millard and Hedges, 1996; Pike, 2000; Pike et al., 2002). The diffusion–adsorption (D–A) model of these authors predicts the spatial distribution of U and U-series isotopes across a bone or tooth enamel section. The constant diffusion of uranium from the outer to the inner surfaces, lead to the development of U-shaped U-concentration profiles. Over time, these profiles will gradually fill-in and flatten as the bone equilibrates with the U in solution (Fig. 8A). The distribution of apparent U-series ages follows a similar pattern, with apparent ages decreasing towards the center of the bone (Fig. 8B). If the adsorption of the uranium is a continuing process without changes in the adsorption rate, the modeled D–A ages will be consistent throughout the bone. The D–A model has the great advantage, in that it allows the identification of bones with deviating U-uptake histories. For example, assuming a two stage U-uptake (here 50% of the uranium was accumulated 10 ka ago, the other 50% 1 ka ago), the U-concentration profile would still look more or less U-shaped, see Figure 8C (it would be difficult to judge from the analytical data whether or not the profile concurred with the D–A model). However, the apparent U-series ages would clearly show an inverted profile (Fig. 8D). U-leaching leads to a U-concentration profile

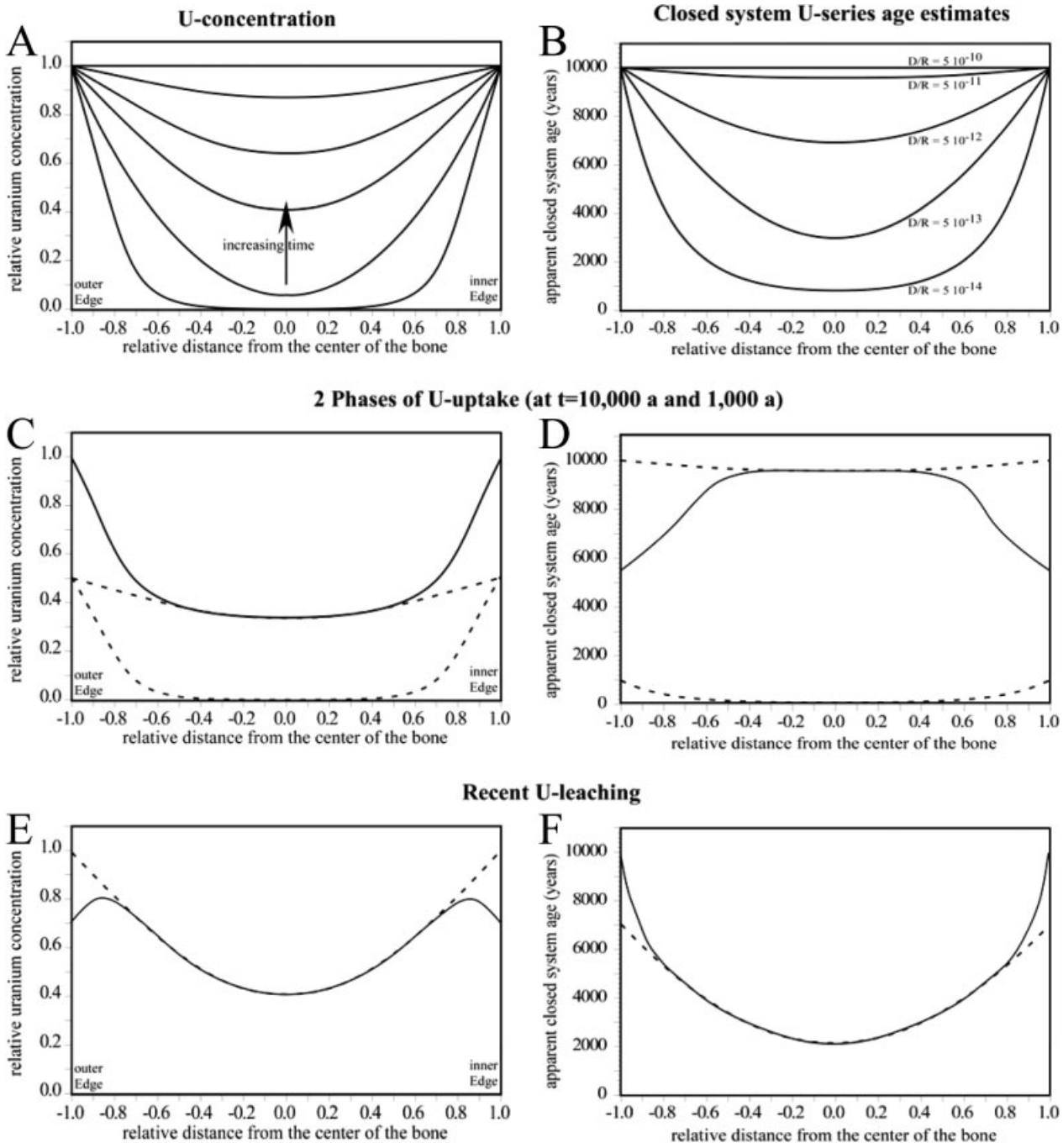

Fig. 8. The diffusion/absorption (D-A) model of Millard and Hedges (1996). **A**: Development of normalized U-concentration profiles according to the D-A model. **B**: Apparent U-series age estimates across a 10 ka bone ($^{234}U/^{238}U = 1$) for different values of the diffusion–adsorption parameters D/R. **C** and **D**: Two phases of U-uptake. Here it is assumed that half of the uranium migrated into the sample between 10,000 and 9,000 years ago and a second phase commenced at 1,000 years ago. The U-concentration distribution (Fig. 8C) seems to conform to the expected U-shaped profile (Fig. 8A). However, the distribution of apparent U-series age estimates (Fig. 8D) clearly shows more recent age estimates at the outside. The dotted lines show the expected U-concentration and U-series age profiles separately for the two uptake events. **E** and **F**: U-leaching. Leaching is demonstrated by decreasing U-concentrations towards the outside of the bone (Fig. 8E). The distribution of apparent U-series age estimates (F) is very similar to the normal age distribution (Fig. 8B), however, the ages near the surface of the bone would overestimate the correct age of the sample. Dotted lines: expected U-concentration and U-series age profiles without leaching (Fig. 8A,B redrawn from Pike et al., 2002).

with decreasing U-concentrations towards the surface of the bone (Fig. 8E). After the measurement of the U-concentration profiles, appropriate analytical strategies can be implemented. For details on the application of the D–A model, see Pike et al. (2002). For his dissertation work, Pike (2000) used solution ICP-MS for the assessment of the U-concentration profile and TIMS for U-series analysis. Samples were obtained by drilling and underwent

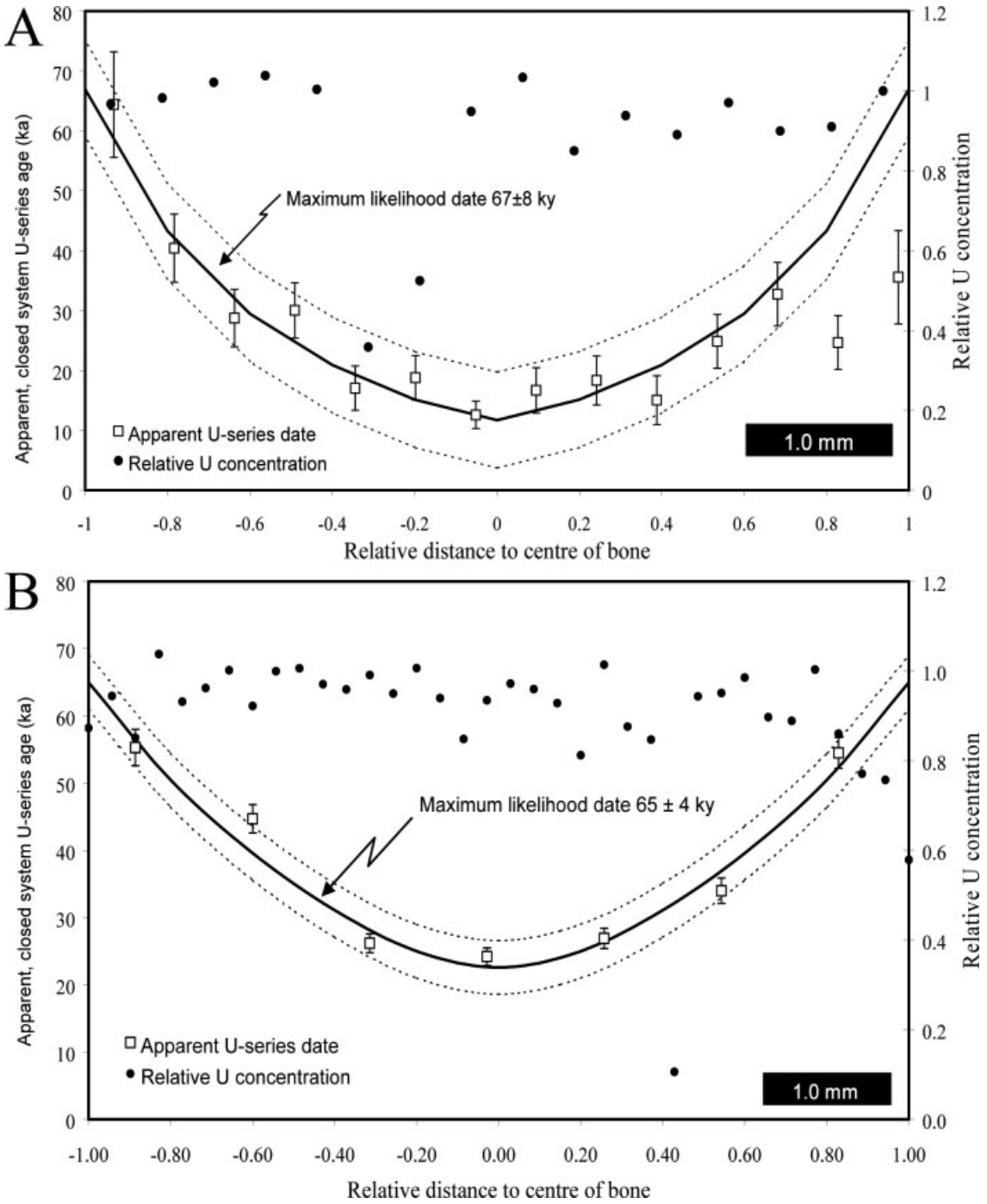

Fig. 9. U-concentration and apparent U-series ages estimates on two bone samples from Steetley Wood (from Pike et al., 2005, original kindly provided by Alistair Pike, University of Bristol) (Reproduced with permission from Pike et al., J Quaternary Sci, 2005, 20, 59–65).

subsequently chemical isotope separation. Following this approach, the full analysis of a bone may take several weeks to months. New developments in in situ U-series microanalysis, using laser ablation multicollector ICP-MS (Eggins et al., 2005) reduce sample preparation to simply cutting a sample to provide a plane surface for the laser scan. The isotopic measurements take about 1 h. Figure 9 shows the results on two bone samples from Steetley Wood Cave (Pike at al., 2005). Note that the U-concentration profile is rather flat, indicating a high diffusion rate into the bone (compare to Fig. 8A).

There is perhaps one caveat to the D–A model. Some bones may have been buried for a significant amount of time with little or no U-uptake. At a later stage, uranium may become mobile in the vicinity of a bone, due to changes in the hydrological system, e.g. erosion leads to the draining of an aquifer. This corresponds to the chemical scenario shown in Figure 8C,D, but the amounts of U-uptake in the later phase would be much larger than in the earlier one. Here, the D–A model may yield significant age underestimations, without the hint of the earlier U-uptake phase. An example for this is perhaps the site of

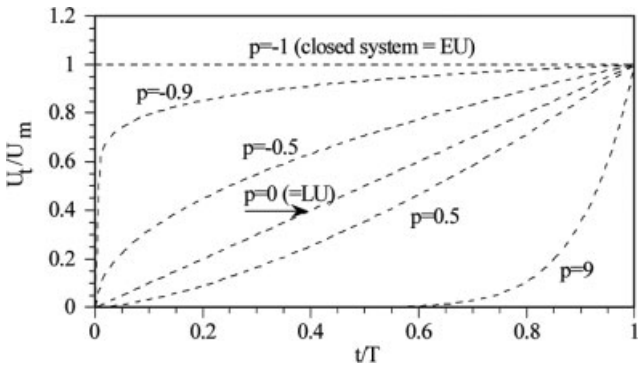

Fig. 10. U-uptake functions according to the p-value system for a series of p-values (from Grün et al., 1988). EU (early U-uptake) and LU (linear U-uptake) are two special cases frequently discussed in literature, because they can be relatively easily modeled.

Hoxne, which is the type locality of the Hoxne Interglacial (Singer et al., 1993). Hoxne has been correlated with marine isotope stage (MIS) 11, therefore, it has an expected age of around 370–415 ka (Bassinot et al., 1994). U-series analysis on bones (Rae and Ivanovich, 1986; Rae et al., 1989) were difficult to interpret (some bones showed leaching), but a number of U-series results from bone surfaces yielded ages of less than 100 ka. On dentine samples, all U-series ages were <60 ka (Schwarcz and Grün, 1993), implying a very late U-uptake.

Open systems can also be recognized by the simultaneous measurement of $^{230}Th/^{234}U$ and $^{231}Pa/^{235}U$ ratios of bone samples (e.g. Chen and Yuan, 1988; Leitner-Wild and Steffan, 1993). At the moment, the D–A model has not yet been adopted for combined Th/U-Pa/U dating. Instead, open ^{230}Th-^{231}Pa systems in bones can be modeled, e.g., using the one parameter uptake equation of Grün et al. (1988), the so called p-value system. A one parameter U-uptake equation, $U(t) = U_m\ (t/T)^{p\,+\,1}$, is used for the modeling of U-uptake, where $U(t)$ is the uranium concentration at the time t, U_m the measured, present day U-concentration, T the age of the sample, and p the uptake parameter. Some representative functions of which are shown in Figure 10. Two special cases are associated with p-values of −1 and 0. A p-value of −1 corresponds to the closed system, or the so-called early uptake (EU) model, which assumes that any uranium in the sample was accumulated shortly after burial and that duration is small compared to the age of the sample. A p-value of 0 corresponds to the so-called linear U-uptake (LU) model. Because these two models are relatively easy to implement mathematically, they have been used in numerous dating studies as limiting cases (see also ESR section below). The p-value diffusion function has no underlying physical meaning (in opposite to the D–A model, see above), but it has the advantage that a single function can be used to model saturating as well as sublinear U-uptake (in contrast to single parameter exponential functions). Nevertheless, any uptake functions derived from the D–A model can be closely assimilated by a p-value function. Furthermore, the real uptake history of a given sample may be more complex than can be modeled by either approach.

Simpson and Grün (1998) used concordance diagrams for their γ spectrometric measurements. These concordance diagrams show the measured $^{230}Th/^{238}U$ versus $^{231}Pa/^{235}U$ ratios, along with $^{234}U/^{238}U$ evolution lines (Fig. 11), whose position in the diagram depend on the U-uptake function (compare Fig. 11A,B). Concordance is obtained when the $^{230}Th/^{238}U$–$^{231}Pa/^{235}U$ data point lies, within error, on the measured $^{234}U/^{238}U$ iso-line. Concordance diagrams can be calculated for any p-value. One should be aware, however, that the iso-$^{234}U/^{238}U$ lines do not change much in their position for U-uptake histories that are more delayed than the linear uptake model (i.e. p > 0). This means that $^{230}Th/^{234}U$–$^{231}Pa/^{235}U$ modeling of samples that have experienced a delayed, sublinear U-uptake history will always be associated with quite large errors. Alternative concordance diagrams were presented by Cheng et al. (1998).

It can be seen that the error of the γ spectrometric measurement is too large to distinguish between closed system, early U-uptake (Fig. 11A) and linear U-uptake (Fig. 11B). In the example given, the γ spectrometric age would range between about 55 ka (some leaching is possible, see below) and 150 ka. The typical errors that can be obtained by TIMS (Edwards et al., 1997; Cheng et al., 1998; small error ellipses in Figs. 11 and 12) would allow far more detailed modeling of U-uptake or loss. If the data had been obtained by TIMS, the open system age would range between 90 and 98 ka (with associated p-values of −0.67 and −0.57, respectively). The concordance plot can also be used to recognize overall U-leaching (Fig. 12). The γ spectrometric measurements of this data set cannot be used to distinguish between closed system (indeed a slight U-uptake is also within error) and 20% U-loss, resulting in an age range of between 80 ka (p = −0.88) and 52 ka (for 20% leaching). TIMS, on the other hand, would result in ages of between 64.2 and 63.5 ka (between 5.5 and 6.5% leaching). It seems clear from these exemplary calculations that there is an urgent need to develop and apply TIMS Th/Pa dating on bones. Apart from the much higher precision, TIMS could be used for an improved Th/Pa D–A model. Suitable samples could be identified through U-concentration profiles with laser ablation ICP-MS.

Dating range

The range of U-series dating depends on the ability to measure isotopic ratios that are different from, but close to equilibrium. This depends on the size of the errors, which is a function of the U-concentrations in the sample and the detection system (see above). TIMS measurements can be used to estimate closed system $^{230}Th/^{234}U$ ages of up to about 500 ka, α spectrometry to about 350 ka and γ spectrometry to about 250 ka. The limits for $^{231}Pa/^{235}U$ dating are ~200, 130, and 100 ka for TIMS, α and γ spectrometry, respectively. Using TIMS, a coral as young as 180 years was measured with a 2-σ error of 5 years (Edwards et al., 1987b). This demonstrates the particular power of U-series dating, when applied to ideally suited material.

The dating range of samples, which have been subject to an open system, can potentially greatly exceed that of closed system samples. If a sample has experienced delayed U-uptake, and its history can be reconstructed e.g. through $^{230}Th/^{238}U$–$^{231}Pa/^{235}U$ analyses, dating in excess of 1 Ma may become feasible.

Errors

Because of the exponential nature of the age function, U-series age errors are asymmetrical (see Fig. 13). Finite ages can be produced as long as the measured $^{230}Th/^{234}U$ ratio is statistically distinctive from equilibrium. Ludwig

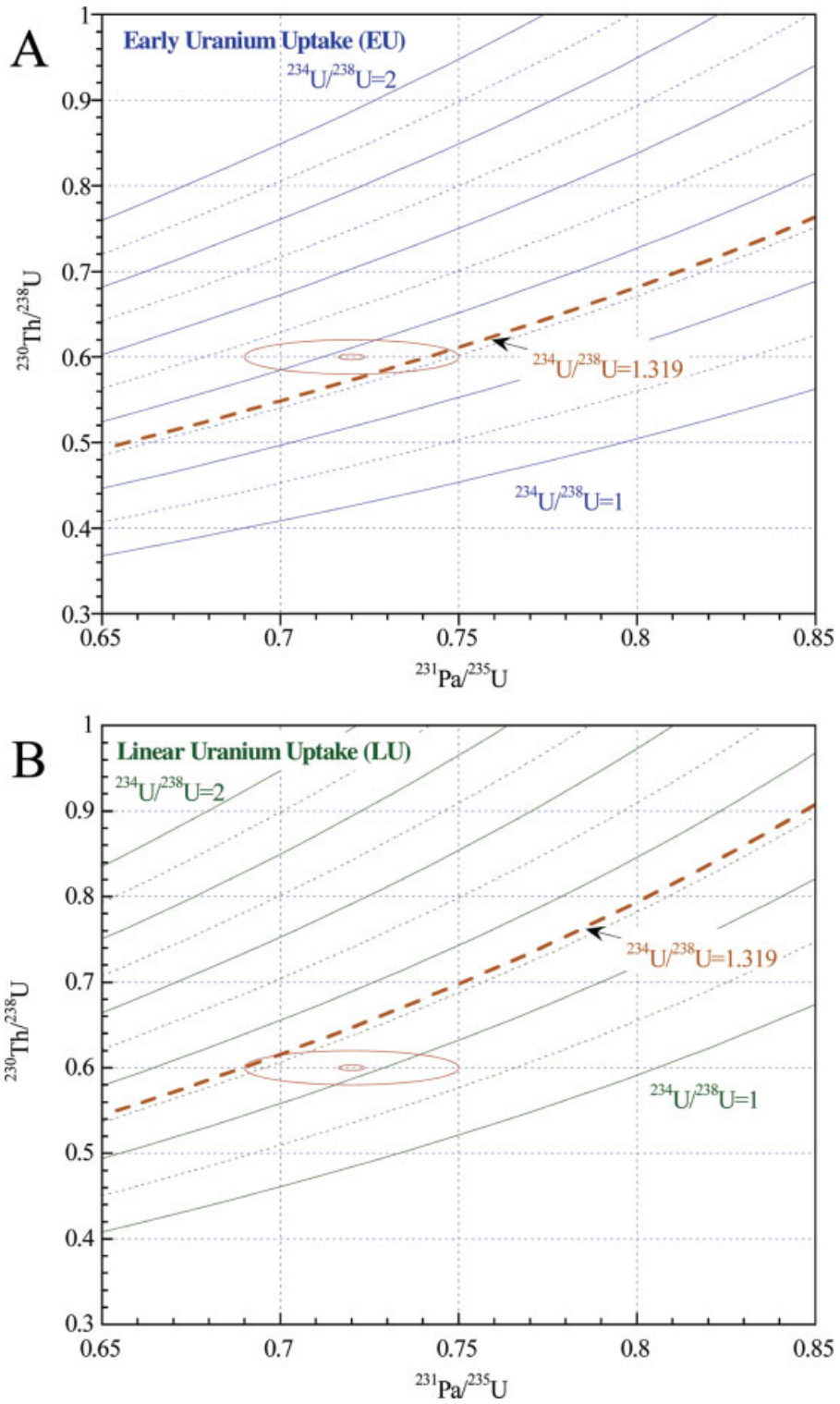

Fig. 11. Concordance diagrams for combined Th/U and Pa/U dating. **A**: Early U-uptake (p = −1, see Fig. 10); **B**: Linear U-uptake (p = 0, see Fig. 10). When the measured $^{230}Th/^{238}U$-$^{231}Pa/^{235}U$ data point lies on the evolution line of the measured $^{234}U/^{238}U$ ratio (dotted line), concordance is achieved. Concordance diagrams can be calculated for any p-value. The errors in the γ spectrometric measurement of the Mungo 3 skull (corrected for detrital ^{232}Th), outer error ellipse, do not allow the distinction between early and linear U-uptake. Typical TIMS errors (inner error ellipse) would allow detailed open system modeling (data from Thorne et al., 1999). [Color figure can be viewed in the online issue, which is available at www.interscience.wiley.com.]

and Titterington (1994) and Ludwig (2003) described the details of the error propagation for U-series age estimations. The Isoplot program (Ludwig, 2001), which can be obtained directly from Kenneth Ludwig (kludwig@bgc.org), offers comprehensive routines for error calculation of U-series analyses. Close to equilibrium, Monte-Carlo strategies are preferred for error calculations.

The main error source for U-series dating of bones lies in the mobility of uranium. Error calculation for open system modeling is not well established, Monte Carlo strategies seem most appropriate for these complex systems. The particular case of linear U-uptake was discussed by Bischoff et al. (1995).

ESR DATING

Electron spin resonance (ESR) is one of several trapped charge dating methods, which are based on the time de-

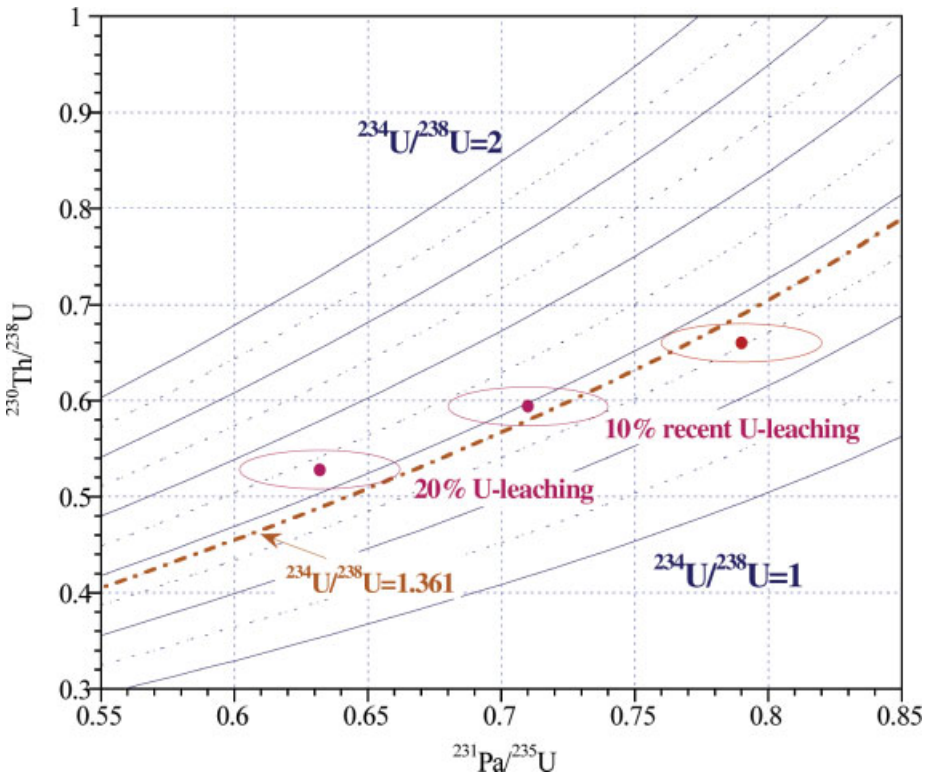

Fig. 12. Concordance diagram for combined Th/U and Pa/U dating for a sample showing leaching (data from the Mungo 3 skull, not corrected for detrital ^{232}Th). If the measured ^{231}Pa/^{235}U ratios are larger than the corresponding Th/U activity ratios in the EU (i.e, closed system) concordance diagram, U-leaching is indicated. Recent U-leaching can be modeled as shown in the diagram (data from Thorne et al., 1999). The ellipses indicate the analytical 1-σ errors. [Color figure can be viewed in the online issue, which is available at www.interscience.wiley.com.]

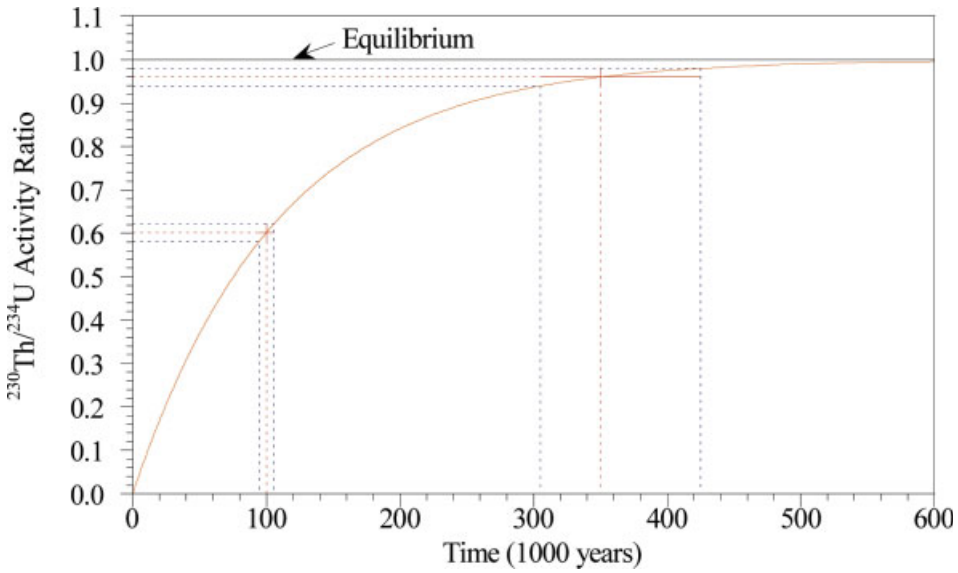

Fig. 13. Errors in U-series dating (dotted lines: mean value and error range). Time evolution of the ^{230}Th/^{234}U ratio is exponential, the symmetrical errors in the measurement of the ^{230}Th/^{234}U ratio leads to asymmetrical age errors, which become larger the closer the measured ^{230}Th/^{234}U ratio approximates equilibrium (both ^{230}Th/^{234}U ratios have the same absolute errors). [Color figure can be viewed in the online issue, which is available at www.interscience.wiley.com.]

pendent accumulation of electrons and holes in the crystal lattice of certain common minerals (e.g. quartz, feldspar, zircon, apatite). In that way, the minerals act as natural dosimeters. The methods differ by the instrumentation and physical processes that are used for the measurement of the trapped charge, and besides ESR comprise of thermoluminescence (TL, see e.g. Aitken, 1985; Mercier et al., 1995a; Prescott and Robertson, 1997), optically stimulated luminescence (OSL, Roberts, 1997; Aitken, 1998) and radioluminescence (RL, Krbetschek et al., 2000). However, only ESR can be applied to bones and teeth, hence to human material. ESR applications in earth sciences were comprehensively reviewed in the book of Ikeya (1993) and ESR dating applications in archaeology and paleoanthropology by Grün, 1997, 2000a, b, 2001), Grün and Stringer (1991) and Rink (1997).

Basic principles

Insulating minerals (such as the mineral phase of tooth enamel, hydroxyapatite) have two energy levels at which electrons may occur: the ground state (valence band) and a higher energy state, the conduction band (see Fig. 14). Electrons are not stable in the forbidden energy zone, which separates these two energy bands. Naturally occurring radioactive isotopes emit a variety of rays, which ion-

ize atoms. Negatively charged electrons are removed from the atoms in the valence band and transferred to the conduction band, positively charged holes remain near the valence band. After a short time of diffusion, most electrons will recombine with holes, returning the mineral back to its original, electrically neutral state. All natural minerals contain defect sites (e.g. lattice defects, interstitial atoms etc.), at which electrons and holes can be trapped. The traps are characterized by the activation energy, which is the energy difference between the conduction band and the trap. The trapped electrons and holes form paramagnetic centers, which can be detected with an ESR spectrometer giving rise to a characteristic ESR signal. Alternatively, ionizing radiation can also split the bonds of molecules resulting in the formation of free radicals (e.g. $CO_3^- \rightarrow CO_2^- + O$), which behave like paramagnetic centers. The latter scheme is the one commonly observed in tooth enamel (Fig. 15).

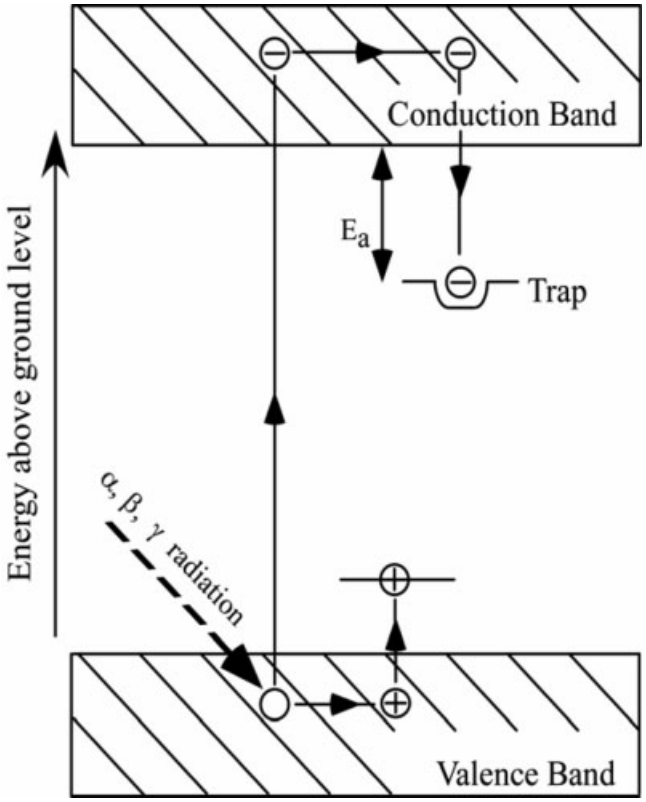

Fig. 14. The basis for ESR dating: trapping of electrons and holes. E_a = activation energy or trap depth (from Grün, in press).

When teeth are formed, the ESR signal is zero. Natural radiation generates new free radicals, trapped electrons and holes. The corresponding ESR signal intensity will increase, until the sample is measured in the laboratory. The signal of the sample is called natural intensity (see Fig. 16), which is dependent on the number of traps, the strength of the radioactivity (dose rate, D) and time. The product of dose rate and time is the dose, D_e, that the sample was exposed to in the past. An age, T, is derived from the simple relationship:

$$D_e = \int_0^T D(t)\mathrm{d}t \qquad (1)$$

If the dose rate is constant, this equation is reduced to: $T = \frac{D_e}{D}$.

The determination of the D_e value is the actual ESR part of the dating procedure. The dose rate is calculated from the analysis of the radioactive elements (mainly Th, U, and K) in the sample and its surroundings. The concentrations of the radioactive elements are converted into dose rates by published tables (see Table 1, below). The determination of the radioactivity that influences the sample is rather complex and has to be carefully evaluated (see Fig. 20, below).

ESR measurement

ESR intensities are measured with off-the-shelf ESR spectrometers (manufactured e.g. by Bruker, JEOL, Varian etc.). An ESR spectrometer has three basic components: a strong electromagnet, a microwave generator (Gunn diode or klystron), and an electronic processing unit. The sample is measured in a cavity, which is connected to the microwave generator by waveguides and

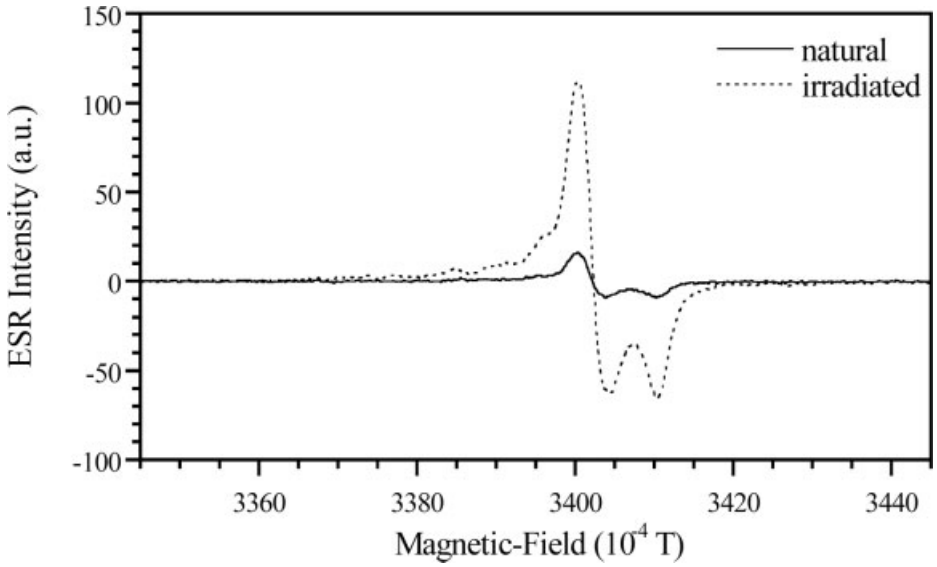

Fig. 15. ESR spectra of tooth enamel (from Grün, in press). The spectrum is dominated by a CO_2^- radical (Callens et al., 1987). The intensity of the ESR signal is often measured from the top of the peak to the base of the second dip, but there are numerous other ways to estimate the intensity of an ESR spectrum (see Grün, 2002).

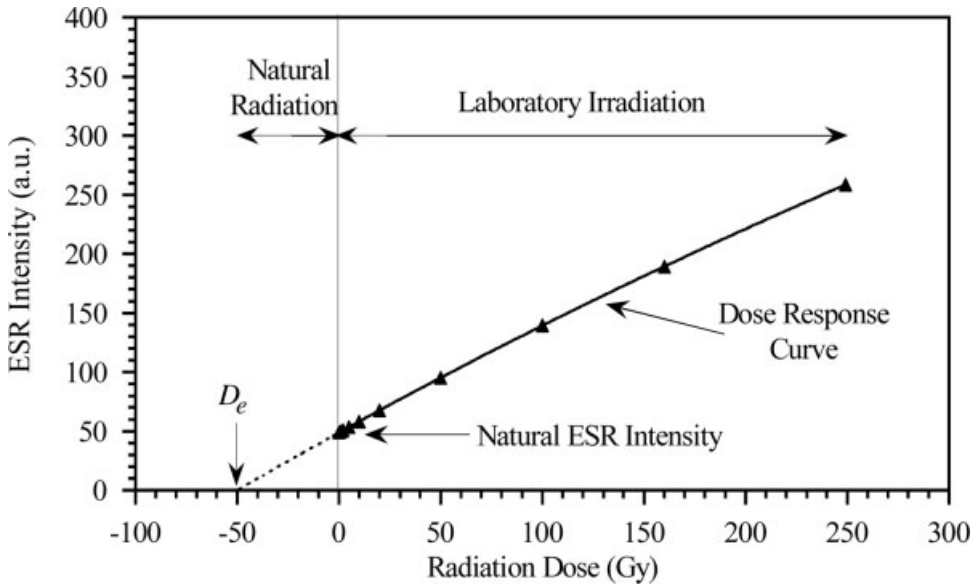

Fig. 16. Dose (D_e) determination using the additive dose method: after measurement of the natural intensity, the sample is irradiated in the laboratory. This leads to the production of more paramagnetic centers (see Fig. 14). Consequently, the signal intensity increases, as determined from the enhanced ESR spectrum (see Fig. 15). The plot of ESR intensity vs. laboratory dose is called the dose response curve. The D_e value results from fitting the data points of the dose response with an exponential function and extrapolation to zero ESR intensity.

TABLE 1. Dose rates for the U and Th decay chains and K (Adamiec and Aitken, 1998)

	$\dot{D}_\alpha$	$\dot{D}_\beta$	$\dot{D}_\gamma$ (μGy/a)
1 ppm $^{238}U + ^{235}U$	2780	146	113
1 ppm ^{232}Th	732	27	48
1% K		782	243

located between the pole shoes of the magnet. The paramagnetic centers have permanent magnetic moments, which are generated by the rotation (spin) of unpaired electrons, specifically by their negative charge (the magnetic moments of paired electrons cancel each other). In an external magnetic field, this magnetic moment can assume two energy states: a ground state, when orientated into the direction of the magnetic field, and an excited state, when orientated into the opposite direction. The transfer of the magnetic moment from the lower to the higher energy level can be induced by absorption of electromagnetic waves with a discrete frequency. The amount of absorbed microwave energy is directly proportional to the number of paramagnetic centers, and, in the end, to the age of the sample. Because the physical dimensions of the waveguide and the cavity are critically dependent on the microwave frequency, the magnetic field is varied linearly for an ESR measurement.

Note that the ESR measurements for dating do not require the determination of the absolute numbers of paramagnetic centers, only relative concentrations (=ESR signal intensities) are needed for the establishment of the dose response curve (see Fig. 16, below). Most modern ESR spectrometers are stable enough that neither internal nor external standards are required.

Measurement of the dose value, D_e

To provide reliable results, the measured ESR signal must have the following properties:

- The initial signal (at $t = 0$) is either zero or can be experimentally determined.
- The signal intensity grows proportionally to the dose received.
- The signals must have a stability, which is at least one order of magnitude higher than the age of the sample.
- The number of traps is constant. Recrystallization, crystal growth or phase transitions must not have occurred.
- The signals should not show anomalous fading.
- The signals are not influenced by sample preparation (grinding, exposure to laboratory light, etc.).

Large systematic errors may arise should any of these points not be fulfilled and the effects not be identified.

The term *equivalent dose* stems from the fact that the laboratory procedures utilize monoenergetic β or γ sources, whereas the dose the sample has received in the past is the sum of multienergetic α, β, γ, and cosmic rays (see below). Thus, the experimentally determined dose value is the β or γ equivalent of the naturally received dose.

For the measurement of D_e, a powdered sample is irradiated in the laboratory to develop a calibration curve of signal intensity versus applied dose for each sample. This plot (dose response curve) is used to extrapolate to zero ESR intensity, which yields the D_e value from the intercept with the *X*-axis (Fig. 16). The dose response curve is not linear (e.g. Grün, 1996), but most often described by a single saturating function (e.g. Brumby, 1992).

D_e estimation on human material

When working on human teeth, it is of course not feasible to work on enamel powder. Grün (1995) suggested to measure fragments instead. These fragments can be reinserted into the original tooth after measurement (see Fig. 17). For the extraction of a tooth enamel fragment, breakage is preferred over cutting because the latter procedure would lead to a loss of material caused by the cut with a diamond blade (around 100 μm). The tooth enamel of many archaeological teeth has developed cracks, at which enamel pieces separate easily (see Fig. 17C). After reinsertion of the measured enamel piece, the teeth look virtually undamaged (Fig. 17D). Some important specimens do not show any natural breaks (e.g. Tabun C2), here it is not possible to extract a sample for ESR measurement.

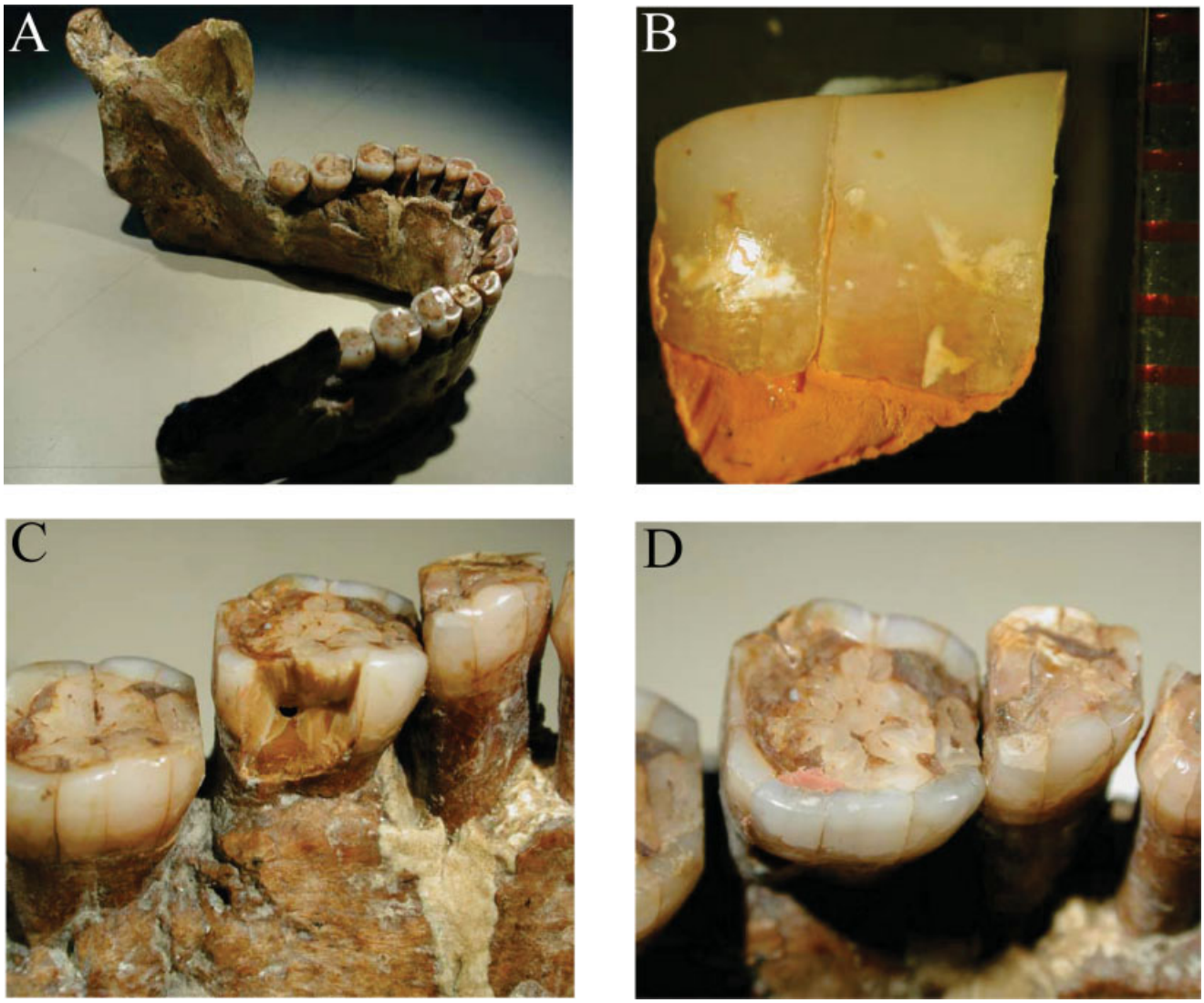

Fig. 17. Removal of a enamel fragment from Tabun C1. **A**: The Tabun C1 mandible. **B**: The fragment removed. **C**: Nearly all teeth in the mandible have cracks along which the enamel separates. Breakage, rather than cutting, has the advantage that no enamel material is lost. **D**: Test refitting of the enamel piece. The tooth appears virtually undamaged (photos kindly provided by C. Stringer, Natural History Museum, London). [Color figure can be viewed in the online issue, which is available at www.interscience.wiley.com.]

The ESR spectra of tooth enamel, which are dominated by the CO_2^- radical (Callens et al., 1987; Vanhaelewyn et al., 2000), are anisotropic. This means, that the shape of the ESR signal depends on the orientation of the tooth enamel fragment in the magnetic field (see Fig. 18). After removal of a fragment from a human tooth (see Fig. 17), it is mounted in a programmable goniometer, which rotates the sample in a horizontal plane. The ESR measurement is then carried out in 10° steps. Figure 19 shows the full breadth of ESR spectra as a function of angle for two orientations of the enamel fragment in the ESR spectrometer. In Figure 19A,C, the dentine/enamel surface is parallel and perpendicular to the rotational plane, respectively. When all spectra are merged, this results in a powder-spectrum, as one can expect from basic physics. A serious problem arises from the observation that the calculated dose values also show angular dependencies (Fig. 19B,D). This is due to the fact that the ESR spectra of the natural sample are qualitatively different to the portion of the ESR intensity that is added to the natural sample through the laboratory irradiation process. Whilst the natural spectrum is dominated by orientated CO_2^- radicals, the laboratory irradiation adds a mix of orientated and nonorientated CO_2^- radicals (Callens et al., 1995, 2002; Brik et al., 1998; Vanhaelewyn et al., 2002; Grün, in preparation). The dose estimations show angular dependencies (Fig. 19B,D), because the natural sample mainly contains oriented CO_2^- radicals whereas laboratory irradiation generates additional nonorientated CO_2^- radicals in the sample. The contribution of the latter radicals to the total signal is angle independent whereas the contribution of the orientated CO_2^- radicals is angular dependent. The net result is that the relative signal intensities of the irradiated samples show an angular variation with respect to the natural sample. A relatively small contribution of the angular CO_2^- radi-

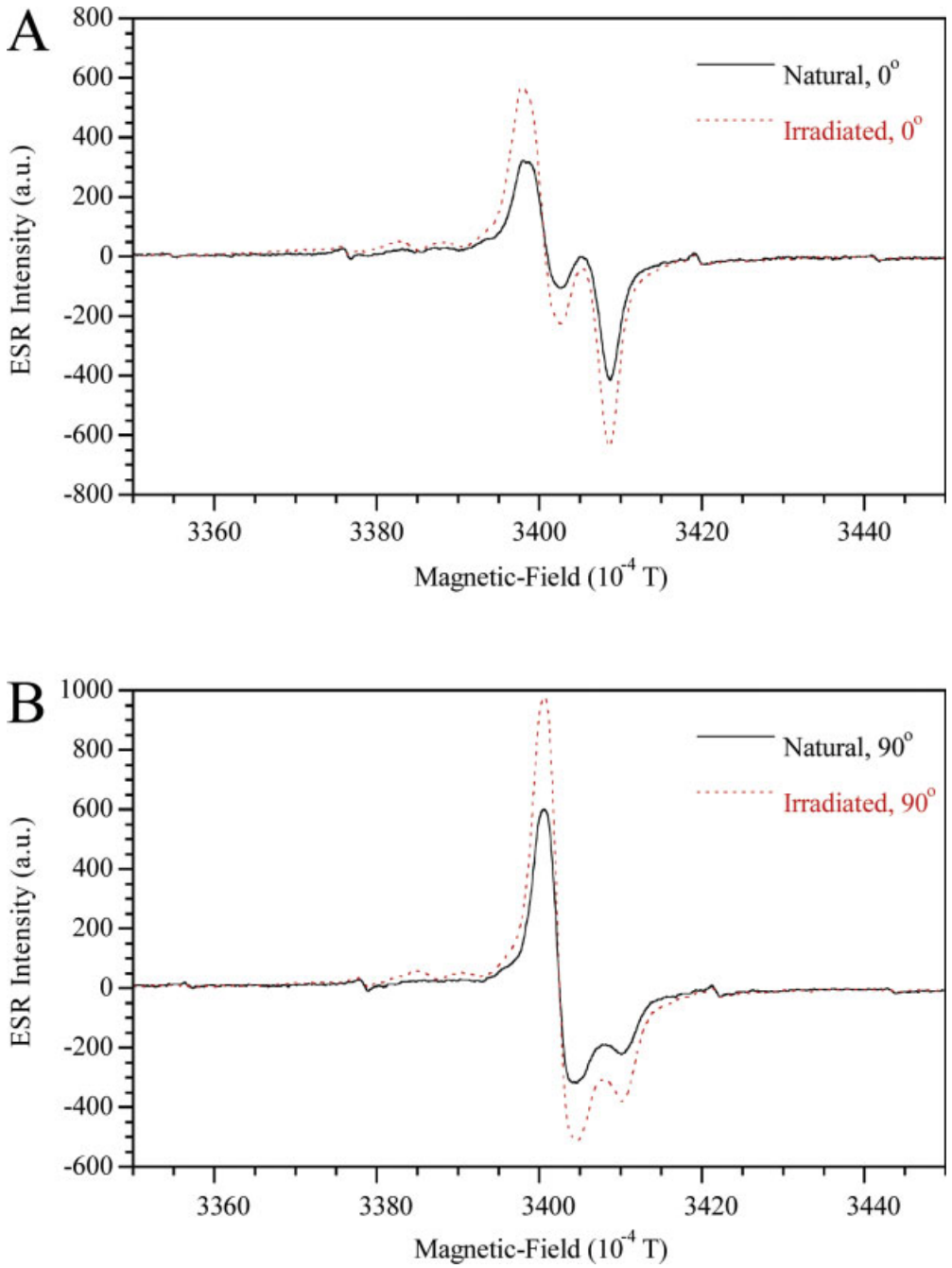

Fig. 18. ESR spectra of enamel fragments with different orientation in the magnetic field. The components of the ESR spectrum split up (compare to powder spectrum in Fig. 15). [Color figure can be viewed in the online issue, which is available at www.interscience.wiley.com.]

cal to the total signal results in relatively small dose values (e.g., around 50° and 230° in Fig. 19C,D), larger contributions in higher dose values (e.g., around 110° and 280° in Fig. 19C,D).

With time, some of the nonorientated CO_2^- radicals will turn into the orientated species (Brik et al., 2000). The occurrence of the two radical species, and the conversion of the one into the other, may be the explanation for some fading that has been observed in some younger samples (Grün and Ward, 2002). The effect of the occurrence of the nonorientated CO_2^- radical on the reliability of D_e measurements has not yet been quantified. It should be noted that this effect is not observable in powder spectra, because the powder spectra of the two CO_2^- species are identical (Grün, 2006). Nevertheless, D_e results derived from powder spectra should contain a similar systematic, yet unresolved, uncertainty. Generally, one would expect that the dose values are underestimated, and that therefore the resulting ages are too young. However, it is not likely that this will cause large systematic errors, as independent age comparisons indicate only a small trend towards ESR age underestimation in the range of 5–10%,

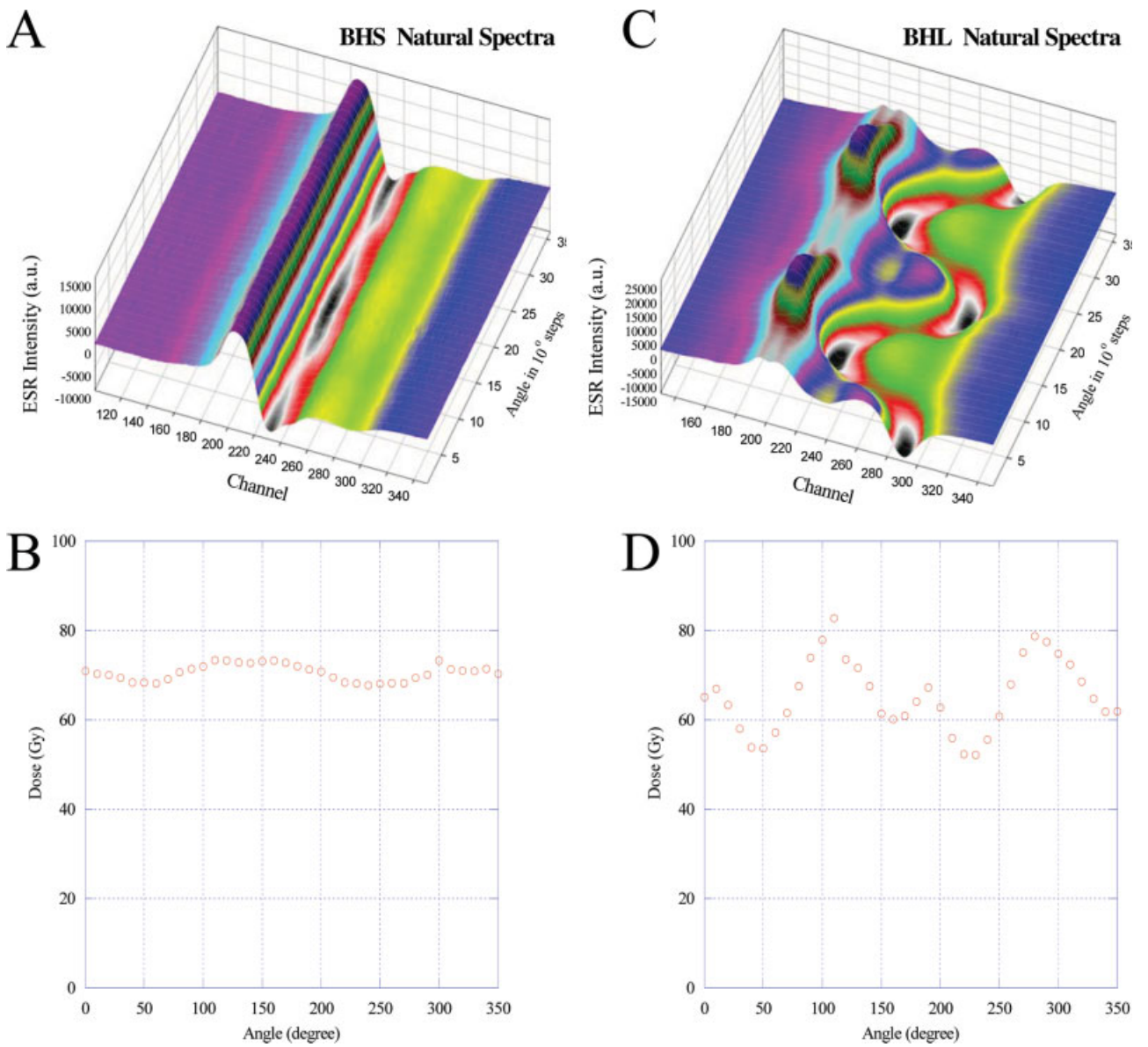

Fig. 19. ESR measurement of an enamel fragment rotated around different axes. ESR spectra of the natural sample are recorded in 10° steps and stacked. **A**: Rotation around the axis parallel to the enamel/dentine boundary. **B**: Dose estimation from spectra recorded in the configuration shown in diagram A. **C**: Rotation around the axis perpendicular to the vertical direction of the tooth (the spectra resulting of the rotation around the third major axis look the same as this diagram). **D**: Dose estimation from spectra recorded in the configuration shown in diagram C. [Color figure can be viewed in the online issue, which is available at www.interscience.wiley.com.]

as for example shown for Border Cave (Grün et al., 2003, see below).

The errors of the parameters describing the dose response curve can either be obtained by analytical expression (Brumby, 1992) or Monte Carlo simulation (Grün and Brumby, 1994).

Determination of the dose rate, $\dot{D}$

The dose rate is calculated from the concentrations of radioactive elements in the sample and its surroundings (only the U and Th decay chains and the ^{40}K-decay are of relevance; a minor contribution comes from ^{87}Rb in the sediment), plus a component of cosmic rays. There are three different ionizing rays, which are emitted from the radioactive elements (see Fig. 20):

- γ rays (photons) have a range of about 30 cm.
- βeta rays (electrons) have a range of about 2 mm.
- α rays (He nuclei: particles consisting of two protons and two neutrons) have only a very short range of about 20–40 μm, because of their large size they collide with many atoms in the crystal lattice, causing visible damage (α-tracks). α Particles are less efficient in producing ESR intensity than β and γ rays. Therefore, the α efficiency has to be determined, which is the ratio of the ESR intensity generated by a given α dose over the ESR intensity generated by an equivalent γ or β dose. α Efficiency values

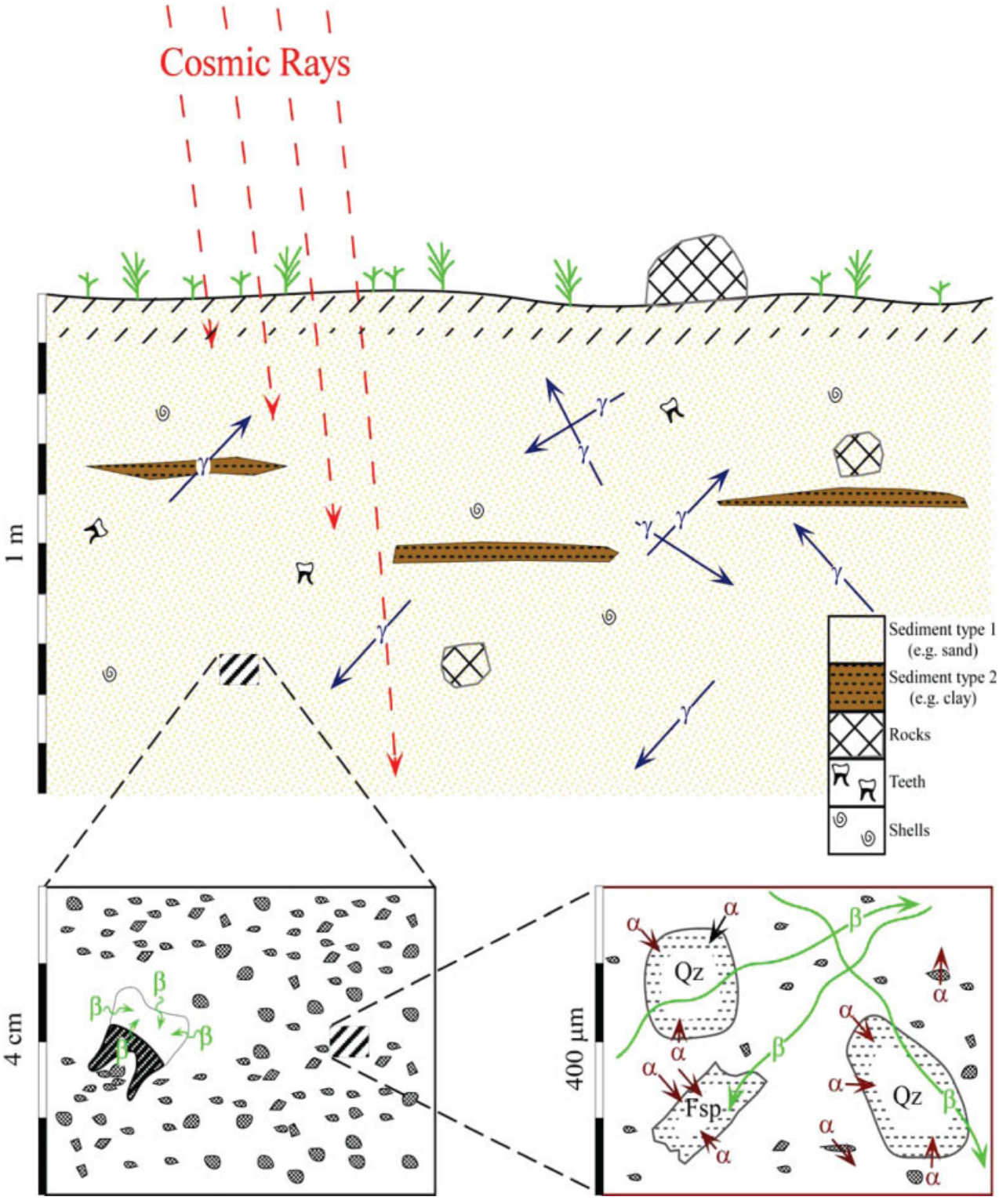

Fig. 20. Schematic representation of the different external components of natural radiation relevant for dose rate calculations (Qz = quartz, Fsp = feldspar). High energy cosmic rays are attenuated once they penetrate the sedimentary layers. For practical purposes, the cosmic ray dose rate becomes negligible at a depth of about 20 m. γ Rays have an average range of about 30 cm. β Rays have average ranges of a few mm. Smaller samples, such as teeth or shells, are completely penetrated by external β rays and the affected volume cannot be removed. α Rays have average ranges of a few tens of µm. In addition to the external dose rate sources, samples receive a portion of the internally generated α, β, and γ rays (from Grün, in press based on S. Stokes as shown in Aitken, 1998: Fig. 2.2). [Color figure can be viewed in the online issue, which is available at www.interscience.wiley.com.]

for tooth enamel are in the range of 0.13 ± 0.02 (Grün and Katzenberger-Apel, 1994).

The concentrations of radioactive elements within the sample are usually very different from its surroundings. Thus, *internal dose rates* and *external dose rates* have to be assessed independently. Furthermore, it is necessary to estimate the cosmic dose rate, which is about 300 μGy/a at sea-level and decreases with depth below ground. Is also dependent on altitude as well as geographic latitude (for more details, see Prescott and Hutton, 1988, 1994).

The conversion of the elemental analysis into dose rates are shown in Table 1. Dose rate calculations become more complicated, when disequilibrium in the U-decay chains or attenuation factors have to be considered (for details see Aitken, 1985, 1998; Grün, 1989).

Estimation of the external dose rate of tooth enamel

The calculation of the external dose rate is dependent on the size of the samples (Fig. 20). The removal of the outer 50 μm of the sample eliminates the volume that was affected by external α irradiation. This volume is routinely removed from the tooth enamel and not further considered. This, however, cannot be done when working on human teeth. It can be shown, however, that the external α contribution on the total dose rate is only a few percent (Grün, 1987). Human tooth enamel has thicknesses in the range of 0.8–1.2 mm, therefore it is not possible to remove the outer 2 mm for the elimination of the external β dose. Therefore, the enamel receives external β radiation, which decreases with depth. As a result, β attenuation factors have to be calculated (for more details see Brennan et al., 1997; Marsh, 1999). The external β dose rate has to be calculated separately from the external γ dose rate, because the β dose rate is generated from the sediment immediately attached to the sample, whereas the γ dose rate originates from all sediment that is within a radius of about 30 cm around the sample (see Fig. 20). The β dose rate from the sediment is derived from the chemical analysis of U, Th, and K and the evaluation of the water contents. Water absorbs some β and γ rays. Its presence in the surrounding sediment has to be considered in the calculation of the β and γ dose rates (Bowman, 1976; Aitken and Xie, 1990).

The γ dose rate can normally not be deduced from laboratory analyses, but has to be measured in situ with a portable, calibrated γ spectrometer or TL dosimeters. This is because most environments show an inhomogeneous distribution of radioactive elements, e.g. caused by layering of sediments (clays usually have a higher radioactivity than sands) or the occurrence of larger rocks (lumpy environment: Schwarcz, 1994). In situ measurements have the advantage of including the present-day water content of the surrounding sediment. A further complication arises if the teeth analyzed were buried in their original jaw. On the one hand, the bone material from a mandible or skull shields a tooth from the sediment dose rate, on the other hand, it provides some γ dose from its internal radioactive elements. This effect can be rather large, in the range of >10% of the total γ dose rate (see Nathan and Grün, 2003).

Many paleoanthropological sites have been completely excavated in the past and it is not possible to measure any external dose rates. In some cases it has been attempted to reconstruct the external γ dose rate from museum sediment samples (see discussion in Grün and Stringer, 2000). This process is usually associated with very large errors because the sediment samples may show a large spread in the concentrations of the radioactive isotopes. Furthermore, any effects of a lumpy environment cannot be addressed (i.e. the original sediments might have contained larger boulders and pebbles etc., which, of course, were not collected - see Schwarcz, 1994).

Estimation of the internal dose rate in tooth enamel

This parameter is mainly generated by α and β rays emitted from elements within the sample. In the tissues of teeth, the U-decay chains are in disequilibrium (see U-series dating methods, above). This affects the average dose rates and can be taken into account mathematically (Grün, 1989). The α efficiency is difficult to determine, because of size requirements for ESR measurements. The most commonly used value for tooth enamel is 0.13 ± 0.02 (Grün and Katzenberger-Apel, 1994), but note that Chen et al. (1994) measured a value of 0.223 ± 0.013.

Dose rate calculations for tooth enamel are further complicated by the fact that enamel and dentine accumulate uranium over time (see U-series section, above). The explicit history of the uranium uptake may have significant implications for the calculation of the average dose rate, and, thus the age of the sample. Conventionally, two uranium uptake models have been calculated: early U-uptake (EU) and linear U-uptake (LU), see also U-series section, above. For the EU model, it is assumed that all the uranium measured today was accumulated by the tooth within a short time after its burial. The linear U-uptake model (LU) predicts that the uranium has been accumulated continuously over time in a linear fashion (see U-uptake functions in Fig. 10). The differences in EU and LU age calculations are small as long as the U-concentrations in the samples are moderate. However, with increasing U-concentrations, the EU–LU age difference increases until the LU age is nearly twice the EU age. In the interpretation of ESR dating results it had generally been assumed that the correct age of a sample was bracketed by the EU and LU age calculations. It has been recognized since, however, that teeth from a considerable number of sites (perhaps in the region of 10–20%) may have U-uptake histories that lie outside the age range defined by the EU and LU models (see below). This may be due to U-leaching or strongly delayed U-uptake caused by changes in the hydrological environment of the samples. It should be emphasized that in these cases, in spite of the very large age range covered by the parametric EU and LU models for teeth containing considerable amounts of uranium, the age results may still be grossly erroneous. Furthermore, there is no first-principle argument that could possibly be used to prefer one model over the other.

To overcome the problem of the unknown U-uptake history, Grün et al. (1988) suggested the analysis of the ESR samples for U-series isotopes. Uranium series dating results are similarly influenced by U-uptake, but to a different extent than ESR (the LU U-series age is always nearly twice the EU age). For combining ESR and U-series dating results, Grün et al. (1988) introduced the p-value system (see Fig. 10 and associated text in the U-series section). The different constituents of teeth usually give somewhat different U-series isotope results. The measurements of U-series isotope data on the bulk tissues of a tooth are used for the establishment of the relationships between apparent U-series ages and p-values, start-

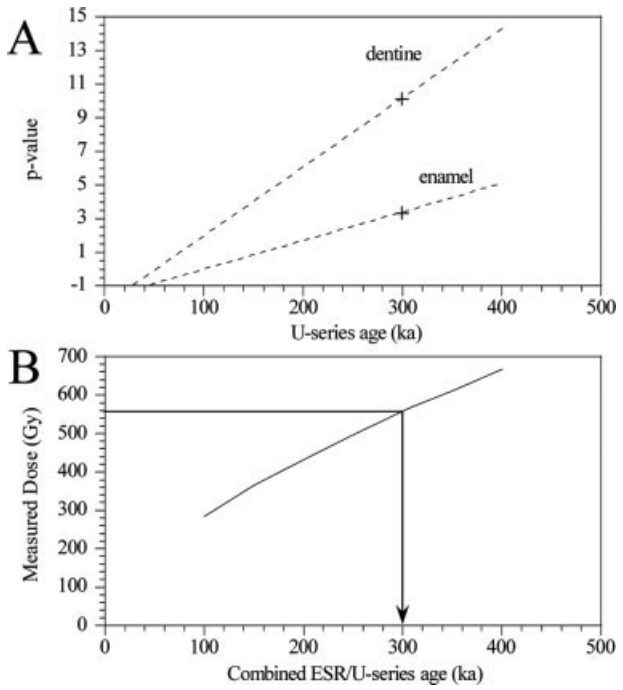

Fig. 21. Combination of U-series and ESR dating (from Grün et al., 1988) for sample 145, a tooth from Hoxne (see also Fig. 22). **A**: Apparent U-series ages are calculated from the measured isotopic ratios (i.e. $^{230}Th/^{234}U$ and $^{234}U/^{238}U$) and a p-value starting from $p = -1$ (for p-values, see Fig. 10). The crosses indicate the p-values for dentine and enamel that are obtained after the calculation of the U-series/ESR age (Fig. B). **B**: Using the relationship between p-values and apparent U-series age estimates (from Fig. A) in combination with all other dose rate parameters, doses are calculated for any given age. The projection of the measured D_e value onto this function yields the combines U-series/ESR (US-ESR) age of the sample. The p-values for the different constituencies of the tooth can be read from Figure A.

ing from the closed system ages (Fig. 21A). The p-value vs. age relationships for uranium in conjunction with all other dose rate parameters are then used to compute dose values for any given age (Fig. 21B). The projection of the measured D_e onto this function yields the combined U-series/ESR age. Returning the calculated age to the functions in Figure 21A yields the corresponding p-values. It is of course not possible to reconstruct the actual U-uptake, which may be episodical. To assess the influence of the model function on age calculation, Grün, 2000c introduced an alternative calculation for combined U-series/ESR dating. In the closed-system U-series/ESR (CSUS-ESR) model, it is assumed that all uranium migrates into the constituents of a tooth at a time corresponding to the closed system U-series age of that tissue. Figure 22B (below) shows the difference in the U-uptake model between the p-value and CSUS models for the constituents of two teeth from Hoxne. The CSUS-ESR model yields the oldest possible age that can be calculated from given U-series and ESR results, whereas p-value system calculations result in the youngest possible age. In most cases the difference between the p-value and CSUS calculations is in the order of a few percent. This indicates that combined ESR/U-series dating is not particularly sensitive on the explicit U-uptake history, as long as no leaching takes place.

It may be educational to return to the site of Hoxne. Using the analytical values of Grün et al. (1988), with the modifications outlined in Grün and Schwarcz (2000), one would obtain EU ages in the range of about 100–210 ka (164 ± 41 ka) and LU ages between 175 and 300 ka (245 ± 50 ka). The enormous age range covered by these two parametric models (100–300 ka!) would still underestimate the expected age of MIS 11, around 370–415 ka (Bassinot et al., 1994). The p-value calculations returned an age of 404^{+33}_{-44} ka and the CSUS-ESR 437 ± 38 ka (here, the model dependency is about 8%, the largest observed so far). Both results agree within error with the expected age range (see Fig. 22A; Grün and Schwarcz, 2000). Figure 22B shows the differences in the uptake functions behind the p-value and CSUS-ESR calculations.

Measurement of radioactive elements and isotopes

A wide range of analytical techniques can be used for the analysis of radioactive elements. In the field, the external γ dose rate can be measured with thermoluminescence dosimeters or a γ spectrometer. Elemental concentrations can be measured with X-ray fluorescence, ICP-MS, neutron activation analysis etc. Uranium and thorium concentrations of the teeth, as well as U-series isotopes can be measured in situ by laser ablation multicollector ICP-MS (Eggins et al., 2005, see above). Where the U-concentrations are too low for the in situ analysis of ^{234}U and ^{230}Th ($U < 0.5$ ppm), their contribution to the total dose rate is usually so small that the uncertainties in the reconstruction of the U-uptake are of minor concern.

Errors in ESR age estimations

The evaluation of random errors is straight-forward. The error in the D_e estimation is usually within 1–5%. Thus far, the systematic error caused by the nonorientated CO_2^- radical has not been assessed. The typical precision of dose rate assessments is in the range of 5–7%. Some systematic errors are introduced by assumptions. These occur because not all parameters are measured or can be measured. For example, the water contents of the sediments might have changed over time, some sediments might have had some radioactive disequilibrium in the U-decay chain (e.g., by Ra-mobilization, Rn-emission, for examples see Prescott and Hutton, 1995; Grün et al., 2006), the α efficiency in ESR is difficult to measure and is based on the analysis of a few samples (Chen et al., 1994; Grün and Katzenberger-Apel, 1994), radioactive disequilibrium within the samples and surrounding sediments are rarely measured, etc.

Although error calculation should be straight-forward, and has been outlined in detail by Aitken (1985: his Appendix B), most publications mix the random and systematic errors and treat them equally. Note that nearly all ESR age estimations are given with 1-σ errors.

If the external dose rate is reconstructed from museum sediment samples, it is usually associated with very large errors (>20%, see above). If the teeth contain significant amounts of uranium, the errors introduced by an unknown U-uptake history may be as high as 50%, if the assumption is made that the EU and LU models bracket the true ages of the samples. If all dose rate parameters can be measured, including U-series isotopes, the 1-σ errors (precision) of ESR ages on teeth are in the range of 5–9%, systematic calibration errors may be as high as 5%.

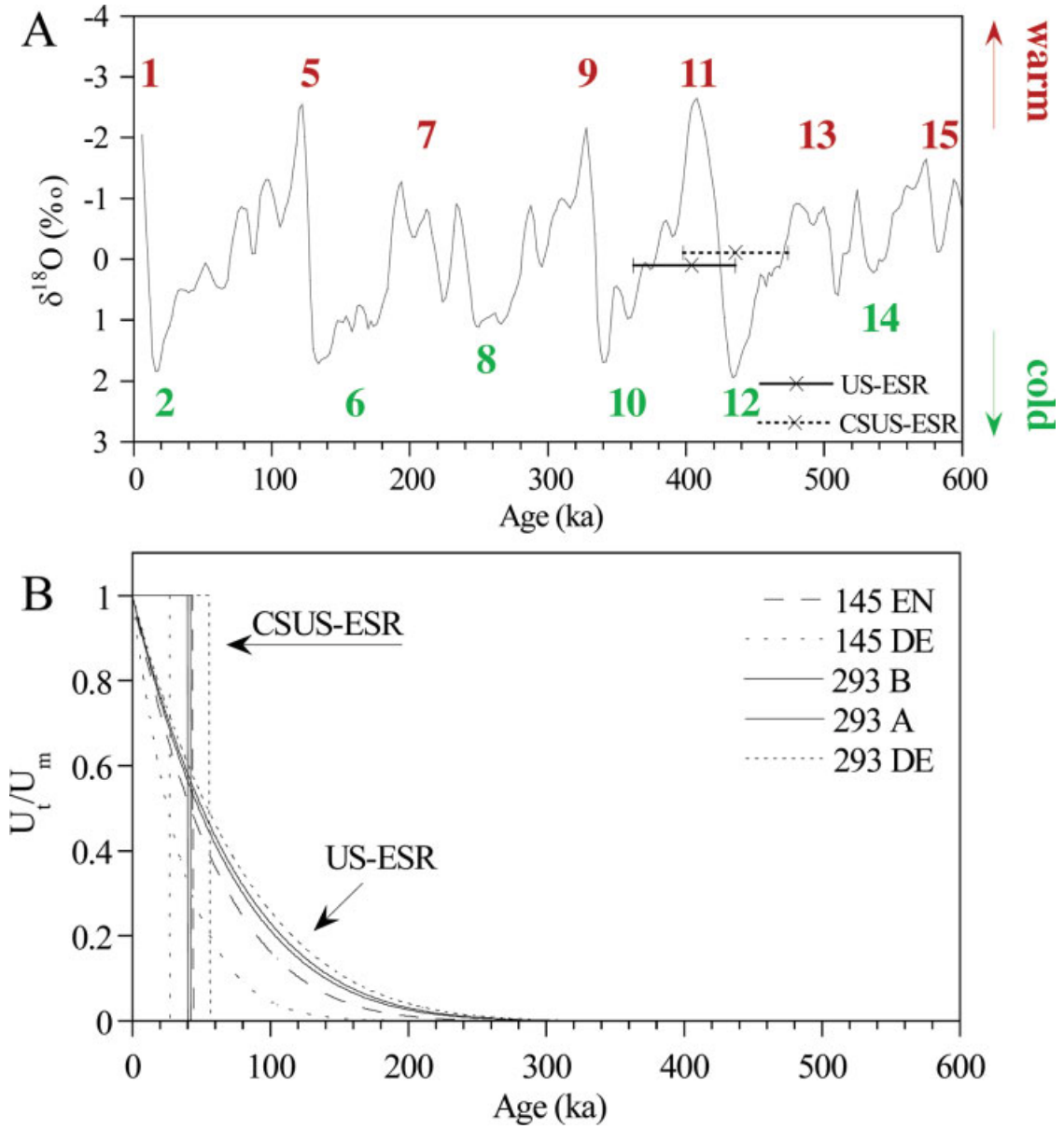

Fig. 22. Dating results for the site of Hoxne. The CSUS-age estimates present the maximum possible age that can be calculated with given ESR and U-series data while the US-ESR yields the minimum age. It is thus possible to check the model sensitivity of combined U-series/ESR dating. The lower diagram shows functions of the U-uptake histories used for the calculation of the US/ESR and CSUS/ESR open system age estimates (from Grün and Schwarcz, 2000). [Color figure can be viewed in the online issue, which is available at www.interscience.wiley.com.]

Because of the considerable amount of uncertainties outlined above, the uninitiated reader might already have come to the conclusion that ESR could be regarded as analytical extravagance with little chronological virtue. A discussion of the ESR results obtained from a series of samples from Border Cave (see below) might serve at least as temporary remedy.

AAR DATING

Nearly all applications of amino acid racemization (AAR) dating on bones and teeth have not been very successful (see below). Nevertheless, this application is covered here not only for the sake of completeness, but also because some new applications on dentine recovered from teeth found in caves seem to have yielded promising results. It could therefore be expected that in the near future, AAR may experience a renaissance in its application on human bones.

Reviews on various aspects of AAR dating were published by Hare et al. (1980, 1997), Miller and Brigham-Grette (1989), Rutter and Blackwell (1996), Wehmiller and Miller (2000). Johnson and Miller (1997) reviewed the archaeological applications of AAR analysis.

Basic principles

AAR dating is a chemical dating technique. Amino acids consist of four basic building blocks attached to a central carbon atom: a carboxylic acid group (COOH), an amino

group (NH_2), a hydrogen atom, and a radical group (e.g. CH_3O for serine, $C_2H_3O_2$ for aspartic acid etc., see Hare, 1969). Amino acids occur in two chiral forms (not superposable on its mirror image), similar in symmetry to the left and right hands. Amino acids are optically active, the L-type (lævorotatory) turns a plane of polarized light to the left, the D-type (dextrorotatory) to the right. L- and D-amino acids are informally called "left-handed" and "right handed", respectively. Nearly all living organisms exclusively produce L-amino acids. After death, L-amino acids convert into the D-type by a process called racemization. For some amino acids, racemization takes place over geological times, their D/L ratio can be used for dating, until equilibrium is achieved (usually D/L $\sim$ 1). AAR dating may be applicable to samples as old as one million years (Murray-Wallace et al., 2001).

Figure 23 shows the two most commonly used reactions for geochronological purposes, the racemization of L to D-aspartic acid and the epimerization of L-isoleucine to D-alloisoleucine, a nonprotein. Racemization involves at least one intermediate step (see Fig. 23A). The hydrogen atom can be removed forming a negatively charged carbon anion. The hydrogen atom has subsequently two possible locations to which it can be reattached. If it attaches at the opposite location, D-aspartic acid is formed. L-isoleucine can convert into D-isoleucine by racemization (both chiral groups are mirrored) and into D-alloisoleucine by epimerization (only one of the central chiral groups is mirrored; Fig. 23B). In general, the conversion rates of L to D and D to L for most racemization reactions are equal. However, this does not apply for the epimerization of isoleucine to alloisoleucine, resulting in equilibrium A/I (alloisoleucine/isoleucine) ratios of about 1.3 (see Hare et al., 1997). Like all chemical reactions, the racemization rate is strongly temperature dependent. The geological reaction rates can be deduced from high temperature heating experiments (e.g. Miller et al., 2001). Figure 24 shows the general effect of the time/temperature dependence of the racemization reaction in a geological sample. If the storage temperature is known, D/L ratios can be used for age estimation. Because of the logarithmic relationship between the D/L ratio and time, the D/L ratio changes rapidly in young samples and more slowly in older ones. This means that the resolution of AAR, assuming more or less constant analytical errors, diminishes with the age of the samples. On the other hand, if the ages of samples are independently known, AAR values can be used for the reconstruction of average storage temperatures of a certain area, i.e. its climatic history (see, for example, the reconstruction of glacial cooling in the southern hemisphere: Miller et al., 1997b).

Measurement

The amino acids are quantitatively measured with a range of chromatographical methods (see Wehmiller and Miller, 2000), such an ion-exchange high-pressure liquid chromatography, gas chromatography (e.g. Engel and Hare, 1985; Murray-Wallace, 1993), and more recently, reversed phase liquid chromatography (Kaufman and Manley, 1998). Each method has specific advantages and disadvantages in sample preparation and measurement resolution, which are discussed in detail by Wehmiller and Miller (2000). All methods have in common that they are fast and relatively inexpensive. This allows the analysis of a large number of samples within a reasonably short time.

Calibration

If all kinetic parameters were known, AAR could be used as an independent numerical dating technique. However, an additional problem arises by the fact that the temperature at a given locality may have changed dramatically during the Quaternary. To address this problem, calibration points are obtained by dating samples with independent geochronological methods, such as radiocarbon or U-series. The D/L ratio of the sample and the independent age estimate are used to fit a certain kinetic model (see Fig. 24), which is usually derived from heating experiments (see above). To minimize the effects of an unknown temperature history, calibration points are obtained for different geological ages (see e.g. Miller et al., 1997a). It has to be noted that the calibration curves a) are model dependent, b) apply only to one species, and c) are restricted to limited geographical areas with closely similar temperature histories. For the dating or correlation of samples of unknown age, it is usually assumed that these experienced the same thermal history as the calibration samples.

Errors

Figure 25 summarizes the principles of error calculation for amino acid age estimations (from Wehmiller and Miller, 2000). It is assumed that a sample with a D/L ratio of 0.3 and an independent age of 125 ka was used as calibration point, a parabolic kinetic function was fitted to the calibration point and a temperature uncertainty of 1.5°C has been assigned to the average storage temperature. A measured D/L ratio of 0.5 would result in a mean age of 350 ka, a typical measurement uncertainty of 5% would result in an age error of $\pm$40 ka. The error from the temperature envelope results in age error of about $\pm$60 ka (the error is slightly asymmetrical). The overall error would be in the 90 ka range. The correct error may be significantly larger, because of uncertainties in the measurement of the D/L ratio of the calibration point, its independent age estimate and the application of equally likely, alternative kinetic models. Because of the large uncertainties caused by extrapolations, it is usually advisable to produce several calibration points with different ages. This allows age interpolations, which are usually associated with significantly smaller errors.

AAR dating of bones

During the 1970s, a large number of papers were published reporting amino acid dating results on bones using either isoleucine or aspartic acid. Rutter and Blackwell (1996) provided a comprehensive compilation of these AAR data, including a large variety of age estimates on human remains, e.g. from Border Cave, Swartklip, and Eyasi and those of the paleoindians from Laguna, Del Mar, San Jacinto, and Sunnyvale (Bada et al., 1974; Bada and Helfman, 1975; Masters and Bada, 1978). Particularly, the results from the paleoindian samples with ages of up to 70 ka caused some controversy (e.g. Bender, 1974), perhaps because other, independent dating methods yielded significantly younger ages for these samples (see Bischoff and Rosenbauer, 1981, 1982; Bada and Finkel, 1982; Taylor, 1983; Taylor et al., 1983, 1985; Stafford et al., 1984, 1990). Bada (1985) attributed the amino acid age-overestimations to an unreliable radiocarbon age estimation on the calibration sample as well as bone diagenesis.

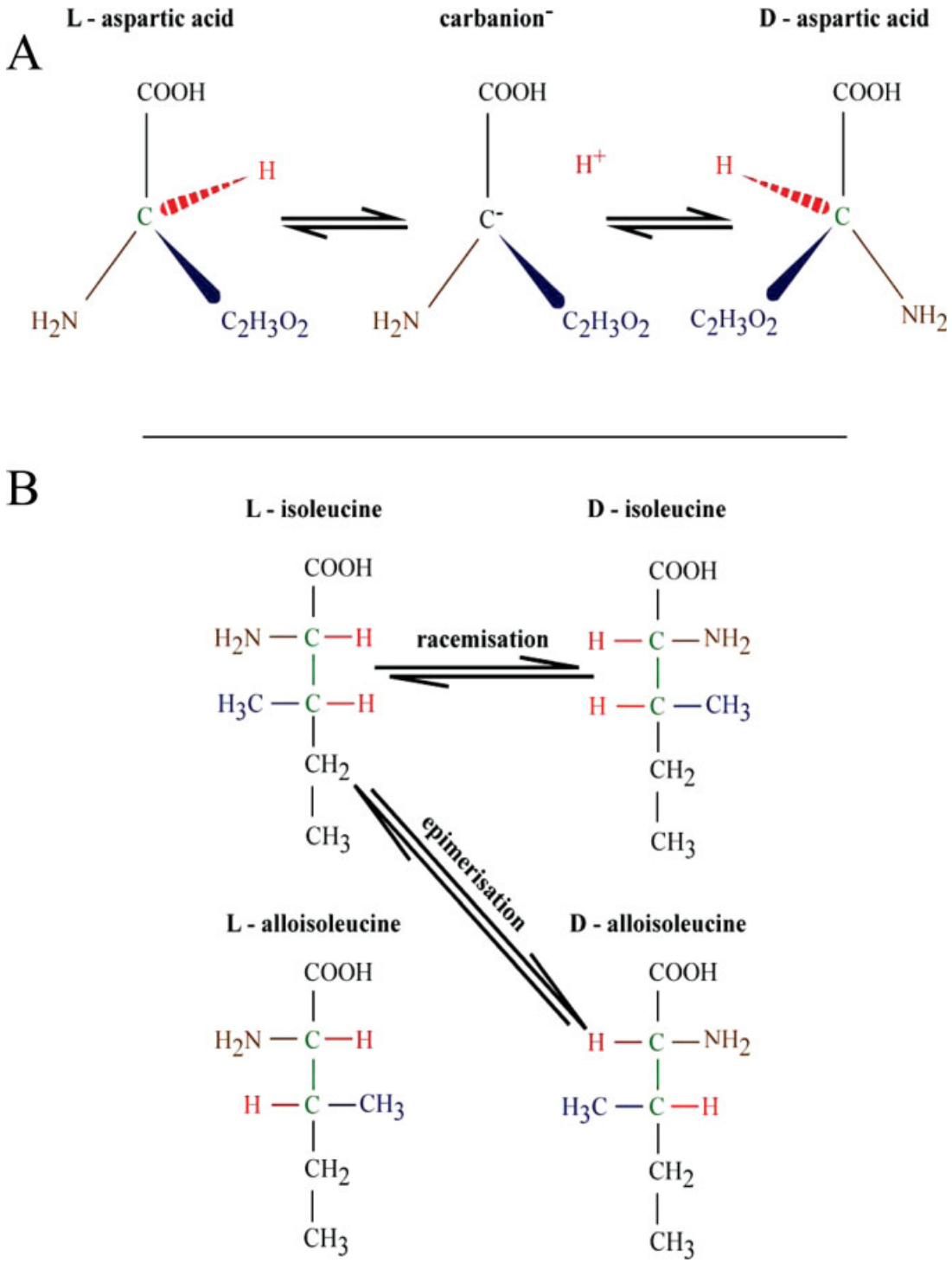

Fig. 23. Racemization and epimerization of the two most commonly used amino acids in geochronology. **A**: Aspartic acid changes from the L- into the D-configuration involving an intermediate step, where the hydrogen atom is removed. This results in the formation of a carbon anion (carbanion). The hydrogen atom can be reattached at its original position, or on the opposite side, then D-aspartic acid is formed. In equilibrium, the solution will contain an equal mixture of L and D forms. The solid lines present bonds lying in the plane of the figure, blue triangles connect groups projected forward and the red dashed triangle groups projected behind the paper plane (after Hare et al., 1997). **B**: L-isoleucine racemization (both the two central carbon configurations are mirrored) and epimerization (only one of the central carbon configurations is mirrored). The rates for the two directional epimerization reactions are different, therefore the solution will equilibrate at an A/I (alloisoleucine/isoleucine) ratio of about 1.3 (after Miller and Brigham-Grette, 1989). [Color figure can be viewed in the online issue, which is available at www.interscience.wiley.com.]

Hare et al. (1997) discussed why AAR ages of bones were notoriously unreliable and could deviate from independent age estimations by up to an order of magnitude. This has been attributed to the porosity of bones, allowing for a number of interfering chemical processes to take place, such as leaching, algal, and bacterial contamination, precipitation of secondary minerals, variable geochemical conditions in the surrounding matrix, inhomogeneity of D/L ratios in different bones from the same skeleton etc. In the end, it seems that Bada et al. (1999) agreed with this judgement.

Nevertheless, some newer studies on cave bear teeth seem to imply that the D/L ratios from the dentine of cave bears can be used for geochronological purposes (Torres et al., 1999, 2002). This may be due to the fact that samples from caves have experienced less temperature and humidity changes than those in open air sites. Preliminary results on a human tooth from Sidron yielded agreeing age estimates for radiocarbon, ESR, and AAR (Torres, unpublished data).

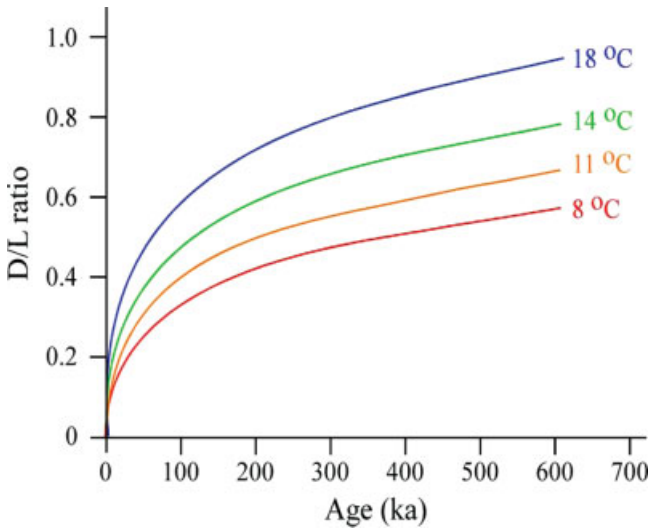

Fig. 24. Age and temperature dependency of D/L ratios. At constant temperatures the D/L ratio is solely a function of time. On the other hand, if the age of the sample is known, the D/L ratio can be used for estimating the average storage temperatures (after Wehmiller and Miller, 2000). [Color figure can be viewed in the online issue, which is available at www.interscience.wiley.com.]

APPLICATIONS

Rather than giving a comprehensive review of all applications of dating techniques to human remains, I focus on a few examples to give insights not only the present state-of-the-art but also the state-of-the-problems.

One of the central questions in paleoanthropology at large, is the chronology of the evolution of modern humans. A hotly debated sub-set is the transition from Neanderthals to modern humans in Europe. The discussion is certainly not helped by the fact that the earliest Upper Paleolithic, the Aurignacian, has sparse physical associations with modern human remains and that some of the formerly associated human remains have turned out to be significantly younger (Smith et al., 1999; Conard et al., 2004, see also Table 3 in Trinkaus, 2005). One question in my mind, that is rarely addressed, is whether the occurrence of some scarce human remains in an archaeological layer necessarily means that these humans

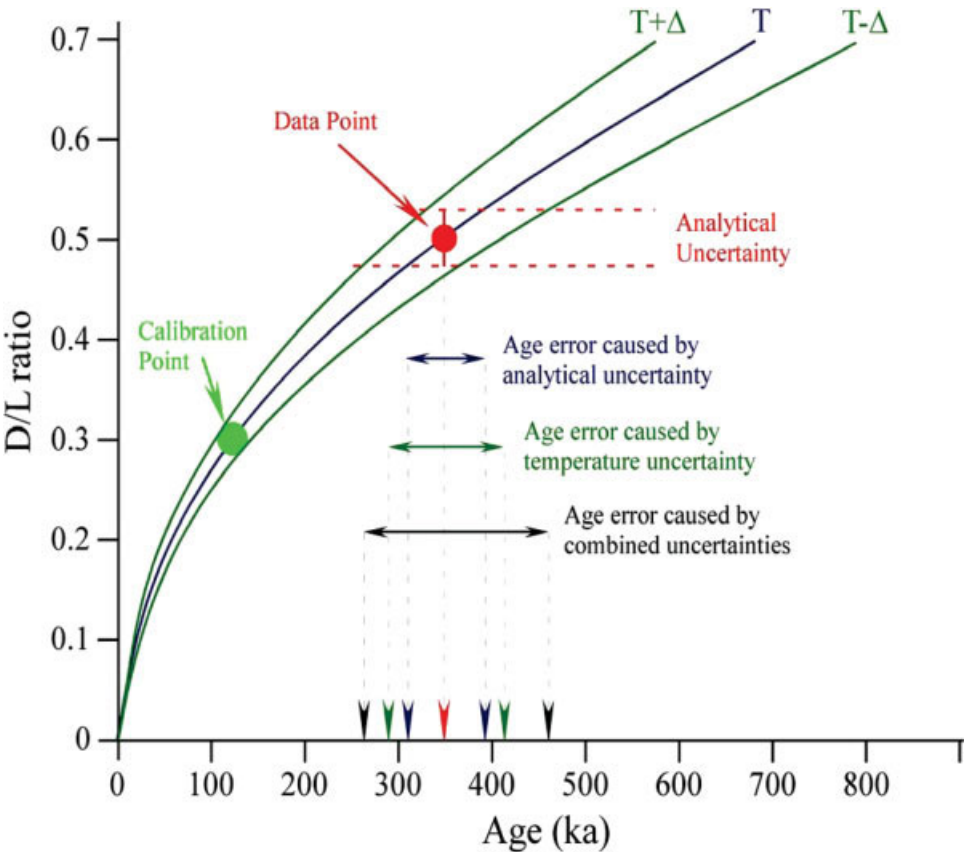

Fig. 25. Error calculation of amino acid age estimations. A calibration point is derived from a sample with a D/L ratio of 0.30 and an independent age estimate of 125 ka. The data point is fitted with a kinetic model for the current mean annual temperature or estimate of the average temperature for the last 125 ka. The kinetic equation may have been derived from heating experiments (e.g. one of the curves in Fig. 24). The sources for the age errors are the analytical uncertainty of the D/L measurement and the uncertainty in the average storage temperature (here = 1.5°C). Additional random errors arise from any uncertainty in the measurement of the calibration point, as well as systematic errors from the application of alternative kinetic functions (after Wehmiller and Miller, 2000).[Color figure can be viewed in the online issue, which is available at www.interscience.wiley.com.]

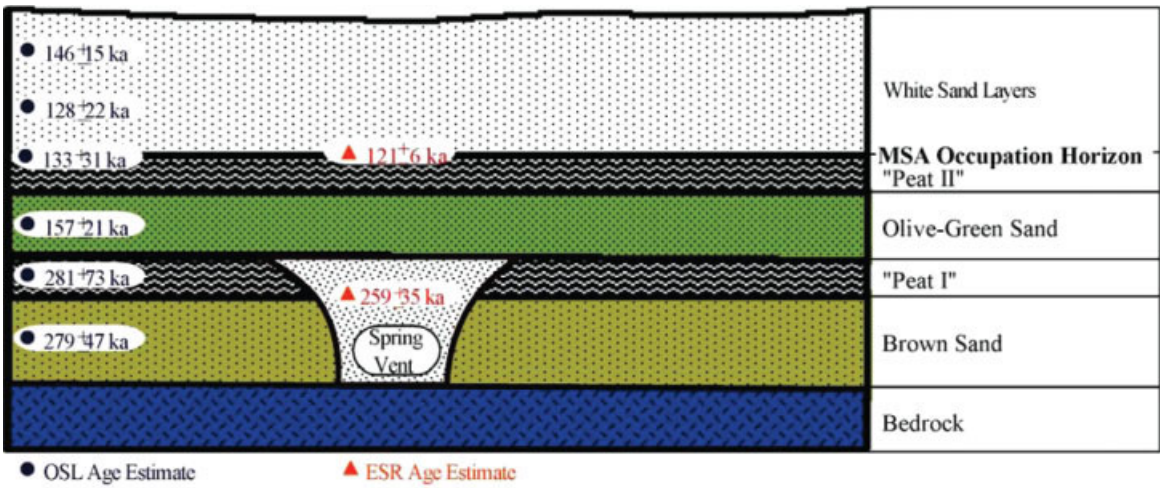

Fig. 26. ESR and OSL dating results of Florisbad in stratigraphical context (from Grün et al., 1996). [Color figure can be viewed in the online issue, which is available at www.interscience.wiley.com.]

actually produced the respective layer. For example, are Neanderthals responsible for the Chatelperronian at St. Cesaire (Leveque and Vandermeersch, 1980), or the "Hobbits" for the archaeology at Lian Bua (Morwood et al., 2004)? Could it be, they were the victims? However, before airing any more such heretic views on taphonomy and its implications for the interpretation of the archaeological record (Mellars, 2004), I prefer to be burnt for my opinions on geochronology and its relative significance for the reconstruction of human evolution.

Africa

It has been established for quite some time that anatomically modern humans occurred in southern Africa significantly earlier than in Europe. The sites of Klasies River Mouth and Border Cave contain human remains that were dated through associated material to between 65 and 110 ka (Deacon et al., 1988; Grün et al., 1990). The Herto fossils from Ethiopia have been dated to between 154 ± 7 and 160 ± 2 ka (Clark et al., 2003; White et al., 2003) and the dating results on Omo Kibish 1 indicate an age of 195 ± 5 ka (McDougall et al., 2005). Because of the sometimes uncertain relationship between the material dated and the human fossils (e.g. Faupl et al., 2003 noted that the samples that were dated to constrain the younger age limit of the Herto fossils originated from a site several hundreds of kilometers away, but see reply by Hart et al., 2003), some valuable additional chronological information could be obtained by analyzing the fossils directly.

Florisbad

In 1932, T.F. Dreyer discovered human cranial fragments at Florisbad (Dreyer, 1938). The partial cranium was part of a natural accumulation of mostly carnivore prey remains, which were trapped in vertical spring vent structures. The human remains show typical damage caused by hyena chewing (Brink, 1987, 1988). The Florisbad fossil hominid remains consist of much of the frontal bone and right side of the face, together with parts of the parietals, maxillae, and the right M^3. Clarke (1985) produced the most recent and realistic reconstruction, in which the face appeared more archaic in shape than previously. The human remains of Florisbad are considered immediate precursors for modern humans in Africa (e.g. McBrearty and Brooks, 2000). The main reason to mention Florisbad here is that it was the first site, at which direct nondestructive ESR analysis was applied to human dental material. The fossil could not be dated by associated material, because, apart from the human remains, the so-called Spring-Collection of Dreyer contained only nonprovenanced material, which actually originated from fossil accumulations spreading perhaps from about 40–400 ka (see Grün et al., 1996).

Although the right M^3 cannot directly be fitted to the skull, it is most likely that it is part of the same individual, considering that all other human bone fragments are. Nonetheless, it is actually the only dental material that can unequivocally be associated with the bones. Two fragments were removed from the tooth and dose values determined. At the time, laser ablation analysis was not available and it had to be assumed that the tooth was virtually uranium free as all other teeth of the site are. The dating results are shown in Figure 26, yielding an age of about 260 ± 35 ka for the dental material. There is general agreement with OSL dates on stratigraphically related sedimentary units, however, all age estimates are associated with very large errors. While the ESR measurements could only be improved to a minor extent, the main error comes from the uncertainty in the reconstruction of the radioactive environment. OSL could be greatly tightened up, using more advanced dating protocols (Murray and Wintle, 2000). The dating results were first perceived with scepticism, they were regarded as "too old." With the new dating results on early modern humans in Ethiopia in the range of 150–200 ka (White et al., 2003; McDougall et al., 2005), the ESR results on Florisbad have become somewhat less provocative.

Border cave

The site is located in KwaZulu, South Africa, on the border with Swaziland. It contains a long stratigraphic sequence covering the Middle and Late Stone Ages (MSA and LSA) as well as Iron Age. Eight anatomically modern hominid specimens were discovered over the years, BC1, BC2, BC6 to B8 are of uncertain provenance, BC4 is asso-

ciated with Iron Age deposits, while BC3 and BC5 were found within MSA contexts (Beaumont et al., 1978; Beaumont, 1980, 1994).

Similar to radiocarbon, ESR dating has undergone a series of changes. Originally considered a simple and rapid technique, dosimetry turned out to be very complicated, particularly when applied to tooth enamel, due to the U-uptake history (see above). Ongoing research into the basic principles have shown that some assumptions used in calculations of ESR age estimates were not correct (e.g. relating to β attenuation, compare Grün, 1986; Brennan et al., 1997; Marsh, 1999). Consequently, the ESR dating results on Border Cave have changed over time, mainly because of advances in dose rate calculations (summarized in Grün and Beaumont, 2001). As mentioned above, new observations on the ESR spectra of tooth enamel fragments indicate yet unresolved complications in the definition of the ESR signal and dose response.

The samples from Border Cave have the advantage of containing very little uranium, which simplifies dose rate calculations and eliminates one of the main sources of uncertainty in ESR age calculations (see above). The external γ dose rate was measured in a detailed survey at the site. The ESR dating results on powdered faunal tooth enamel samples from the archaeological sequence at Border Cave are in reasonable agreement with independent age results (e.g. Miller et al., 1999; Bird et al., 2003, see Fig. 27, below). There is perhaps the indication of small ESR age underestimations (Grün and Ward, 2002). Because the uncertainties in the dose rate calculations are well constrained, one would have to conclude that the systematic errors in the dose estimation, due to the effect of different species of CO_2^- radicals (see description of the ESR spectra in tooth enamel, above), are unlikely to be larger than 5–10%.

On the basis of the study of nitrogen contents and infrared splitting factors, Sillen and Morris (1996) suggested that the Border Cave 5 mandible could be of Iron Age (i.e. around 1,000 years old). In contrast to most of the human remains at Border Cave, which were found in the spoil heap of a non-archaeological digging exercise (the local farmer mistook the aeolian dust for guano), BC5 was found in situ at the base of the 3 WA (white ash) layer. The proposed Iron Age for BC5 implied that the excavators had missed a 1.5 m deep pit from the Iron Age layers at the top of the sedimentary deposits down to the base of 3WA. This did not entirely delight the excavator in charge.

A small fragment was removed from the mandibular third right molar and measured with ESR, yielding a dose value of 150 ± 5 Gy. The internal U-distribution was measured with laser ablation ICP-MS. The analytical results convert to an age of 74 ± 5 ka, in agreement with the stratigraphically expected age (see Fig. 27). For anthropology, the results confirm the antiquity of BC5 and modern human remains in southern Africa in general. For ESR, the study demonstrates that powder and fragment measurements yield stratigraphically consistent age results, and these are in close agreement with other, independent age assessments. Nonetheless, research has to continue to solve the problem of the effect of the two species of the CO_2^- radicals (see above).

Tuinplaas

The human remains of Tuinplaas (Springbok Flats, South Africa) consist of a nearly complete skeleton with a large cranium (Broom, 1929). The provenance of the skeleton is uncertain, and only MSA artifacts were found in the surroundings of the human remains, which led to a loose association between the fossil and the artifacts (Van Riet Lowe, 1929). Radiocarbon dating yielded ages of about 5,600 BP for a calcareous crust covering the bones (Vogel and Marais, 1971) and about 590 BP for a bone sample (Hedges et al., 1996a). The samples for the latter analysis were suspected to be contaminated. Pike et al. (2004) carried out a laser ablation U-series analysis, shown in Figure 28. The U-profile does not pass the quality criteria of the D–A model, i.e. it does not show a U-shaped profile, but indicates U-leaching at the outside (decreasing U-concentrations). Thus, the chronological information that can be derived from the laser ablation analysis, is that the specimen should be older than the apparent U-series age estimates in the center of the bone and younger than the apparent ages at the surface of the bone (U-leaching leads to older apparent U-series ages, see Fig. 8). These considerations lead to an age bracket of 10–23 ka for this specimen, implying that it is not related to the MSA artifacts (though there is a general question as to when the MSA/LSA transition takes place in southern Africa, see e.g. Wadley and Jacobs, 2004).

There are a range of other human fossils from Africa in various stages of ESR/U-series analysis, including samples from the Cave of Hearths, Hudjiespunt, Irhoud, Kabwe, Omo Kibish 1, Sale, and Thomas 1 and 3. Some of the samples have excellent stratigraphical control, others have not. As mentioned above, the quality of the chronological information derived from ESR analysis is critically dependent on how well the radioactive environment can be reconstructed.

The Near East

The human fossil record of the Levant provides a vital link between Africa and the world outside this continent. Thus far, human fossils were analyzed from Tabun, Skhul, and Qafzeh. This paper is not the forum to discuss the taxonomical implications of the anatomical features of the human fossils from the Levant. Here, I simply follow the classifications that were used by my collaborators over the years and call the human remains from Tabun, Kebara, and Amud Neanderthals and those from Skhul and Qafzeh, early modern humans. There are numerous publications, however, which beg to differ (see e.g. Kramer et al., 2001 and references therein).

Tabun

The cave of Tabun is located in Mount Carmel, Israel. The archaeological sequence at Tabun is one of the longest and apparently most complete in Southwestern Asia, and has become a reference site for the evolution of archaeological technologies in the Levant (Jelinek, 1982a, b; Bar-Yosef, 1989). Garrod's excavations (Garrod and Bate, 1937) led to the recovery of one of the most complete Neanderthal skeletons ever discovered, Tabun I (C1), an adult female. In addition, a virtually complete adult mandible was found, Tabun II (C2). The hominid material was described by McCown and Keith (1939).

There has been a long-standing discussion as to why the luminescence (Mercier et al., 1995b) and ESR dating sequences do not agree (see summary in Grün and Stringer, 2000). When comparing the two data sets of Mercier et al. (1995b) and Grün and Stringer (2000; Fig. 29), one can clearly observe a systematic shift between the

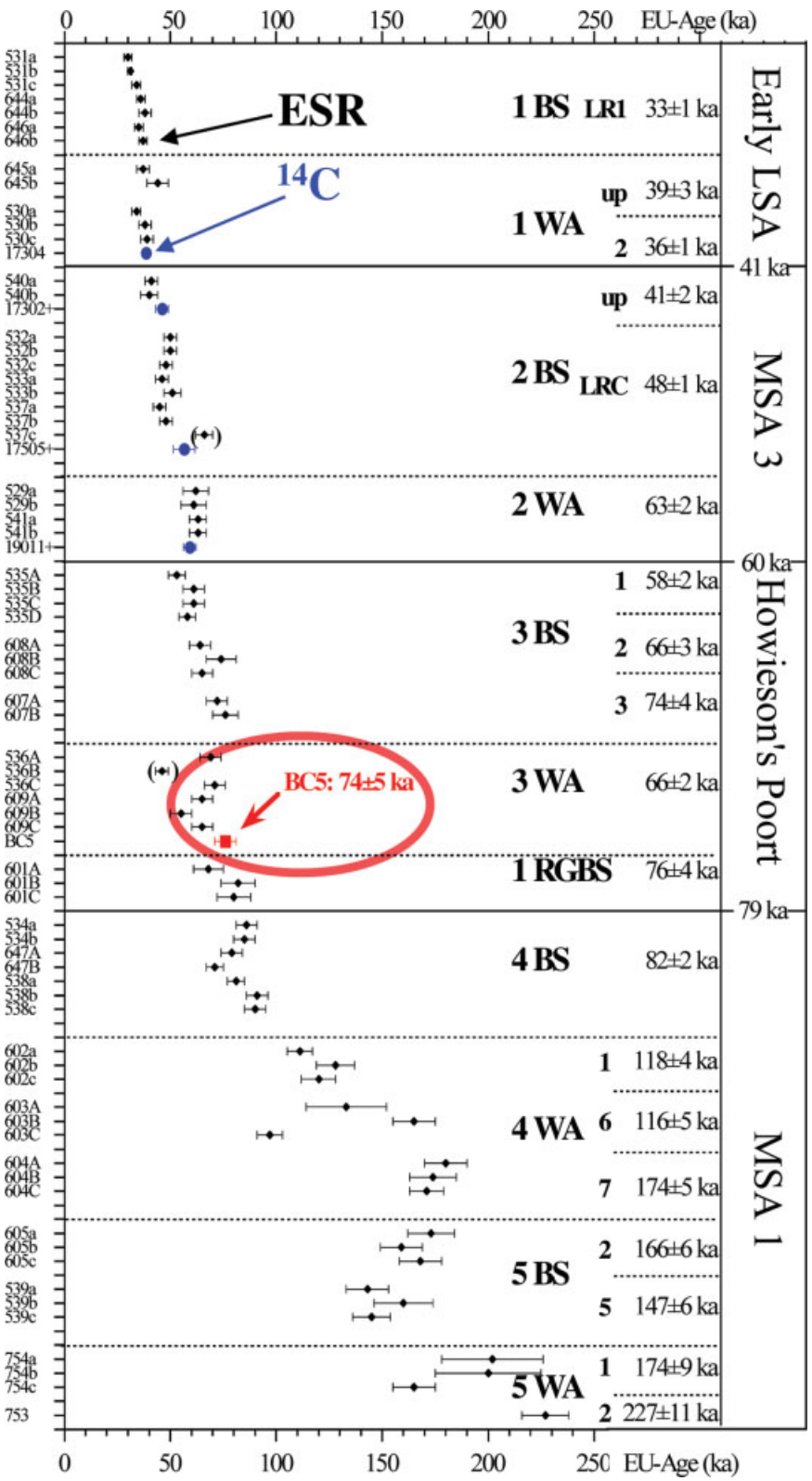

Fig. 27. The age of BC5 in context with the revised ESR chronology for Border Cave (Grün and Beaumont, 2001). Lowercase letters following the sample number on the left axis denote subsamples of a single tooth, capital letters separate enamel fragments. The two bracketed results were not used for the calculation of the average ages of the units. ESR shows slightly younger ages than radiocarbon (data from Bird et al., 2003), which may be the effect of the two CO_2^- radicals (Figure from Grün et al., 2003). [Color figure can be viewed in the online issue, which is available at www.interscience.wiley.com.]

mean values. However undesirable the large error ranges of the analyses are, the two data sets agree within error. For the sake of completeness, one should perhaps mention that Rink et al. (2003) reported the dates of two apatite vein samples without making any contributions to the chronology of the site, and a single tooth found in situ in Layer E_d (Rink et al., 2004), which yielded an age obviously agreeing with the luminescence chronology. From this Rink et al. (2004) concluded that the other ESR dating studies at the site had been considerably flawed.

In 1998, Schwarcz and Simpson used γ spectrometry on two bone samples from the Tabun C1 skeleton. They con-

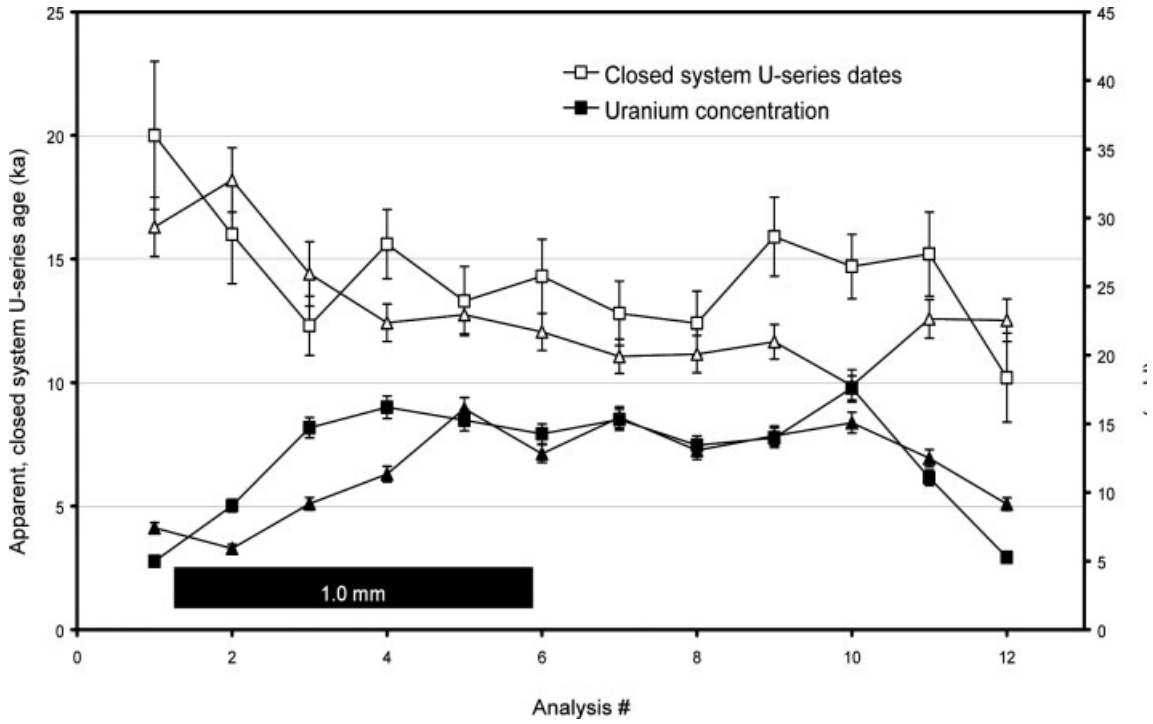

Fig. 28. U-concentration and apparent U-series ages across a bone fragment from Tuinplaas. The U-profiles indicate U-leaching, which is at least partly responsible for the elevated apparent U-series ages in these regions. Squares and triangles show the results of two separate profiles (from Pike et al., 2004 original kindly provided by Alistair Pike, University of Bristol).

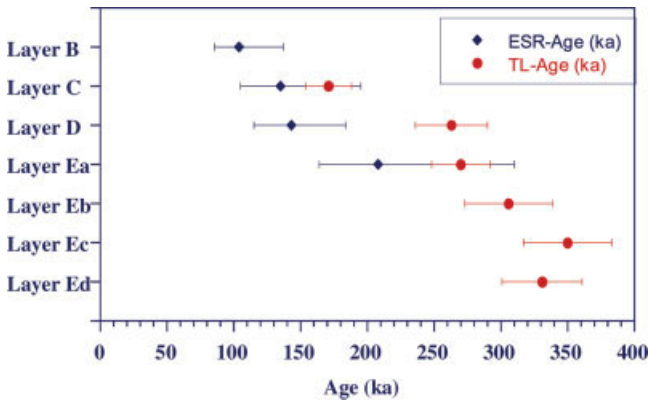

Fig. 29. Results of the ESR (Grün et al., 1991; Grün and Stringer, 2000) and luminescence (Mercier et al., 1995b) dating studies on samples from Tabun. [Color figure can be viewed in the online issue, which is available at www.interscience.wiley.com.]

cluded that their results indicated a late Middle Paleolithic, perhaps even early Upper Paleolithic age of the specimen. Their data are shown in Figure 30. The closed system Th/U and Pa/U ages cover a very wide age range (Fig. 30A). This becomes significantly worse, when the data are plotted in the concordance diagrams and open systems are allowed (Fig. 30B,C). It is evident that the quality of the γ spectrometric results simply does not allow us to draw any chronological conclusions (the large errors in the measurements would allow virtually any date between a few thousand years and infinity).

A dental sample from Tabun C1 was analyzed by ESR and for U-series isotopes (Grün and Stringer, 2000). Again, the chronological interpretation of the results is not straight-forward. Because there was no sediment attached to Tabun C1 and its stratigraphic position is somewhat ambiguous (Bar-Yosef and Callander, 1999), it is not possible to carry out ESR age calculations. Instead, in the first instance, one can only use the dose value and compare it to other teeth from the site (Fig. 31A). Unfortunately, these data are severely scattered, so that a clear attribution to a specific layer is impossible. The same applies to the uranium concentration in the dentine (Fig. 31B). Surprisingly, the U-series data on dentine samples from layers B to E_a, cluster tightly and are progressively older (Fig. 31C). The U-series result from the C1 dentine is closest to the result of faunal material from Layer B. In the case of Tabun, rather than being able to carry out a straight-forward dating analysis, the ESR and U-series results could only be used to obtain some indication of the provenance of the skeleton, i.e. that it most probably relates to Layer B. If this assumption is correct, the ESR data could then be used for some tentative age calculations using the full breadth of possible radioactive environments. All such calculations resulted in model ages, which were significantly older than the Middle to Upper Paleolithic Transition, MUPT, which has been dated in various parts in Europe and the Middle East to between about 35 and 42 ka BP.

An isolated human tooth, BC7, was also analyzed with ESR (Coppa et al., 2005). Similar to the study of C1, the data could only be used to speculate about the provenance of the tooth. Model calculations pointed to an age contemporaneous with Layer B.

Skhul

Along with the site of Qafzeh, the cave site of Skhul has significant bearing for our understanding of modern

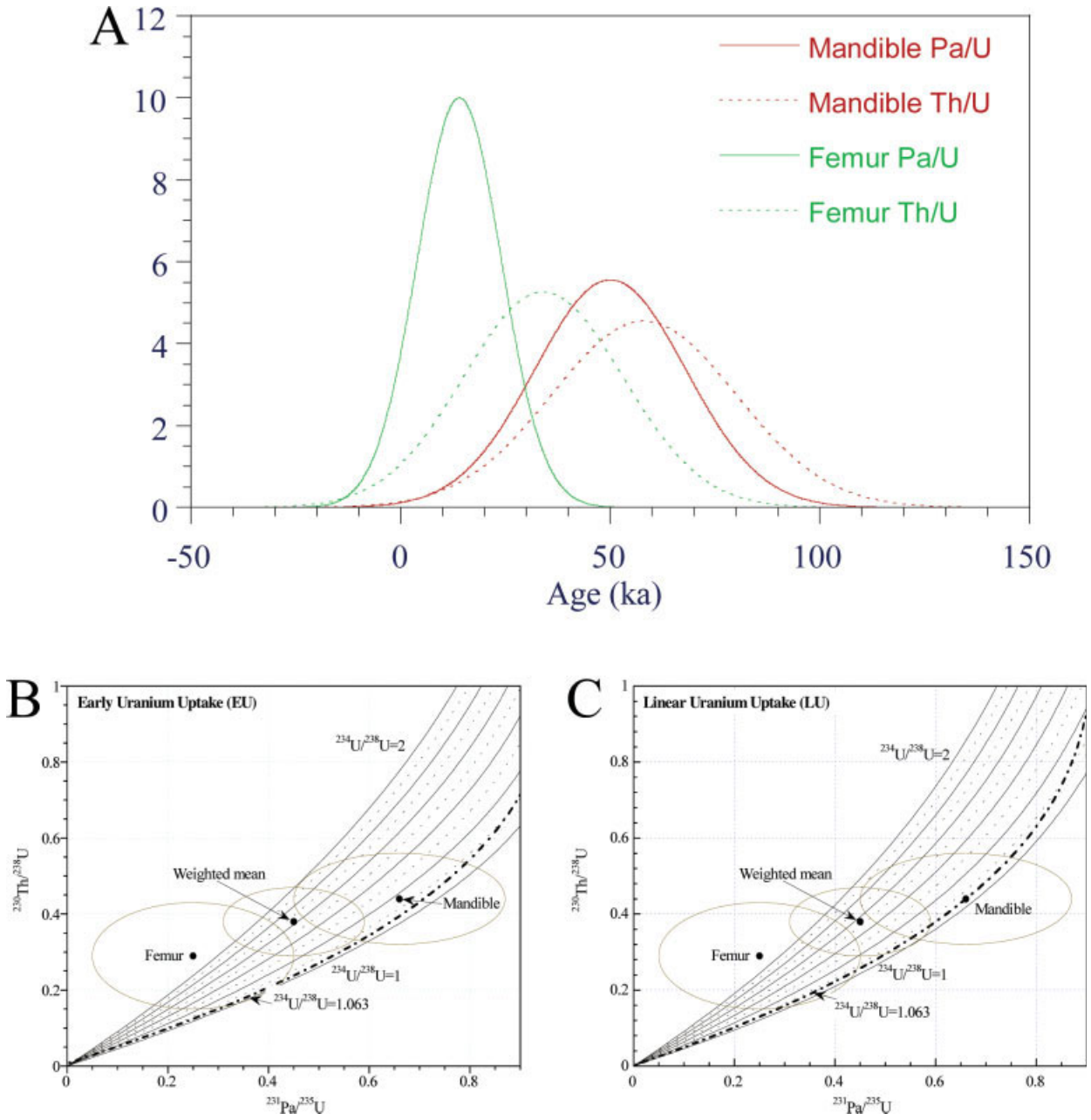

Fig. 30. Results of the γ spectrometric measurements on bone fragment from Tabun C1 (data from Schwarcz et al., 1998). **A**: Closed system data shown as Gaussian distributions. **B**: EU concordance diagram. **C**: LU concordance diagram. [Color figure can be viewed in the online issue, which is available at www.interscience.wiley.com.]

human evolution. Located only a few hundred meters away from Tabun, the site has revealed a significant number of intentional burials (Garrod and Bate, 1937; McCown, 1937; McCown and Keith, 1939), the human remains of which all show modern human features. Associated material was dated in a number of studies, closed system ESR ages on faunal teeth in the range of about 55–100 ka were reported by Stringer et al. (1989) and 46–88 ka by McDermott et al. (1993), U-series ages on faunal teeth in the range of 43–80 ka were obtained by McDermott et al. (1993) and TL on burnt flint in the range of about 99–134 ka by Mercier et al. (1993).

A more recent study by Grün et al. (2005) involved ESR analysis of a dental fragment from Skhul II, γ spectrometric, and TIMS U-series analyses on bones from Skhul IX. Similar to most other studies, the γ spectrometric analysis contained limited chronological information (Fig. 32). The samples display delayed U-uptake (as shown by the fact that the $^{230}Th/^{234}U$–$^{231}Pa/^{235}U$ data point lies above the closed system iso-$^{234}U/^{238}U$ line), but open system modeling would also include very high p-values corresponding to virtually infinite age estimates. A TIMS U-series analysis on the surface of one of the bone fragments yielded an age on 131 ± 2 ka. Considering that the γ spectrometric analysis strongly implied delayed U-uptake, this TIMS result is more likely a minimum age result than an age underestimate resulting from U-leaching.

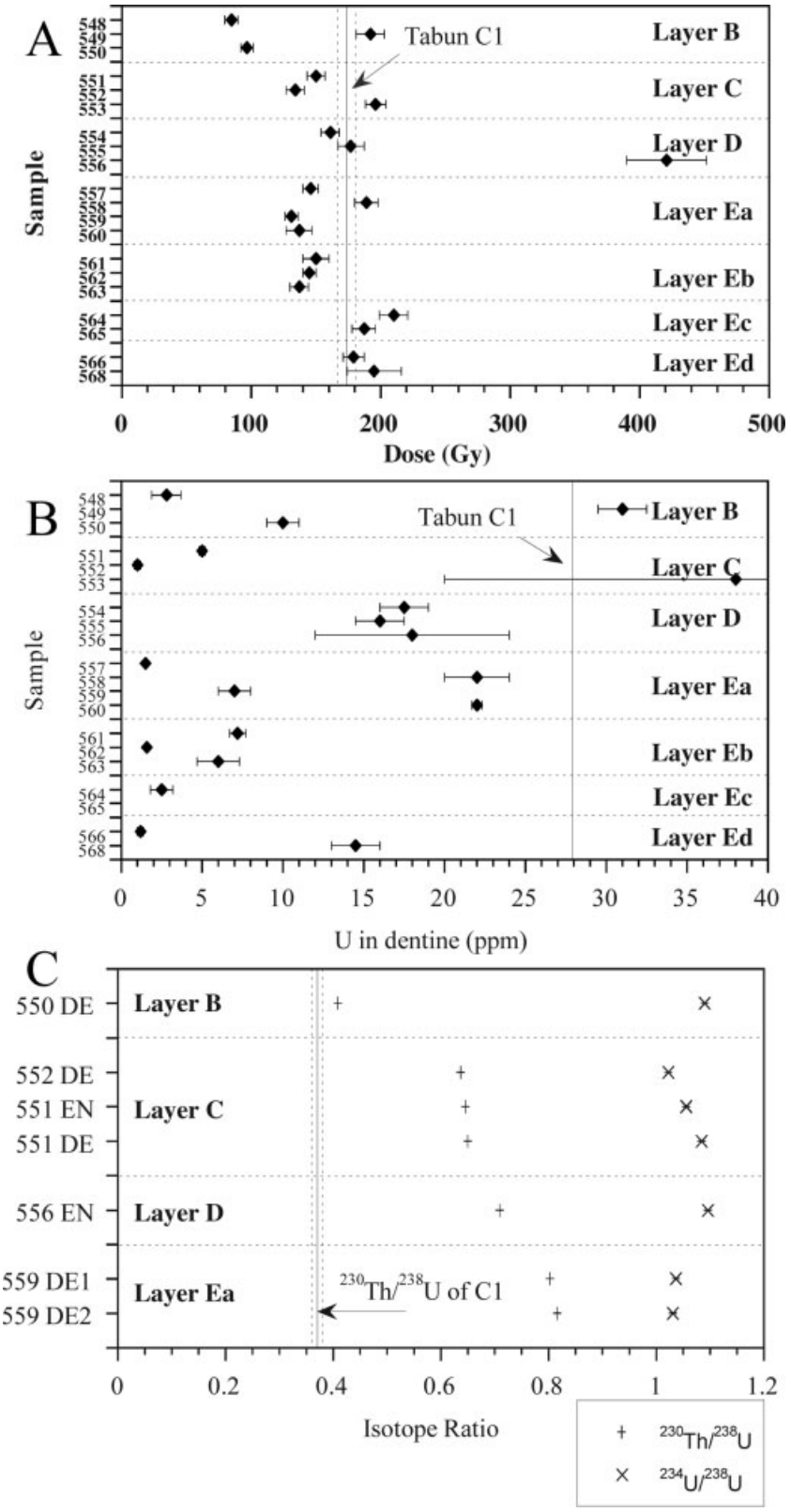

Fig. 31. Results of the analysis of a dental fragment of Tabun C1 (from Grün and Stringer, 2000). **A**: Dose estimation in context to previous analyses on faunal teeth. **B**: Uranium concentration in the dentine of C1 in context to previous analyses on faunal teeth. **C**: U-series analysis in the dentine of C1 in comparison to previous analyses on faunal teeth. The U-series data from the different layers show surprisingly little scatter and allow a correlation of C1 to Layer B.

In contrast to the results on Skhul IX, the apparent TIMS U-series analysis on the dentine from Skhul II yielded only 32.1 ± 0.8 ka. This is in line with the U-series results on the dentine of other teeth (Fig. 33A). Most of these teeth remain unprovenanced with respect to their location within the site, except for sample 1058, a pig tooth in clear association with Skhul V and sample 1057, a bovid tooth associated with Skhul IX (for more details, see Grün et al., 2005). The dental U-series results could imply either that a reasonable number of samples, including

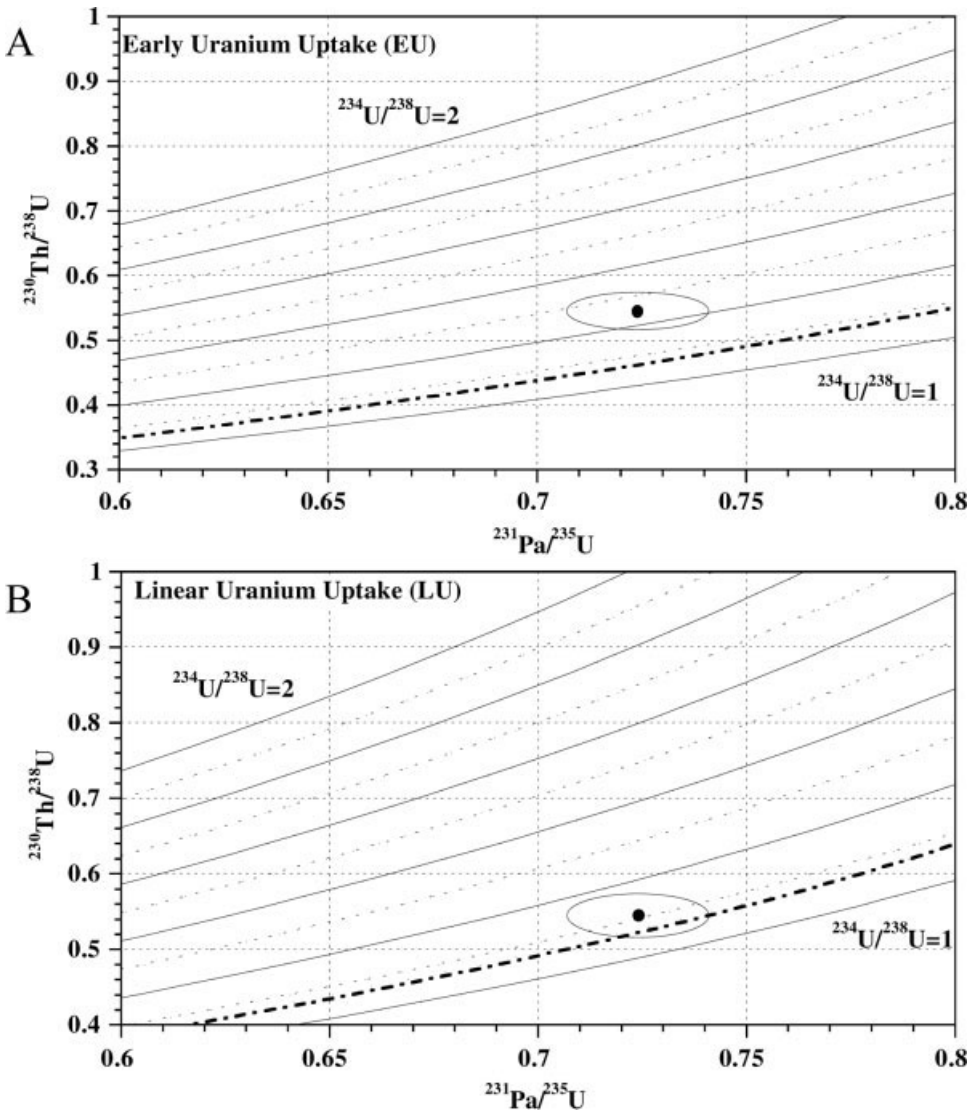

Fig. 32. EU (**A**) and LU (**B**) concordance diagrams for bone fragments from Skhul IX (from Grün et al., 2005). The data show a general trend of delayed U-accumulation. Open system modeling would include very high p-values corresponding to virtually infinite age results.

some of the human remains, are of an age perhaps synchronous with the MUPT, or that the samples with somewhat higher U-concentrations had experienced a delayed U-uptake, as indicated by the arrow in Figure 33B. When applying combined U-series/ESR dating, none of the samples are close to the MUPT (Fig. 34A) and there is a general, broad trend of delayed uptake (expressed in p-values, see Fig. 10, above) in those samples with higher U-concentration (Fig. 34B). The sample from Skhul II, having the highest U-concentration, indicates the most delayed uptake. Because of the uncertainties in the reconstruction of the radioactive environment, Grün et al. (2005) also modeled how wrong the assumptions for the γ dose rate have to be, to accommodate MUPT ages (Fig. 35). For the combined U-series/ESR age of Skhul II to coincide with the MUPT, the values for the reconstruction of the external dose rate have to be out by at least 3-σ. Most other samples, including those in clear association with Skhul V and IX, cannot accommodate a MUPT age.

At this stage it is not possible to decide whether the burial samples are of the same age population or whether Skhul IX is significantly older than II and V. If the burials took place within a short time span, then the best age estimate lies between 100 and 135 ka. If Skhul IX was older than II and V, perhaps around 140 ka, then the best estimate for II and V is 98^{+19}_{-10} ka. The open system age results on the burials are in close agreement with the thermoluminescence results of Mercier et al. (1993).

Qafzeh

This site has played a central role in our understanding of modern human evolution. Qafzeh cave near Nazareth contained the remains of at least 20 human individuals (infants, children and adults), some of which seemed to have been intentionally buried. Qafzeh was first excavated in the 1930s by Neuville and in a second phase during 1965–1979 by Vandermeersch (Oakley et al., 1975; Vandermeersch, 1981). The luminescence dating result of 92 $\pm$ 6 ka on burnt flints associated with the early modern human fossils from Qafzeh (Valladas et al., 1988) initiated a major revision of our Eurocentric perception of modern human evolution. The luminescence age estimate was confirmed by dating analysis of faunal teeth using ESR (Schwarcz et al., 1988) and U-series (McDermott et al., 1993). The skull of Qafzeh 6 was analyzed with γ spectrometry by Yokoyama et al. (1997), who obtained

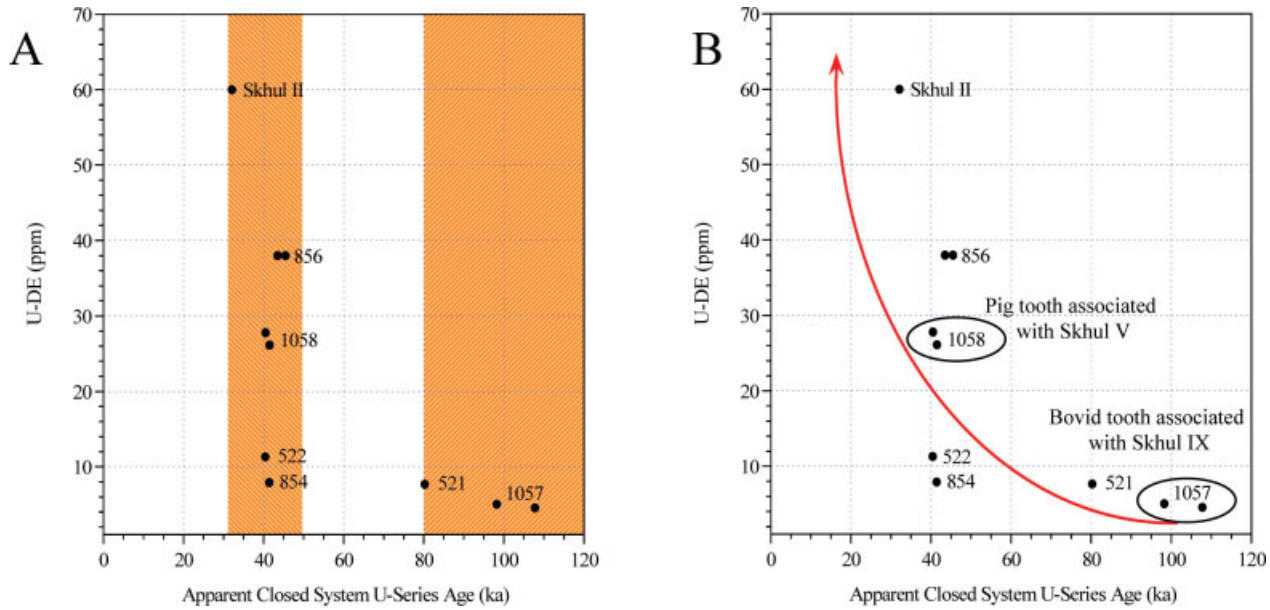

Fig. 33. **A**: Apparent U-series ages of the samples from Skhul. Apart from samples 1057 and 1058, the faunal material (521, 522, 854, and 856) is unprovenanced with respect to its location within the site. The closed system age estimates fall into two ranges, from about 30 to 50 ka and 80 to 120 ka (shaded areas). This could either mean that the samples are of two different age groups where the younger one could be close to the Middle/Upper Paleolithic Transition, or that the samples with higher U concentrations underwent a later stage of U-uptake, as indicated by Fig. B). **B**: The samples with younger apparent U-series ages have higher U-concentrations. This could have been caused by some later U-uptake as indicated by the arrow (Figure from Grün et al., 2005). [Color figure can be viewed in the online issue, which is available at www.interscience.wiley.com.]

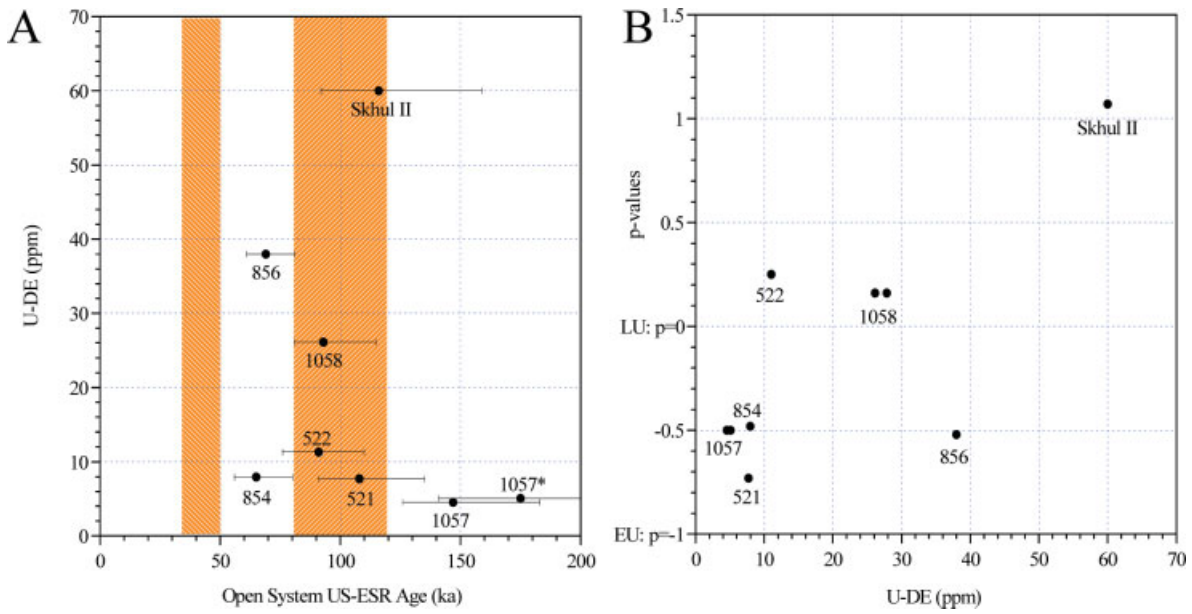

Fig. 34. **A**: Combined US-ESR age estimates of the samples from Skhul. The two shaded areas, which present the two age ranges discussed in Figure 33A, are included for cross reference. **B**: Plot of p-value (a measure of the delay in U-accumulation, see Fig. 10) versus U-concentration. There is a general trend that the samples with higher U-concentration experienced more delayed U-uptake (compare Fig. 33B) (Figure from Grün et al., 2005). [Color figure can be viewed in the online issue, which is available at www.interscience.wiley.com.]

$^{230}Th/^{234}U$ and $^{231}Pa/^{235}U$ age estimates of 80^{+24}_{-18} ka and 94^{+10}_{-8} ka, respectively. The concordance plot of these analytical data sets are shown in Figure 36. Because of the inherent problems of γ spectrometry to measure ^{234}U, the calculated $^{234}U/^{238}U$ ratio has a large error. It can be seen that the 1-σ error envelope of the $^{230}Th/^{234}U$–$^{231}Pa/^{235}U$ measurements does not overlap with the mean $^{234}U/^{238}U$ value (Fig. 36A). If open systems are considered, the data set at one end implies U-uptake with a p-value of about $p \approx 0.6$, corresponding to an age of about 120 ka (see Fig. 36B), and at the other end leaching of about 70%, corresponding to an age of 34 ka (Fig. 36C). If it was possible to

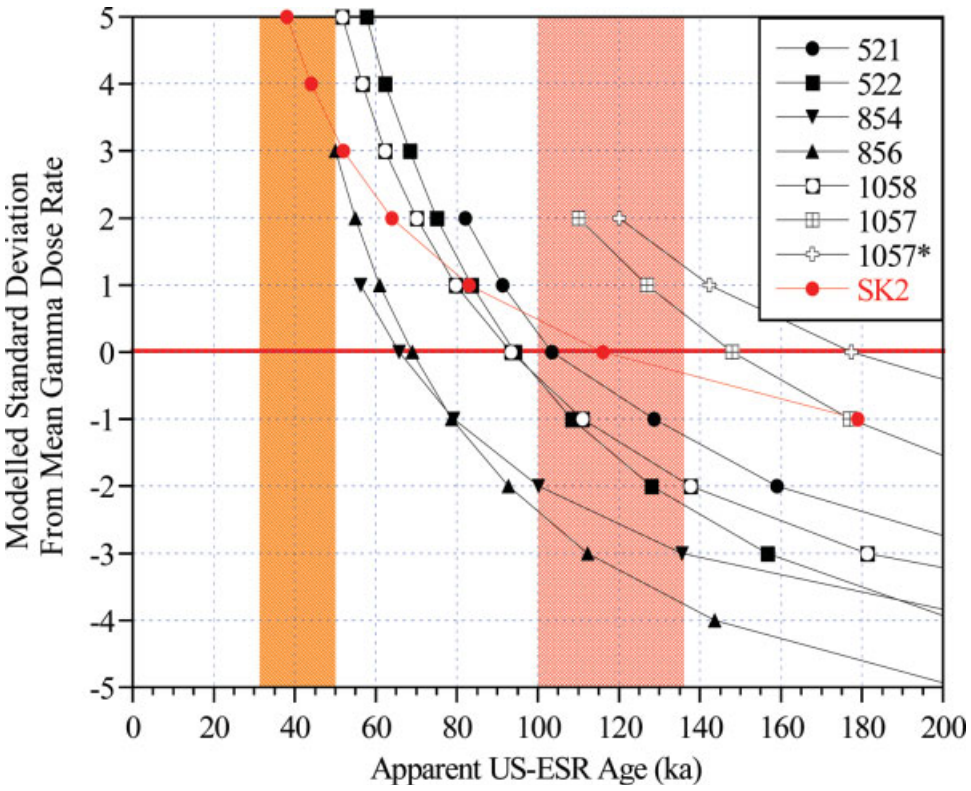

Fig. 35. Relationship between calculated US-ESR ages and the estimate of the external γ dose rate, expressed in units of standard deviations from the mean of the samples from Skhul. The first shaded area corresponds to the one in Figure 33A, the second (100–135 ka) marks the estimated time range for the burials (Figure from Grün et al., 2005). [Color figure can be viewed in the online issue, which is available at www.interscience.wiley.com.]

tighten the $^{234}U/^{238}U$ ratio (e.g. by TIMS or laser ablation), more precise results could be obtained.

There is a range of other human fossils from the Levant in various stages of analysis, including Amud, Kebara, Qafzeh 10 and 12, and Skhul 1.

Europe

In Europe, the transition from the Middle Paleolithic (generally associated with Neanderthals) to the Upper Paleolithic (generally associated with modern humans) is well documented and reasonably well dated (see e.g. Bocquet-Appel and Demars, 2000; Mellars, 2004, 2006, but also Pettitt and Pike, 2001 reviewing the pitfalls of radiocarbon chronologies). Generally, this transition takes place around 35,000–42,000 years BP. Of particular interest are the sites where Neanderthals have survived for much longer and those sites where modern humans potentially arrived much earlier.

There is no doubt that radiocarbon dating has played an outstanding role for establishing the chronology of modern human prehistory in Europe by providing many reliable dating results on human remains. One can hardly agree more with Mellars (2006), who foreshadows a new radiocarbon revolution as a result of the drastically improved pretreatment techniques (Bronk Ramsey et al., 2004b; Higham et al., 2006b, see above). Nevertheless, for any pretreatment technique to produce reliable results, the sample must contain at least some unaltered, original organic material. When bones are older than 30,000 years, they become more and more diagenetically altered and exchange significant amounts of their radiocarbon pool with the environment. As a result, at least some samples may not contain any pristine organic matter, and their radiocarbon results become questionable.

Vindija

This site has acquired an important place in the discussion of the Neanderthal/modern human transition in Europe, after radiocarbon results of 29,080 ± 400 BP and 28,020 ± 360 BP were obtained on samples from the Neanderthal posterior mandible fragment (Vi-207) and a superior fragment of the left parietal (Vi-208), respectively (Smith et al., 1999). The implications were that Neanderthals in this region had survived the initial colonization of Europe by modern humans, and that cultural interactions between Neanderthals and modern people may have taken place, particularly as the Vindija Cave contained a diverse Upper Paleolithic artifact assemblage (Karavanic and Smith, 1998). Particular weight was given to the observation that the two samples gave closely similar results. Nitrogen isotopes in two bone samples revealed the Neanderthals as top predators, more likely to develop effective hunting strategies rather than relying on scavenging (Richards et al., 2000).

Previously, the mandible (Vi-207) had been analyzed by γ spectrometry (Karavanic et al., 1998; see Fig. 37A,B). The concordance diagrams imply that the closed system estimate (45 ka) is a minimum age for the sample and that the more likely age is around the LU model, resulting in a mean age of 113 ka (of course, the open system results are associated with very large errors). The γ spectrometric results were dismissed by Smith et al. (1999), because the technique had obviously led to uninterpretable results for a split-base bone point (Fig. 37C,D). These results meant that this undoubtedly Upper Paleolithic tool had a minimum age of around 68 ka.

Because the samples from Vindija were the youngest Neanderthal remains analyzed by a numerical dating technique thus far, enormous inferences were made with respect to the colonization pattern of modern humans and

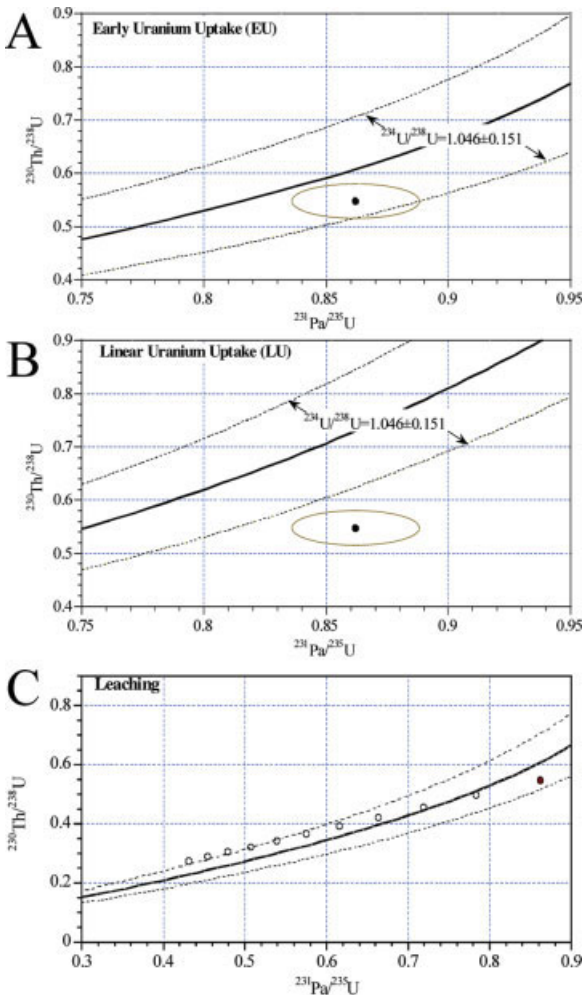

Fig. 36. Concordance diagrams for the γ spectrometric results on Qafzeh 6 (data from Yokoyama et al., 1997). **A**: EU concordance diagram. **B**: LU concordance diagram. **C**: Effect of leaching (in 10% steps relative to the measured U-concentration, error ellipse of the Th/U-Pa/U measurement omitted for clarity). Because of the large error in the estimation of the $^{234}U/^{238}U$ ratio, open system modeling would allow for ages between about 34 ka (70% leaching, Fig. 36C) and 120 ka ($p \approx -0.6$, Fig. 36A,B). [Color figure can be viewed in the online issue, which is available at www.interscience.wiley.com.]

the possibility of cultural and genetic exchange (Smith et al., 1999). The site had the advantage of showing signs of cryoturbation as well as bioturbation of the cultural layers by cave bears in some areas, which made it easy to cast doubt on the stratigraphic integrity of the site (e.g. d'Errico et al., 1998, see discussion by Straus, 1999; Zilhao and d'Errico, 1999; Karavanic and Smith, 2000).

Higham et al. (2006a) carried out new radiocarbon analyses on the previously dated samples using the new ultrafiltration pretreatment technique. They reported revised results of 31,390 ± 220 BP (Vi-208) and 32,400 ± 1,200 BP (Vi-207), but left the chronological door ajar by mentioning that *the "true" ages should be in the vicinity of 32,000 B.P. or slightly older*. Higham et al. (2006a) also presented a critical review of the few human fossils that have returned age estimates contemporaneous with the MUPT in Europe, which at present, do seemingly not allow for any far-reaching arguments.

Banyoles

The dating study of the Banyoles mandible (Grün et al., 2006) is included in this review to show the state-of-the-art of our present analytical capabilities. Maroto (1993) published a comprehensive review on all aspects of scientific research on this specimen. The mandible was found in a travertine near the township of Banyoles (Bañolas), Catalonia, Spain. For a long time it has puzzled anthropologists. Because of its robustness, its taxonomy changed from Neanderthal (e.g. Hernández-Pacheco and Obermaier, 1915) to pre-Neanderthal (e.g. de Lumley, 1971/2, 1973; de Lumley, 1982; Stringer et al., 1984) and back to Neanderthal (Sánchez, 1993; Strauss et al., 1993). Nevertheless, it was thought to represent early Neanderthals rather than late ones. The dating results on the encasing travertine of 45 ± 5 ka (Julia and Bischoff, 1991) were thus somewhat surprising. The remaining question was, whether the mandible could have been reworked.

To address the question of the antiquity of the Banyoles mandible, a direct dating study was carried out by Grün et al. (2006). In a first step, a piece of tooth enamel was removed from the right M_3 and analyzed by ESR. The piece of enamel had so cleanly separated from the dentine that is was not possible to measure the dentine U-concentration with laser ablation ICP-MS. On request, three small pieces of dentine were collected for U-series analysis (Fig. 38A). The largest dimension of the largest piece (DE1) was 1.3 mm, the other pieces (DE2 and DE3) were considerably smaller. Instead of measuring tracks, it was decided to analyze U-series isotopes by drilling holes with the laser ($\phi = 85$ μm). Because of the configuration of our mass spectrometer with a single ion counter in the center of the detector-array, ^{230}Th and ^{234}U have to be measured separately. Thus, the material ablated from the holes result in either $^{234}U/^{238}U$ or $^{230}Th/^{238}U$ ratios. The $^{234}U/^{238}U$ ratios from the different locations are very homogeneous. In contrast, the $^{230}Th/^{238}U$ ratios and the U concentrations vary greatly. The large variations of the $^{230}Th/^{238}U$ values are astonishing: hole H1 gives an apparent age of about 300 years, while H2, less than 200 μm apart, about 57 ka. Because of this surprising small-scale variation in the $^{230}Th/^{238}U$ values, two laser ablation scans were run across the top of DE1 in the same track (the second scan ablating material from deeper into the sample). The approximate position of the scans are indicated in Figure 38B. The first scan did not penetrate either of holes H1 and H2, while the second scan ran completely through H1 (causing the apparent drop in U-concentration in Scan 2; see Fig. 38C) and just touched the top of H2. The scans show increasing the U-concentrations from H1 to H2, while the $^{230}Th/^{238}U$ values decrease, confirming the observations made earlier from the holes.

The dentine clearly underwent at least two U-accumulation stages, the first several tens of thousands of years ago, possibly during the initial burial phase, and a second one, perhaps starting about 1,400 years ago and continuing to very recent times. This later U-accumulation phase was most likely initiated by the activation of percolating waters from historic quarrying and drainage activities. In 812, the monastery of Sant Esteve was founded on what was then undrained waste land. To control the level of the lake, the monks laid a network of irrigation ditches, which turned a virtually uninhabitable place into an agricultural and industrial area (see Constans, 1985).

TIMS U-series analysis on the encasing travertine matrix confirmed the apparently young ages reported by

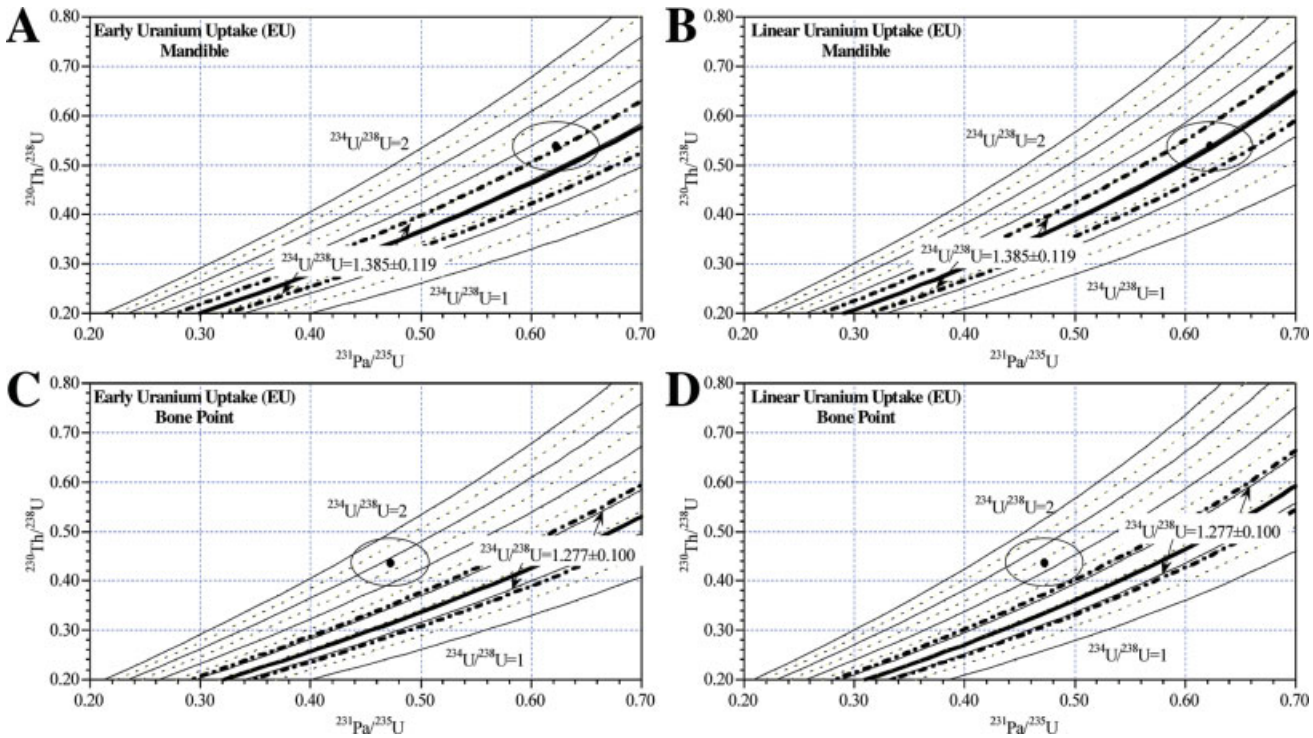

Fig. 37. Concordance diagrams for the γ spectrometric results on samples from Vindija (data from Karavanic et al., 1998). **A** and **B**: EU and LU concordance diagrams of the mandible (Vi-207). **C** and **D**: EU and LU concordance diagrams of a split-base bone point. Allowing for open system, the mandible would have a minimum age of 42 ka and a maximum age in excess of 150 ka. The data of the undoubtedly Upper Paleolithic split-base point imply an age of older than 68 ka. [Color figure can be viewed in the online issue, which is available at www.interscience.wiley.com.]

Julia and Bischoff (1991). However, U-mobilization was indicated. The combined ESR/U-series ages were in the range of 62 ka, which is a few thousand years older then the encasing matrix. This could either mean that the encasing travertine was an open system and had accumulated a small amount of uranium, or that the mandible was reworked. However, from whatever radioactive environment it was reworked from, it could be only a few thousand years older than the matrix. An age in the region of 150 ka, to be contemporaneous with the youngest Neanderthal precursors, can categorically be excluded.

Australia

Australasia holds an important key to understanding when the ideas and genes associated with the "out of Africa" migration of *H. sapiens* took place, as well as the speed and the likely pattern of dispersal. There seems consensus that only *Homo sapiens* colonized the continent, but the age of this event remains in dispute. It remains a critical issue in world archaeology to pinpoint the timing of this colonization event, because of the profound implications for deciphering the archaeological record of when modern humans reached different parts of the planet and whether behavioral modernity arose in more than one place at different times.

Dating analysis of human remains had become difficult in Australia, because the remains of their ancestors are sacred to the Aboriginal communities. The development of virtually non-destructive techniques have led to a more open mind towards dating, partly because of the keen interest of the traditional landowners to know more about their cultural heritage.

Mungo 3

The Willandra Lakes area (which includes Lake Mungo), in western New South Wales, has yielded the remains of more than 150 different individuals (Webb, 1989), including the world's first cremation, Mungo I (Bowler et al., 1970). More recently, one of the world's longest human track ways has been described by Webb et al. (2006). In 1974, a complete skeleton, Lake Mungo III, was found in the fringing lunette. The body was intentionally buried and had been covered with powdered red ochre (Bowler and Thorne, 1976). It is a gracile individual and indistinguishable from living Aboriginal Australians (Thorne, 1980).

Detailed sedimentological studies concluded in 1998 that the burial was carried out before the development of the soil horizon on the lower Mungo unit (Bowler, 1998). This was later revised to accommodate an alternative sedimentary history, implying that the burial took place contemporaneously with the formation of the lower Mungo soil (Bowler and Magee, 2000; Bowler et al., 2003). Based on correlated radiocarbon data, an age of 28,000 to 30,000 BP was deduced (Bowler and Thorne, 1976). A subsequent thermoluminescence dating study by Oyston (1996) yielded age estimates in the range of about 36–50 ka, indicating that the age of LM3 may be well beyond the practical limits of radiocarbon dating of about 40 ka (Chappell et al., 1996).

A detailed dating study was carried out on the skeleton and its surrounding sediments, involving OSL dating of the sediment layer in which the skeleton was buried, TIMS U-series dating of the calcitic coating and bone shavings, γ spectrometric analysis on the skull and ESR

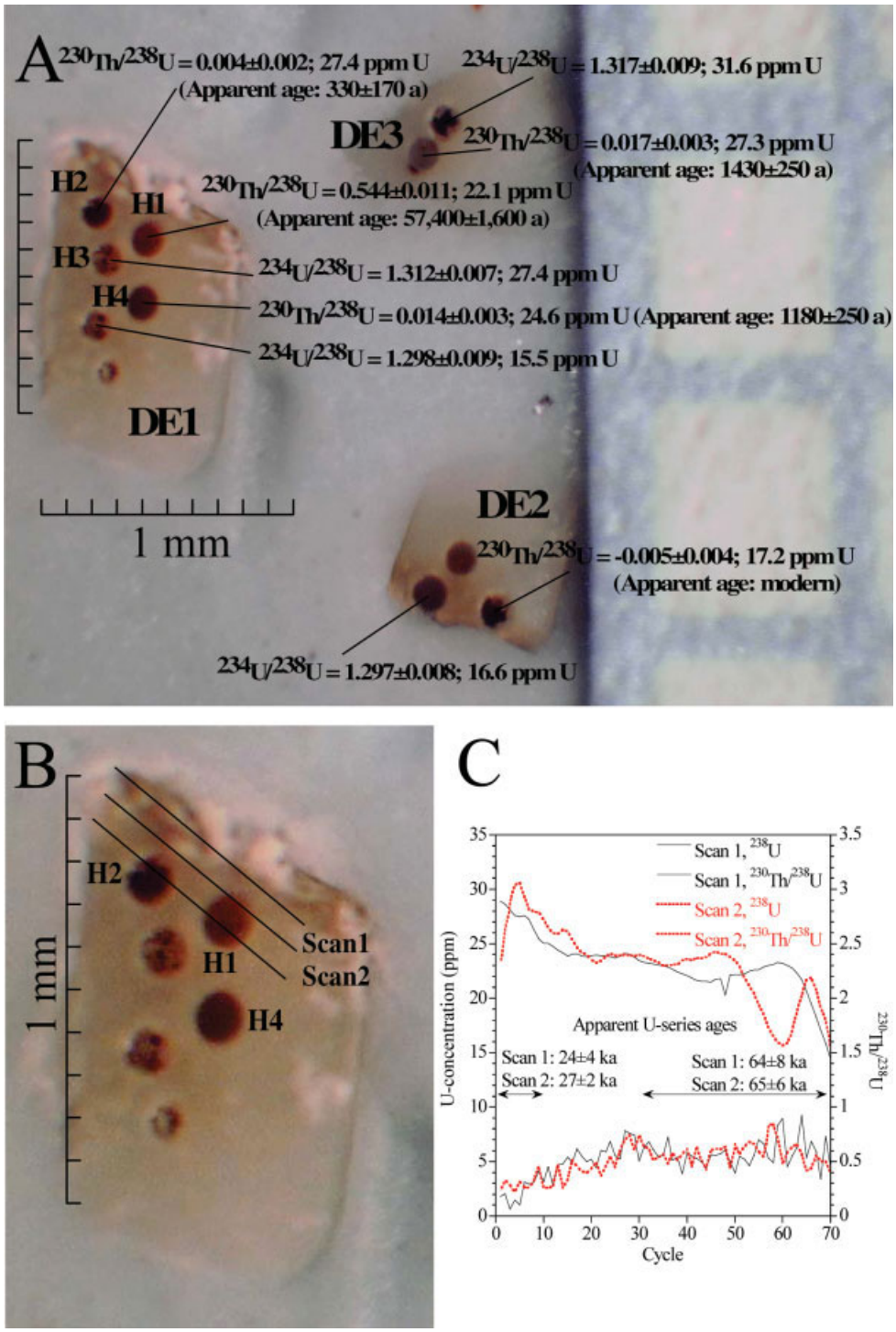

Fig. 38. Laser ablation in situ U-series analysis of dentine fragments from the Banyoles mandible. Because of the configuration of the Neptune ICP-MS with only a single central ion counter, this can either be used for the measurement of ^{234}U or ^{230}Th, thus the material ablated from the holes give either $^{234}U/^{238}U$ or $^{230}Th/^{238}U$ ratios. **A**: Results of drilling holes with the laser into three dentine fragments DE1–DE2 (the squares on the right are from 1 mm metric paper). Because of the small scale variations in the $^{230}Th/^{238}U$ ratio in DE1 (compare results from H1 and H2) two laser ablation scans were run across the top surface of DE1. **B**: Position of the successive scans across the top of DE1. **C**: U-concentration and $^{230}Th/^{238}U$ profiles of the two scans. The dip in the U-concentration of the second scan (around cycle 60) is caused by the laser hitting hole H1. Note that this does not affect the resulting $^{230}Th/^{238}U$ ratios (from Grün et al., 2006). [Color figure can be viewed in the online issue, which is available at www.interscience.wiley.com.]

dating of tooth enamel (Thorne et al., 1999). These authors concluded that the age of the skeleton was 62 ± 6 ka. This led to an animated discussion, which raised a range of speculations as to why this age estimate was so utterly wrong. Connoisseurs of scientific contention will delight in the exchanges of Bowler and Magee (2000), Gil-

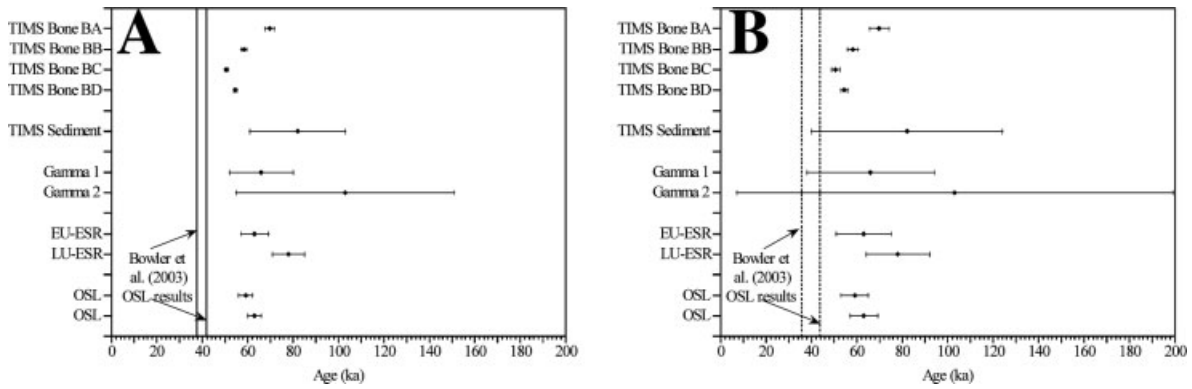

Fig. 39. Comparison of the dating results relating to Mungo 3 of Bowler et al. (2003) with those of Thorne et al. (1999). **A**: 1-σ errors and **B**: 2-σ errors.

lespie and Roberts (2000), Grün et al. (2000), and Brown (2000). This discussion raised funds for a subsequent, systematic OSL dating exercise, which concluded that both the Mungo 3 and Mungo 1 burials occurred at 40 ± 2 ka (Bowler et al., 2003).

For the review of the site, there are no new data to support one or the other result. A question was raised whether the dose rate received by the tooth from the mandible and skull (with high U-concentrations) was significantly higher than the dose rate from the sediment (with low concentrations of radioactive elements). The configuration of the Mungo burial was modeled by Nathan and Grün (2003), who concluded that the maximum effect was a shift of 3 ka towards younger ages, well within the reported uncertainty of 6 ka (Thorne et al., 1999). Neither somewhat more advanced approaches to spectrum evaluation for dose estimation (Grün, 2006), nor adjustments in the β dose calculation (using Marsh, 1999 instead of Brennan et al., 1997) lead to any different ESR dating results. It is perhaps educational to have a closer look at the uncertainties involved.

The γ spectrometric results discussed in Thorne et al. (1999), are actually shown in Figures 11 and 12, above. The difference between the two graphs is that the first considers detrital ^{230}Th whereas the second one does not. As discussed above, the true errors of the data set are considerable, and a 1-σ age range of 55–150 ka is obtained when the data are corrected for detrital ^{230}Th (because of the modeling of U-uptake) and 80–55 ka when not correcting for detrital ^{230}Th (leaching is then implied by the data). Figure 39A shows the results obtained by Thorne et al. (1999) together with the OSL range proposed by Bowler et al. (2003). In spite of the larger errors of the γ spectrometric results and the U-series age on the calcitic matrix, none of the Thorne et al. (1999) data agree within a 1-σ error with those of Bowler et al. (2003). This changes to some extent when 2-σ errors are plotted (Fig. 39B). However, neither the TIMS U-series nor the ESR and OSL results overlap with the Bowler OSL window. Whether the OSL of Thorne et al. (1999) data can be disregarded, because they originated from some distance away from the burial, as suggested by Bowler and Magee (2000), is an open question. The samples were collected in what was thought to be sedimentary equivalent positions with the help of a colleague, who was intimately familiar with the stratigraphy of the site.

There is no doubt that all bone shavings should have the same age. The TIMS data display a trend that the apparently older samples have lower U-concentrations. This can be interpreted in two ways (Fig. 40): say the specimens are 70 ka old (Fig. 40A), then the different U-concentrations would correspond to different modes of U-uptake within the bone samples (as it is observed in simple bone profiles, see Figures 8 and 9, or the example from Skhul, Fig. 34). On the other hand, if the bones were 50 ka old (Fig. 40B), the subsamples may have originally accumulated some more uranium, which was subsequently partially leached. The more uranium was leached, the older the apparent U-series result. According to the D–A model, leaching is somewhat more likely, because it predicts higher apparent U-series ages for lower U-concentrations (see Fig. 8E,F) whereas general U-uptake would result in younger apparent U-series ages (see Fig. 8A,B). Leaching would also be corroborated by the γ spectrometric results on the skull (Fig. 11). Nevertheless, other explanations are also viable and the U-series data as such give no hint, as to which of these scenarios may be applicable. When modeling, it is clear that U-mobilization has taken place (apart from the fact the bones must have acquired their uranium post mortem in the first place), but virtually any modeling exercise yields similarly good (or bad) results. Nevertheless, if leaching in the 20% range had occurred, then the TIMS results would indeed overlap with the OSL window. Leaching of 20% of the uranium from the dentine of the tooth sample would also result in overlap with the ESR results (2-σ). Until recently, there were no data available that showed unequivocal U-leaching from dentine and it was thought, if it was happening at all, it would only be in exceptional circumstances. However, recent studies on a range of Australian megafauna sites provided such samples (Grün et al., in press) and U-leaching from dentine now seems possible in warm, semiarid environments. Perhaps it is worthwhile noting that all of Bowler et al.'s (2003) data are based on the application of a single dating technique. One systematic error source would have approximately the same effect on all individual dating results.

To sum up, disregarding all factors of what could possibly go wrong with OSL, if some U-leaching has occurred in the tissues analyzed by Thorne et al. (1999), the data could overlap with the results of Bowler et al. (2003). The discussion above shows that the two data sets are not entirely exclusive, however, one is really pushed hard when trying to reconcile them. Clearly more research is required. Laser ablation ICP-MS on bone profiles could lead to some understanding of the overall U-uptake his-

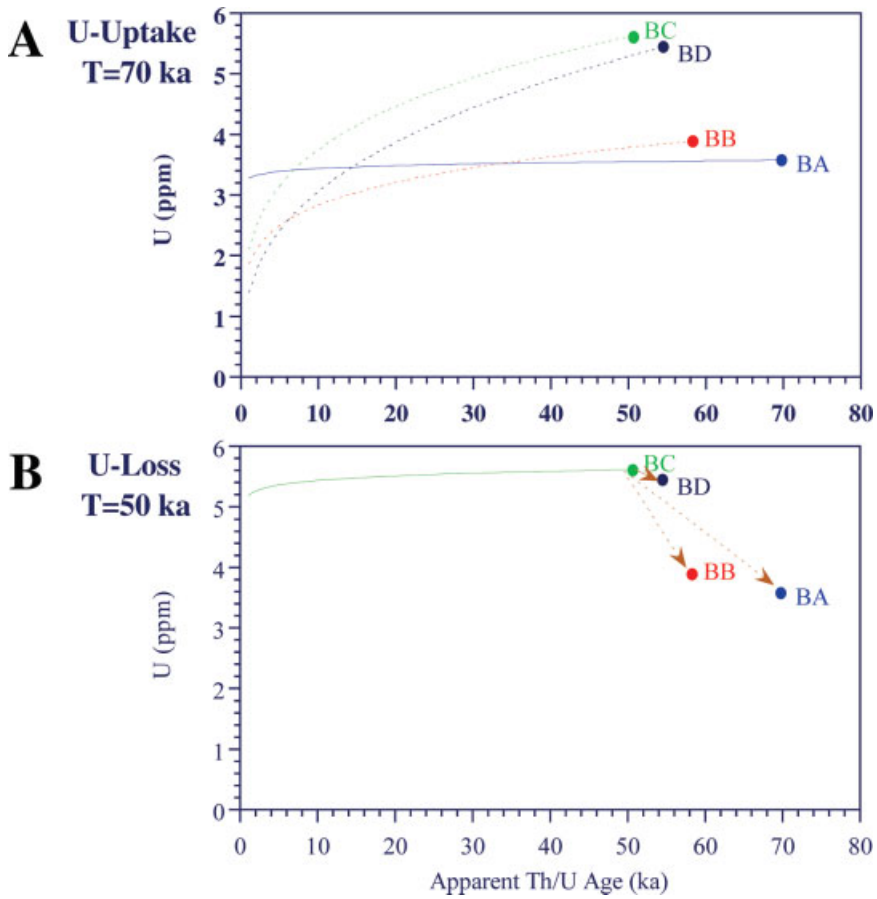

Fig. 40. Scenarios for U-uptake for the TIMS results on bone shavings (BA–BD) from Mungo 3. There is a trend of older apparent U-series ages with decreasing U-concentrations. This could either be caused by different adsorption rates (Fig. 40A), or an initial adsorption with subsequent different leaching rates (Fig. 40B). **A**: If LM3 was 70 ka old, the U-series results would imply different absorption rates into the bone sub-samples (similar to different volumes in Fig. 8). **B**: If LM3 was 50 ka old, the U-series results would imply different amounts of U-leaching. [Color figure can be viewed in the online issue, which is available at www.interscience.wiley.com.]

tory in the Mungo 3 bones and combined TIMS $^{230}Th/^{234}U$ and $^{231}Pa/^{235}U$ analysis may resolve the issue of the age of the Mungo 3 skeleton.

CONCLUSIONS

Some readers may find it surprising that the central topic of this review is the behavior of uranium and its daughter isotopes in bones and teeth. The element is highly mobile and it is our ability to reconstruct the history of uranium mobilization in the samples that holds the key for obtaining reliable age estimates on human fossils beyond the radiocarbon dating range. Greatly improved pretreatment techniques have recently provided a boost for radiocarbon dating opening the door for dating bones routinely to perhaps 55 ka (always on the proviso that the samples do actually contain pristine organic material of that age that can be extracted). Beyond the range of radiocarbon, numerical dating of human remains is only possible with U-series and ESR.

Inasmuch as one (i.e. I) would like to make a straightforward case for claiming general reliability for the dating approaches of human remains other than radiocarbon, there is obviously still a long way to go. Advances in technology and methodology now allow the virtual non-destructive analysis of human remains using ESR and laser ablation U-series. ESR has the inherent flaw of becoming useless for dating, when the radioactive environment of the dental material cannot be reconstructed. The dose values as such can at best be used for tentative age speculations. On the other hand, the better the radioactive environment can be reconstructed, the more significant is the geochronological information from ESR, particularly when used in conjunction with U-series dating. It seems that the review is a floccinaucinihilipilification of γ spectrometry for U-series dating analyses. The errors involved in the analysis usually (but not always!) prohibit a meaningful estimation of chronological results. γ Spectrometry nevertheless gives some insight into a general trend of U-mobilization in the bones. Th/U dating of bones and teeth certainly has value for providing minimum age estimates, however, for reliability, it seems advantageous to substantiate any Th/U results with either ESR (recognizing the restrictions outlined above), or to further develop combined mass-spectrometric Th/U–Pa/U dating. Whether or not AAR can be revived as a dating method for cave material remains to be seen.

Having been critical of the state-of-the-art of direct dating, one should perhaps not forget that conventional age assignments through associated material is potentially fraught with significantly more sources of chronological inaccuracies. As examples may serve the arguments of d'Errico et al. (1998), d'Errico and Goni (2003) for deciding, which sites show coherent stratigraphies and dating results, and which ones don't (see also responses by Mellars, 1999; Otte, 1999; Strauss, 1999 to the earlier paper with a response by Zilhao and d'Errico, 1999). In context of the Mungo 3 burial, serious, perhaps justified, concerns were raised about the relevance of samples some 300 m away from the burial. In extreme cases, the samples used for dating were collected hundreds of km away from the fossil (see discussion about the dating of the Herto fossils,

above). Problems arising from taxonomical issues, e.g. whether Lagar Velho is a Neanderthal hybrid (Duarte et al., 1999) or not (Tattersall and Schwartz, 1999) or whether *Homo floresiensis* (Brown et al., 2004) is related to *Homo erectus* (Falk et al., 2005a), a microcephalic *Homo sapiens* (Weber et al., 2005; Martin et al., 2006, see also reply by Falk et al., 2005b), an australopithecine (Hawks, 2005), or anything in between, are better left unexplored in the context of this paper. Here and in many other cases, direct dating analysis could provide crucial pieces to the puzzle that yields the correct chronology of human evolution.

ACKNOWLEDGMENTS

I thank Sara Stinson for initiating this paper, reminding me tirelessly about its due date and constructive comments. I thank four anonymous thoughtful referees for improving the manuscript. I thank Tegan Kelly, University of Tasmania, for corrections. I am very grateful to Fiona Grün for drawing the background of Figure 3, Konrad Hughen, Woods Hole Oceanographic Institution, for providing Figure 4, and Chris Stringer, Natural History Museum, London, for providing the photos in Figure 17. Alistair Pike, University of Bristol, kindly provided the original drawings for Figures 9 and 28.

LITERATURE CITED

Aitken MJ. 1985. Thermoluminescence dating. New York: Academic Press.

Aitken MJ. 1998. Optical dating. Oxford: Oxford University Press.

Aitken MJ, Xie J. 1990. Moisture correction for annual γ dose. Ancient TL 8:6–9.

Arnold JR, Libby WF. 1949. Age determinations by radiocarbon content: Checks with samples of known age. Science 110:678–680.

Arnold JR, Libby WF. 1951a. World-wide distribution of natural radiocarbon. Phys Rev 81:64–69.

Arnold JR, Libby WF. 1951b. Radiocarbon dates. Science 113: 111–120.

Bada L. 1985. Amino acid racemization of fossil bones. Annu Rev Earth Planet Sci 13:214–268.

Bada JL, Finkel R. 1982. Comment on Uranium series ages of the Del Mar Man and Sunnyvale skeletons. Science 217:755.

Bada JL, Helfman PM. 1975. Amino acid racemization dating of fossil bones. World Archaeol 7:160–173.

Bada JL, Schroeder RA, Carter GF. 1974. New evidence for the antiquity of man in North America deducted from aspartic acid racemization. Science 184:791–793.

Bada JL, Wang XS, Hamilton H. 1999. Preservation of key biomolecules in the fossil record: Current knowledge and future challenges. Philos Trans R Soc London. 354:77–87.

Bard E. 1997. Nuclide production by cosmic rays during the last ice age. Science 277:532–533.

Bard E. 1998. Geochemical and geophysical implications of the radiocarbon calibration. Geochim Cosmochim Acta 62:2025–2038.

Bard E, Arnold M, Hamelin B, Tisnerat-Laborde N, Cabioch G. 1998. Radiocarbon calibration by means of mass spectrometric $^{230}Th/^{234}U$ and ^{14}C ages of corals: An updated database including samples from Barbados, Mururoa and Tahiti. Radiocarbon 40:1085–1092.

Bard E, Hamelin B, Fairbanks RG, Zindler A. 1990. Calibration of ^{14}C timescale over the past 30,000 years using mass spectrometric U-Th ages from Barbados corals. Nature 345:405–410.

Barnola JM, Raynaud D, Korotkevich YS, Lorius C. 1987. Vostok ice core provides 160,000-year record of atmospheric CO_2. Nature 329:408–414.

Bar-Yosef O. 1989. Geochronology of the Levantine Middle Palaeolithic. In: Mellars P, Stringer, CB, editors. The human revolution: Behavioural and biological perspectives on the origin of modern humans. Edinburgh: Edinburgh University Press. p 589–610.

Bar-Yosef O, Callander J. 1999. The woman from Tabun: Garrod's doubts in historical perspective. J Hum Evol 37:879–885.

Bassinot FC, Labeyrie LD, Vincent E, Quidelleur X, Shackleton NJ, Lancelot Y. 1994. The astronomical theory of climate and the age of the Brunhes-Matuyama magnetic reversal. Earth Planet Sci Lett 126:91–108.

Beaumont PB. 1980. On the age of Border Cave hominids 1-5. Palaeontologia Africana 23:21–33.

Beaumont PB. 1994. Report to the KwaZulu Monuments Council on excavations at Border Cave near Ingwavuma in July–August 1987 and on the results of related investigations up until December 1993. Kimberley: McGregor Museum.

Beaumont PB, de Villiers H, Vogel JC. 1978. Modern man in sub-Saharan Africa prior to 49 000 years B.P.: A review and evaluation with particular reference to Border Cave. S Afr J Sci 74:409–419.

Beck JW, Richards DA, Edwards RL, Silverman BW, Smart PL, Donahue DJ, Hererra-Osterheld S, Burr GS, Calsoyas L, Jull AJT, Biddulph D. 2001. Extremely large variations of atmospheric ^{14}C concentration during the last glacial period. Science 292:2453–2458.

Bender ML. 1974. Comment on reliability of amino acid racemization dating and paleotemperature analysis on bones. Nature 252:378–381.

Bird MI, Ayliffe JK, Fifield LK, Turney CSM, Cresswell RG, Barrows TT, David B. 1999. Radiocarbon dating of "old" charcoal using a wet oxidation, stepped-combustion procedure. Radiocarbon 41:1–14.

Bird MI, Fifield LK, Santos GM, Beaumont PB, Zhou Y, di Tada ML, Hausladen PA. 2003. Radiocarbon dating from 40 to 60 ka BP at Border Cave, South Africa. Quaternary Sci Rev 22:943–947.

Bischoff JL, Rosenbauer RJ. 1981. Uranium series dating of human skeletal remains from the Del Mar and Sunnyvale sites, California. Science 213:1003–1005.

Bischoff JL, Rosenbauer RJ. 1982. Reply. Science 217:756.

Bischoff JL, Rosenbauer RJ, Moench AF, Ku TL. 1995. U-series age equations for uranium assimilation by fossil bones. Radiochim Acta 69:127–135.

Blanc AC. 1939. L'homme fossile du Mont Circé. L'Anthroplogie 49:253–264.

Bocquet-Appel JP, Demars PY. 2000. Neanderthal contradiction and modern human colonization of Europe. Antiquity 74:544–552.

Bourdon B, Henderson GM, Lundstrom CC, Turner SP, editors. 2003. Uranium-series geochemistry. Reviews in Mineralogy and Geochemistry, Vol. 52. Washington, DC: Mineralogical Society of America.

Bowler JM. 1998. Willandra Lakes revisited: Environmental framework for human occupation. Archaeol Oceania 33:120–155.

Bowler JM, Johnston H, Olley JM, Prescott JR, Roberts RG, Shawcross W, Spooner NA. 2003. New ages for human occupation and climatic change at Lake Mungo, Australia. Nature 421:837–840.

Bowler JM, Jones R, Allen H, Thorne AG. 1970. Pleistocene human remains from Australia: A living site and human cremation from Lake Mungo, western New South Wales. World Archaeol 2:39–60.

Bowler JM, Magee JW. 2000. Redating Australia's oldest human remains: A sceptic's view. J Hum Evol 38:719–726.

Bowler JM, Thorne AG. 1976. Human remains from Lake Mungo. In: Kirk RL, Thorne AG, editors. The origin of the Australians. Canberra: Australian Institute of Aboriginal Studies. p 127–138.

Bowman SGE. 1976. Thermoluminescence dating, the evaluation of radiation dosage, Unpublished PhD Thesis. Oxford: University of Oxford.

Brennan BJ, Rink WJ, McGuirl EL, Schwarcz HP, Prestwich WV. 1997. β Doses in tooth enamel by "One Group" theory and the Rosy ESR dating software. Radiat Meas 27:307–314.

Brik A, Haskell E, Brik V, Scherbina O, Atamanenko O. 2000. Anisotropy effects of EPR signals and mechanisms of mass transfer in tooth enamel and bones. Appl Radiat Isot 52: 1077–1083.

Brik AS, Haskell EH, Scherbina OI, Brik VB, Atamanenko ON. 1998. Alignment of CO_2- radicals of tooth enamel with heating. Mineralogie J (Kiev) 20:46–60.

Brink JS. 1987. The archaeozoology of Florisbad, Orange Free State. Memoirs Van Die Nasionale Museum Bloemfontein 24:1–151.

Brink JS. 1988. The taphonomy and palaeoecology of the Florisbad spring fauna. Palaeoecol Afr 19:169–179.

Bronk Ramsey C. 2001. Development of the radiocarbon calibration program. Radiocarbon 43:355–363.

Bronk Ramsey C. 2005. OxCal Program v3.10 (http://www.rlaha.ox.ac.uk/oxcal/oxcal.htm).

Bronk Ramsey C, Higham T, Bowles A, Hedges REM. 2004a. Improvements to the pretreatment of bone at Oxford. Radiocarbon 46:155–163.

Bronk Ramsey C, Higham T, Leach P. 2004b. Towards high-precision AMS: Progress and limitations. Radiocarbon 46:17–24.

Bronk Ramsey C, Pettitt PB, Hedges REM, Hodgins GWL, Owen DC. 2000a. Radiocarbon dates from the Oxford AMS system, Archaeometry datelist 29. Archaeometry 41:243–254.

Bronk Ramsey C, Pettitt PB, Hedges REM, Hodgins GWL, Owen DC. 2000b. Radiocarbon dates from the Oxford AMS system, Archaeometry datelist 30. Archaeometry 41:459–479.

Broom R. 1929. The Transvaal fossil human skeleton. Nature 123:415–416.

Brown P. 2000. Australian Pleistocene variation and the sex of Lake Mungo 3. J Hum Evol 38:743–749.

Brown P, Sutikna T, Morwood MJ, Soejono RP, Jatmiko, Saptomo EW, Due RA. 2004. A new small-bodied hominin from the Late Pleistocene of Flores, Indonesia. Nature 431:1055–1061.

Brumby S. 1992. Regression analysis of ESR/TL dose response data. Radiat Meas 20:595–599.

Buck CE, Cavanagh WG, Litton CD. 1996. Bayesian approach to interpreting archaeological data. Chichester: Wiley.

Burr GS, Beck JW, Taylor FW, Recy J, Edwards RL, Cabioch G, Carriere T, Danahue DJ, O'Malley JM. 1998. A high resolution radiocarbon calibration between 11,700 and 12,400 calendar years BP derived from ^{230}Th ages of corals from Espiritu Santo Island, Vanuatu. Radiocarbon 40:1093–1105.

Callens F, Moens P, Verbeeck R. 1995. An EPR study of intact and powdered human tooth enamel dried at 400°C. Calcif Tissue Int 56:543–548.

Callens F, Vanhaelewyn G, Matthys P. 2002. Some recent multifrequency electron paramagnetic resonance results on systems relevant for dosimetry and dating. Spectrochim Acta Part A 58:1321–1328.

Callens FJ, Verbeeck RMH, Matthys PFA, Martens LC, Boesman ER. 1987. The contribution of CO_3^{3-} and CO_2^- to the ESR spectrum near $g = 2$ of powdered human tooth enamel. Calcif Tissue Int 41:124–129.

Chappell J, Head J, Magee J. 1996. Beyond the radiocarbon limit in Australian archaeology and Quaternary research. Antiquity 70:543–552.

Chen T, Yang Q, Wu E. 1994. Antiquity of *Homo sapiens* in China. Nature 368:55,56.

Chen TM, Yuan S. 1988. Uranium-series dating of bones and teeth from Chinese Palaeolithic sites. Archaeometry 30: 59–76.

Cheng H, Edwards RL, Hoff J, Gallup CD, Richards DA, Asmerom Y. 2000. The half-lives of uranium-234 and thorium-230. Chem Geol 169:17–33.

Cheng H, Edwards RL, Murrell MT, Benjamin TM. 1998. Uranium-thorium-protactinium dating systematics. Geochim Cosmochim Acta 62:3437–3452.

Cherdyntsev VV. 1971. Uranium-234. Jerusalem: Israel Program for Scientific Translations.

Clark JD, Beyene Y, WoldeGabriel G, Hart WK, Renne PR, Gilbert H, Defleurq A, Suwa G, Katoh S, Ludwig KR, Boisserie JR, Asfawkk B, White TD. 2003. Stratigraphic, chronological and behavioural contexts of Pleistocene *Homo sapiens* from Middle Awash, Ethiopia. Nature 423:747–752.

Clarke RJ. 1985 A new reconstruction of the Florisbad cranium, with notes on the site. In: Delson E, editor. Ancestors: The hard evidence. New York: Alan Liss. p 301–355.

Conard NJ, Bolus M. 2003. Radiocarbon dating the appearance of modern humans and timing of cultural innovations in Europe: New results and new challenges. J Hum Evol 44: 331–371.

Conard NJ, Grootes PM, Smith FH. 2004. Unexpectedly recent dates for human remains from Vogelherd. Nature 430:198–201.

Constans LG. 1985. Diplomatari de Banyoles. I. Banyoles: Centre d'Estudis Comarcals.

Coppa A, Grün R, Stringer C, Eggins S, Vargiu R. 2005. Newly recognized Pleistocene teeth from Tabun Cave, Israel. J Hum Evol 49:301–315.

Deacon HJ, Talma AS, Vogel JC. 1988. Biological and cultural development of Pleistocene people in an old world southern continent. In: Prescott JR, editor. Early Man in the southern hemisphere. Supplement to Archaeometry: Australian Studies. Adelaide: Univeristy of Adelaide. p S23–S31.

de Lumley H. 1982. Origine et évolution de l'Homme. Paris: Laboratoire de Préhistoire du Musée de l'Homme.

de Lumley MA. 1971/ 2. La mandíbula de Bãnolas. Ampurias 33/34:1–91.

de Lumley MA. 1973. Anténéandertaliens et Néandertaliens du bassin méditerranéen occidental européen. Études Quaternaires, 2, Marseille.

d'Errico F, Goni MFS. 2003. Neandertal extinction and the millennial scale climatic variability of OIS 3. Quaternary Sci Rev 22:769–788.

d'Errico F, Zilhao J, Julien M, Baffier D, Pelegrin J. 1998. Neanderthal acculturation in western Europe? A critical review of the evidence and its interpretation. Curr Anthropol 39(Suppl.): S1–S44.

Dreyer TF. 1938. The archaeology of the Florisbad deposits. Argeol Navors nas Mus Bloemfontein 1:65–77.

Duarte C, Mauricio J, Pettitt PB, Souto P, Trinkaus E, Van Der Plicht H, Zilhao J. 1999. The early Upper Paleolithic human skeleton from the Abrigo do Lagar Velho (Portugal) and modern human emergence in Iberia. Proc Natl Acad Sci USA 96:7604–7609.

Edwards RL, Chen JH, Ku TL, Wasserburg GJ. 1987b. Precise timing of the last interglacial period from mass spectrometric determination of thorium-230 in corals. Science 236:1547–1553.

Edwards RL, Chen JH, Wasserburg GJ. 1987a. ^{238}U-^{234}U-^{230}Th-^{232}Th systematics and the precise measurement of time over the past 500,000 years. Earth Planet Sci Lett 81:175–192.

Edwards RL, Cheng H, Murrell MT, Goldstein SJ. 1997. Protactinium-231 dating of carbonates by thermal ionization mass spectrometry: Implications for Quaternary climate change. Science 276:782–786.

Eggins SM, Grün R, McCulloch M, Pike A, Chappell J, Kinsley L, Shelley M, Murray-Wallace C, Spötl C, Taylor L. 2005. In situ U-series dating by laser-ablation multi-collector ICPMS: New prospects for Quaternary geochronology. Quaternary Sci Rev 24:2523–2538.

Eggins S, Grün R, Pike A, Shelley A, Taylor L. 2003. ^{238}U, ^{232}Th profiling and U-series isotope analysis of fossil teeth by laser ablation-ICPMS. Quaternary Sci Rev 22:1373–1382.

Engel MH, Hare PE. 1985. Gas liquid chromatographic separation of amino acids and their derivatives. In: Garret GC, editor. Chemistry and biochemistry of amino acids. New York: Chapman and Hall. p 462–479.

Falk D, Hildebolt C, Smith K, Morwood MJ, Sutikna T, Brown P, Jatmiko, Saptomo EW, Brunsden B, Prior F. 2005a. The brain of LB1, Homo floresiensis. Science 308:242–245.

Falk D, Hildebolt C, Smith K, Morwood MJ, Sutikna T, Jatmiko, Saptomo EW, Brunsden B, Prior F. 2005b. Response to comment on "The brain of LB1, Homo floresiensis". Science 310:236.

Faupl P, Richter W, Urbanek C. 2003. Dating of the Herto hominin fossils. Nature 426:621–622.
Finkel R, Suter M. 1993. AMS in the earth sciences: techniques and applications. Adv Anal Chem 1:1–114.
Garrod D, Bate D. 1937. The Stone age of Mount Carmel, Vol. 1. Oxford: Oxford University Press.
Gillespie R, Roberts RG. 2000. On the reliability of age estimates for human remains at Lake Mungo. J Hum Evol 38: 727–732.
Goldstein SJ, Stirling CH. 2003. Techniques for measuring uranium-series nuclides: 1992–2002. Rev Mineral Geochem 52: 23–57.
Goslar T, Hercman H, Pazdur A. 2000. Comparison of U-series and radiocarbon dates of speleothems. Radiocarbon 42:403–414.
Grün R. 1986. β dose attenuation in thin layers. Ancient TL 4:1–8.
Grün R. 1987. α dose attenuation in thin layers. Ancient TL 5:6–8.
Grün R. 1989. Electron spin resonance (ESR) dating. Quaternary Int 1:65–109.
Grün R. 1995. Semi non-destructive, single aliquot ESR dating. Ancient TL 13:3–7.
Grün R. 1996. Errors in the dose assessment introduced by the use of the "linear part" of a saturating dose response curve. Radiat Meas 26:297–302.
Grün R. 1997. Electron spin resonance dating. In: Taylor RE, Aitken MJ, editors. Chronometric dating in archaeology. New York: Plenum. p 217–261.
Grün R. 2000a. Electron spin resonance dating. In: Ciliberto E, Spoto G, editors. Modern analytical methods in art and archaeology chemical analyses, Series 155. New York: Wiley. p 641–679.
Grün R. 2000b. Dating beyond the radiocarbon barrier using U-series isotopes and trapped charges. In: Creagh DC, Bradley DA, editors. Radiation in art and archeometry. Amsterdam: Elsevier. p 472–493.
Grün R. 2000c. An alternative for model for open system U-series/ESR age calculations: (Closed system U-series)-ESR, CSUS-ESR. Ancient TL 18:1–4.
Grün R. 2001. Trapped charge dating (ESR TL OSL). In: Brothwell DR, Pollard AM, editors. Handbook of archaeological sciences. Chichester: Wiley. p 47–62.
Grün R. 2002. ESR dose estimation on fossil tooth enamel by fitting the natural spectrum into the irradiated spectrum. Radiat Meas 35:87–93.
Grün R. Electron spin resonance dating. Encyclopedia of Quaternary science. Elsevier, in press.
Grün R. 2006. A simple method for the rapid assessment of the qualitative ESR response of fossil samples to laboratory irradiation. Radiat Meas 41:682–689.
Grün R, Abeyratne M, Head J, Tuniz C, Hedges REM. 1997. AMS ^{14}C analysis of teeth from archaeological sites showing anomalous ESR dating results. Quaternary Sci Rev 16:437–444.
Grün R, Beaumont P. 2001. Border Cave revisited: A revised ESR chronology. J Hum Evol 40:467–482.
Grün R, Beaumont P, Stringer CB. 1990. ESR dating evidence for early modern humans at Border Cave in South Africa. Nature 344:537–539.
Grün R, Beaumont P, Tobias PV, Eggins S. 2003. On the age of Border Cave 5 human mandible. J Hum Evol 45:155–167.
Grün R, Brink JS, Spooner NA, Taylor L, Stringer CB, Franciscus RG, Murray AS. 1996. Direct dating of Florisbad hominid. Nature 382:500–501.
Grün R, Brumby S. 1994. The assessment of errors in the past radiation doses extrapolated from ESR/TL dose response data. Radiat Meas 23:307–315.
Grün R, Eggins S, Wells RT, Rhodes E, Bestland E, Spooner N, Forbes M, McCulloch M. A cautionary tale from down-under: Dating the Black Creek Swamp megafauna site on Kangaroo Island, South Australia. Quaternary Geochronology 1:142–150.
Grün R, Katzenberger-Apel O. 1994. An α irradiator for ESR dating. Ancient TL. 12:35–38.
Grün R, Maroto J, Eggins S, Stringer C, Robertson S, Taylor L, Mortimer G, McCulloch M. 2006. ESR and U-series analyses of enamel and dentine fragments of the Banyoles mandible. J Hum Evol 50:347–358.
Grün R, Schwarcz HP. 2000. Revised U-series/ESR model ages for teeth from the Hoxnian type locality. Quaternary Sci Rev 19:1151–1154.
Grün R, Schwarcz HP, Chadam JM. 1988. ESR dating of tooth enamel: Coupled correction for U-uptake and U-series disequilibrium. Nucl Tracks Radiat Meas 14:237–241.
Grün R, Spooner NA, Thorne A, Mortimer G, Simpson JJ, McCulloch MT, Taylor L, Curnoe D. 2000. Age of the Lake Mungo 3 skeleton, reply to Bowler & Magee and to Gillespie & Roberts. J Hum Evol 38:733–741.
Grün R, Stringer C, McDermott F, Nathan R, Porat N, Robertson S, Taylor L, Mortimer G, Eggins S, McCulloch M. 2005. U-series and ESR analyses of bones and teeth relating to the human burials from Skhul. J Hum Evol 49:316–334.
Grün R, Stringer CB. 1991. ESR dating and the evolution of modern humans. Archaeometry 33:153–199.
Grün R, Stringer CB. 2000. ESR and U-series analyses of dental material from Tabun C1. J Hum Evol 39:601–612.
Grün R, Stringer CB, Schwarcz HP. 1991. ESR dating of teeth from Garrod's Tabun Cave collection. J Hum Evol 20:231–248.
Grün R, Ward K. 2002. A long-term fading study for ESR intensity measurement and dose evaluation on fossil tooth enamel. Radiat Meas 35:269–274.
Grün R, Wells R, Eggins S, Spooner N, Aubert M, Brown L, Rhodes E. Electron spin resonance dating of Australia megafauna sites. Aust J Earth Sci, in press.
Hare PE. 1969. Geochemistry of proteins, peptides and amino acids. In: Eglington G, Murphy MTJ, editors. Organic geochemistry. Berlin: Springer. p 438–463.
Hare PE, Hoering TC, King Je K, editors. 1980. Biogeochemistry of amino acids. New York: Wiley.
Hare PE, von Endt DW, Kokis JE. 1997. Protein and amino acid diagenesis dating. In: Taylor RE, Aitken MJ, editors. Chronometric dating in archaeology. New York: Plenum. p 261–296.
Hart WK, WoldeGabriel G, Katoh S, Renne PR, Suwa G, Asfaw B, White TD. 2003. A reply to Faupl et al. Nature 426: 622.
Hassan AA, Termine JD, Haynes CV Jr. 1977. Mineralogical studies on bone apatite and their implications for radiocarbon dating. Radiocarbon 19:364–374.
Hawks J. 2005. www.johnhawks.net/weblog/fossils/flores/.
Hedges REM. 2000. Radiocarbon dating. In: Ciliberto E, Spoto G, editors. Modern analytical methods in art and archaeology. Chemical Analyses Series 155. New York: Wiley. p 465–502.
Hedges REM, Housley RA, Pettitt PB, Bronk Ramsey C, van Klinken GJ. 1996b. Radiocarbon dates from the Oxford AMS system: Archaeometry data list 21. Archaeometry 38: 181–207.
Hedges REM, Lee-Thorp JA, Tuross NC. 1996a. Is tooth enamel carbonate a suitable material for radiocarbon dating? Radiocarbon 37:285–290.
Hernández-Pacheco E, Obermaier H. 1915. La mandíbula neandertaloide de Bañolas. Comisión de Investigaciones Paleontológicas y Prehistóricas, 6, Madrid.
Higham T, Bronk Ramsey C, Karavanic I, Smith FH, Trinkaus E. 2006a. Revised direct radiocarbon dating of the Vindija G(1) upper Paleolithic Neandertals. Proc Natl Acad Sci USA 103:553–557.
Higham T, Petchey F. 2000. Radiocarbon dating in archaeology: Methods and applications. In: Creagh DC, Bradley DA, editors. Radiation in art and archaeometry. Amsterdam: Elsevier. p 255–284.
Higham TFG, Jacobi RM, Bronk Ramsey C. 2006b. AMS radiocarbon dating of ancient bone using ultrafiltration. Radiocarbon 48:179–195.
Hughen KA, Lehman S, Southon J, Overpeck J, Marchal O, Herring CJ, Turnbull C. 2004a. ^{14}C activity and global carbon cycle changes over the past 50,000 years. Science 303: 202–207.
Hughen KA, Baillie MGL, Bard E, Beck JW, Bertrand CJH, Blackwell PG, Buck CE, Burr GS, Cutler KB, Damon PE,

Edwards RL, Fairbanks RG, Friedrich M, Guilderson TP, Kromer B, McCormac G, Manning S, Bronk Ramsey C, Reimer PJ, Reimer RW, Remmele S, Southon JR, Stuiver M, Talamo S, Taylor FW, van der Plicht J, Weyhenmeyer CE. 2004b. MARINE04 marine radiocarbon age calibration, 0-26 cal kyr BP. Radiocarbon 46:1059–1086.

Ikeya M. 1993. New applications of electron spin resonance—Dating, Dosimetry and Microscopy. Singapore: World Scientific.

Ivanovich M, Harmon RS, editors. 1992. Uranium series disequilibrium: Application to environmental problems in the earth sciences. Oxford: Oxford University Press.

Jacobi RM, Higham TFG, Bronk Ramsey C. 2006. AMS radiocarbon dating of Middle and Upper Palaeolithic bone in the British Isles: Improved reliability using ultrafiltration. J Quaternary Sci 21:557–573.

Jelinek AJ. 1982a. The Middle Paleolithic in the Southern Levant with comments on the appearance of modern man (*Homo sapiens*). In Ronen A, editor. The transition from lower to Middle Paleolithic and the origin of modern man. BAR International Series.151:57–101.

Jelinek AJ. 1982b. The Tabun Cave and Paleolithic man in the Levant. Science 216:1369–1375.

Johnson BJ, Miller GH. 1997. Archaeological applications of amino acid racemization. Archaeometry 39:265–287.

Julià R, Bischoff JL. 1991. Radiometric dating of Quaternary deposits and the hominid mandible of Lake Banyolas, Spain. J Archaeol Sci 18:707–722.

Karavanic I, Paunovic M, Yokoyama Y, Falgueres C. 1998. Neanderthals and Upper Palaeolithic in Vindija Cave, Croatia: Controversies about layer G1. l'Anthropologie 102:131–141.

Karavanic I, Smith FH. 1998. The Middle/Upper Paleolithic interface and the relationship of Neanderthals and early modern humans in the Hrvatsko Zagorje, Croatia. J Hum Evol 34:223–248.

Karavanic I, Smith FH. 2000. More on the Neanderthal problem: The Vindija case. Curr Anthropol 41:838–840.

Kaufman DS, Manley WF. 1998. A new procedure for determining DL amino acid ratios in fossils using reverse phase liquid chromatography. Quaternary Sci Rev 17:987–1000.

Kitagawa H, van der Plicht J. 1998a. A 40,000 year varve chronology from Lake Suigetsu, Japan: Extension of the ^{14}C calibration curve. Radiocarbon 40:505–515.

Kitagawa H, van der Plicht J. 1998b. Atmospheric radiocarbon calibration to 45,000 year BP: Late glacial fluctuations and cosmogenic isotope production. Science 279:1187–1190.

Kitagawa H, van der Plicht J. 2000. Atmospheric radiocarbon calibration beyond 11,900 BP from Lake Siugetsu laminated sediments. Radiocarbon 42:369–380.

Kramer A, Crummett TL, Wolpoff MH. 2001. Out of Africa and into the Levant: Replacement or admixture in Western Asia. Quaternary Int 75:51–63.

Krbetschek MR, Trautmann T, Dietrich A, Stolz W. 2000. Radioluminescence dating of sediments: Methodological aspects. Radiat Meas 32:493–498.

Ku TL. 2000. Uranium-series methods. In: Noller JS, Sowers JM, Lettis WR, editors. Quaternary geochronology methods and applications. Washington, DC: American Geophysical Union. p 101–114.

Latham AG. 2001. Uranium-series dating. In: Brothwell DR, Pollard AM, editors. Handbook of archaeological sciences. Chichester: Wiley. p 63–72.

Leitner-Wild E, Steffan I. 1993. Uranium-series dating of fossil bones from Alpine caves. Archaeometry 35:137–146.

Leveque F, Vandermeersch B. 1980. Discovery of a human fossil in a Castelperronien layer at Saint-Cesaire (Charente-maritime). CR Acad Sci Paris, Serie D 291:187–189.

Levin I, Kromer B, Francey RJ. 1996. Continuous measurements of ^{14}C in atmospheric CO_2 at Cape Grim. In: Francey RJ, Dick AL, Dereck N, editors. Baseline atmospheric program Australia 1994–1995. Melbourne: CSIRO. p 106–107.

Liritzis Y. 1980. $^{230}Th/^{234}U$ dating of speleothems in Petralona. Anthropos (Athens) 7:143–150.

Liritzis Y. 1982. Petralona dating controversy. Nature 299: 280–281.

Loosli HH, Heimann M, Oeschger H. 1980. Low-level gas proportional counting in an underground laboratory. Radiocarbon 22:461–469.

Ludwig KR. 2001. User manual for Isoplot/Ex rev. 2.49. Berkeley Geochronology Centre, Special Publication 1a.

Ludwig KR. 2003. Mathematical-statistical treatment of data and errors for $^{230}Th/U$ geochronology. Rev Mineral Geochem 52:631–656.

Ludwig KR, Titterington DM. 1994. Calculation of $^{230}Th/U$ isochrons, ages, and errors. Geochim Cosmochim Acta 58:5031–5042.

Lyon AJ. 1970. Dealing with data. Oxford: Pergamon Press.

Mann WB, Marlow WF, Hughes EE. 1961. The half-life of carbon-14. Int J Appl Radiat Isot 11:57–67.

Manning MR, Melhuish WH. 1994. Atmospheric ^{14}C record from Wellington. In: Trends: A compendium of data on global change. Carbon Dioxide Information Analysis Center, Oak Ridge National Laboratory, US Department of Energy, Oak Ridge, Tennessee, USA. (Digital data on http://cdiac.esd.ornl.gov/trends/co2/welling.htm).

Maroto J, editor. 1993. La mandíbula de Banyoles en el context dels fòssils humans del pleistocè. Sèrie monogràphica 13. Girona: Centre d'Investigacions Arqueològiques.

Marsh RE. 1999. β-gradient isochrons using electron paramagnetic resonance: Towards a new dating method in archaeology. MSc thesis, McMaster University, Hamilton.

Martin RD, MacLarnon AM, Phillips JL, Dussubieux L, Williams PR, Dobyns WB. 2006. Comment on "The Brain of LB1, *Homo floresiensis*". Science 216:999b.

Masters PM, Bada JL. 1978. Amino acid racemization dating of bone and shell. Adv Chem 171:117–138.

McBrearty S, Brooks AS. 2000. The revolution that wasn't: A new interpretation of the origin of modern human behavior. J Hum Evol 39:453–563.

McCown TD. 1937. Mugharet Es-Skhul. Description and excavations. In: Garrod DA, Bate DMA, editors. The Stone Age of Mount Carmel, Vol 1: Excavations at the Wady El-Mughara. Oxford: Clarendon Press. p 91–107.

McCown TD, Keith A. 1939. The Stone Age of Mount Carmel, Vol. 2. The fossil human remains from the Levalloiso-Mousterian. Oxford: Clarendon Press.

McDermott F, Grün R, Stringer CB, Hawkesworth CJ. 1993. Mass-spectrometric U-series dates for Israeli Neanderthal/early modern hominid sites. Nature 363:252–255.

McDermott F, Stringer C, Grün R, Williams CT, Din VK, Hawkesworth CJ. 1996. New Late-Pleistocene Uranium-Thorium and ESR dates for the Singa hominid (Sudan). J Hum Evol 31:507–516.

McDougall I, Brown FH, Fleagle JG. 2005. Stratigraphic placement and age of modern humans from Kibish, Ethiopia. Nature 433:733–736.

Mellars P. 1999. The Neanderthal problem continued. Curr Anthropol 40:341–350.

Mellars P. 2004. Neanderthals and the modern human colonization of Europe. Nature 432:461–465.

Mellars P. 2006. A new radiocarbon revolution and the dispersal of modern humans in Eurasia. Nature 439:931–935.

Mercier N, Valladas H, Bar-Yosef O, Vandermeersch B, Stringer C, Joron J-L. 1993. Thermoluminescence date for the Mousterian burial site of Es-Skhul, Mt. Carmel. J Archaeol Sci 20:169–174.

Mercier N, Valladas H, Valladas G. 1995a. Flint thermoluminescence dates from the CFR laboratory at Gif: Contributions to the study of the chronology of the Middle Palaeolithic. Quaternary Sci Rev 14:351–364.

Mercier N, Valladas H, Valladas G, Reyss JL, Jelinek A, Meignen L, Joron JL. 1995b. TL dates of burnt flints from Jelinek's Excavations at Tabun and their implications. J Archaeol Sci 22:495–509.

Millard AR. 1993. Diagenesis of archaeological bone: The case of uranium uptake. DPhil Thesis, University of Oxford, Oxford, UK.

Millard AR, Hedges REM. 1996. A diffusion-adsorption model of uranium uptake by archaeological bone. Geochim Cosmochim Acta 60:2139–2152.

Miller GH, Beaumont PB, Deacon HJ, Brooks AS, Hare PE, Jull AJT. 1999. Earliest modern humans in southern Africa dated by isoleucine epimerization in ostrich eggshell. Quaternary Sci Rev 18:1537–1548.

Miller GH, Brigham-Grette J. 1989. Amino acid geochronology: Resolution and precision in carbonate fossils. Quaternary Int 1:111–128.

Miller GH, Hart CP, Roark EB, Johnson BJ. 2001. Isoleucine epimerization in eggshells of the flightless Australian birds, *Genyornis* and *Dromaius*. In: Goodfriend GA, Colins MJ, Fogel ML, Macko SA, Wehmiller JF, editors. Perspectives in amino acid and protein geochemistry. New York: Oxford University Press.

Miller GH, Magee JW, Johnston BJ, Fogel ML, Spooner NA, McCulloch MT, Ayliffe LK. 1997a. Pleistocene extinction of *Genyornis newtoni*: Human impact on the Australian megafauna. Science 283:205–208.

Miller GH, Magee JW, Jull AJT. 1997b. Low-latitude glacial cooling in the Southern Hemisphere from amino acids in emu eggshells. Nature 385:241–244.

Morwood MJ, Brown P, Jatmiko, Sutikna T, Saptomo EW, Westaway KE, Due RA, Roberts RG, Maeda T, Wasisto S, Djubiantono T. 2005. Further evidence for small-bodied hominins from the Late Pleistocene of Flores, Indonesia. Nature 437: 1012–1017.

Morwood MJ, Soejono RP, Roberts RG, Sutikna T, Turney CSM, Westaway KE, Rink WJ, Zhao JX, van den Bergh GD, Due RA, Hobbs DR, Moore MW, Bird MI, Fifield LK. 2004. Archaeology and age of a new hominin from Flores in eastern Indonesia. Nature 431:1087–1091.

Murray AS, Wintle AG. 2000. Luminescence dating of quartz using an improved single-aliquot regenerative-dose protocol. Radiat Meas 32:57–73.

Murray-Wallace CV. 1993. A review of the application of the amino acid racemisation reaction to archaeological dating. The Artefact 16:19–26.

Murray-Wallace CV, Brooke BP, Cann JH, Belperio AP, Bourman RP. 2001. Whole-rock aminostratigraphy of the Coorong Coastal Plain, South Australia: Towards a 1 million year record of sea-level highstands. J Geol Soc London 158:111–124.

Nathan R, Grün R. 2003. γ dosing and shielding of a human tooth by a mandible and skull cap. Ancient TL 21:79–84.

Newesely H. 1989. Fossil bone apatite. Appl Geochem 4:233–245.

Noller JS. 2000. Lead-210 geochronology. In: Noller JS, Sowers JM, Lettis WR, editors. Quaternary geochronology methods and applications. Washington, DC: American Geophysical Union. p 115–120.

Noller JS, Sowers JM, Lettis WR, editors. 2000. Quaternary geochronology methods and applications. Washington, DC: American Geophysical Union.

Nydahl R, Lövseth K. 1983. Tracing bomb ^{14}C in the atmosphere 1962–1980. J Geophys Res 88:3621–3642.

Oakley KP, Campbell BG, Molleson TI. 1975. Catalogue of fossil hominids, Part 3: Americas, Asia, Australia. London: British Museum (Natural History).

Otte M. 1999. The Neanderthal problem continued. Curr Anthropol 40:350–352.

Oyston B. 1996. Thermoluminescence age determinations for the Mungo III human burial, Lake Mungo, southeastern Australia. Quaternary Sci Rev 15:739–749.

Petit JR, Jouzel J, Raynaud D, Barkov NI, Barnola JM, Basile I, Bender M, Chappellaz J, Davis M, Delaygue G, Delmotte M, Kotlyakov VM, Legrand M, Lipenkov VY, Lorius C, Pepin L, Ritz C, Saltzman E, Stievenard M. 1999. Climate and atmospheric history of the past 420,000 years from the Vostok ice core, Antarctica. Nature 399:429–436.

Pettitt PB, Pike AWG. 2001. Blind in a cloud of data: Problems with the chronology of Neanderthal extinction and anatomically modern human expansion. Antiquity 75:415–420.

Piepenbrink H. 1989. Examples of chemical changes during fossilisation. Appl Geochem 4:273–280.

Pike AWG. 2000. Uranium series dating of archaeological bone by thermal ionization mass spectrometry. DPhil Thesis, University of Oxford, Oxford, UK.

Pike AWG, Eggins S, Grün R, Hedges REM, Jacobi RM. 2005. U-series dating of the Late Pleistocene mammalian fauna from Wood Quarry (Steetley), Nottinghamshire, UK. J Quaternary Sci 20:59–65.

Pike AWG, Eggins S, Grün R, Thackeray F. 2004. U-series dating of TP1, an almost complete human skeleton from Tuinplaas (Springbok Flats), South Africa. S Afr J Sci 100:381–383.

Pike AWG, Hedges REM, Van Calsteren P. 2002. U-series dating of bone using the diffusion-adsorption model. Geochim Cosmochim Acta 66:4273–4286.

Pike AWG, Pettitt PB. 2003. U-series dating and human evolution. Rev Mineral Geochem 52:607–630.

Prescott JR, Hutton JT. 1988. Cosmic ray and γ ray dosimetry for TL and ESR. Nucl Tracks Radiat Meas 14:223–227.

Prescott JR, Hutton JT. 1994. Cosmic ray contributions to dose rates for luminescence and ESR dating: Large depths and long-term time variations. Radiat Meas 23:497–500.

Prescott JR, Hutton JT. 1995. Environmental dose rates and radioactive disequilibrium from some Australian luminescence dating sites. Quaternary Sci Rev 14:439–448.

Prescott JR, Robertson GB. 1997. Sediment dating by luminescence: A review. Radiat Meas 27:893–922.

Rae A, Hedges EM, Ivanovich M. 1989. Further studies of uranium series dating of fossil bone. Appl Geochem 4:331–337.

Rae AM, Ivanovich M. 1986. Successful application of uranium series dating of fossil bone. Appl Geochem 1:419–426.

Reimer PJ, Baillie MGL, Bard E, Bayliss A, Beck JW, Bertrand, CJH, Blackwell PG, Buck CE, Burr GS, Cutler KB, Damon PE, Edwards RL, Fairbanks RG, Friedrich M, Guilderson TP, Hogg AG, Hughen KA, Kromer B, McCormac G, Manning S, Bronk Ramsey C, Reimer RW, Remmele S, Southon JR, Stuiver M, Talamo S, Taylor FW, van der Plicht J, Weyhenmeyer CE. 2004. INTCAL04 terrestrial radiocarbon age calibration, 0-26 cal kyr BP. Radiocarbon 46:1029–1059.

Reimer PJ, Baillie MGL, McCormac G, Reimer RW, Bard E, Beck JW, Blackwell PG, Buck CE, Burr GS, Edwards RL, Friedrich M, Guilderson TP, Guilderson TP, Hogg AG, Hughen KA, Kromer B, Manning S, Southon JR, Stuiver M, van der Plicht J, Weyhenmeyer CE. 2006. "Radiocarbon calibration curve spanning 0 to 50,000 years BP based on paired $^{230}Th/^{234}U/^{238}U$ and ^{14}C dates on pristine corals" by R.G. Fairbanks et al. (Quaternary Science Reviews 24 (2005) 1781–1796) and "Extending the radiocarbon calibration beyond 26,000 years before present using fossil corals" by T.-C. Chin et al. (Quaternary Science Reviews 24 (2005) 1797–1808). Quaternary Sci Rev 25:855–862.

Renne PR. 2000. K-Ar and $^{40}Ar/^{39}Ar$ dating. In: Noller JS, Sowers JM, Lettis WR, editors. Quaternary geochronology methods and applications. Washington, DC: American Geophysical Union. p 77–100.

Richards MP, Pettitt PB, Trinkaus E, Smith FH, Paunovic M, Karavanic I. 2000. Neanderthal diet at Vindija and Neanderthal predation: The evidence from stable isotopes. Proc Nat Acad Sci USA 97:7663–7666.

Rink WJ. 1997. Electron spin resonance (ESR) dating and ESR applications in Quaternary science and archaeometry. Radiat Meas 27:975–1025.

Rink WJ, Bartoll J, Goldberg P, Ronen A. 2003. ESR dating of archaeologically relevant authigenic terrestrial apatite veins from Tabun Cave, Israel. J Archaeol Sci 30:1127–1138.

Rink WJ, Schwarcz HP, Ronen A, Tsatskin A. 2004. Confirmation of a near 400 ka age for the Yabrudian industry at Tabun Cave, Israel. J Archaeol Sci 31:15–20.

Robert J, Miranda CF, Muxart R. 1969. Mesure de la période du protactinium 231 par microcalorimétrie. Radiochim Acta 11: 104–108.

Roberts RG. 1997. Luminescence dating in archaeology: From origins to optical. Radiat Meas 27:819–892.

Roddick C. 1987. Generalised numerical error analysis with applications to geochronology and thermodynamics. Geochim Cosmochim Acta 51:2129–2135.

Rutter NW, Blackwell B. 1996. Amino acid racemization dating. In: Rutter NW, Catto NR, editor. Pleistocene dating methods: Problems and applications. Geotext 2. Ottawa: Geological Association of Canada. p 125–166.

Sánchez F. 1993. Presencia de carácteres autapomórficos neandertalenses en la mandíbula de Banyoles. In: Maroto J, editor. La mandíbula de Banyoles en el context dels fòssils humans del pleistocè. Sèrie monogràfica 13. Girona: Centre d'Investigacions Arqueològiques. p 179–188.

Saunders L, Fleming R. 1957. Mathematics and statistics for use in the biological and pharmaceutical sciences. London: The Pharmaceutical Press.

Schotterer U, Oeschger H. 1980. Low-level scintillation counting in a underground laboratory. Radiocarbon 22:505–511.

Schroeder JB, Hauser TM, Klody GM, Norton GA. 2004. Initial results with low energy single stage AMS. Radiocarbon 46: 1–4.

Schwarcz HP. 1989. Uranium series dating of Quaternary deposits. Quaternary Int 1:7–17.

Schwarcz HP. 1993. Uranium series dating and the origin of modern man. In: Aitken MJ, Stringer CB, Mellars PA, editors. The origins of modern humans and the impact of chronometric dating. Princetown: University of Princetown Press. p 12–26.

Schwarcz HP. 1994. Current challenges to ESR dating. Quaternary Sci Rev 13:601–605.

Schwarcz HP. 1997. Uranium series dating. In: Taylor RE, Aitken MJ, editors. Chronometric dating in archaeology. New York: Plenum. p 159–182.

Schwarcz HP, Bietti A, Buhay WM, Stiner M, Grün R, Segre A. 1991. On the examination of Grotta Guattari: Uranium series and electron spin resonance dates. Curr Anthropol 32:313–316.

Schwarcz HP, Grün R. 1993. ESR dating of the lower industry. In: Singer R, Gladfelter BG, Wymer JJ, editors. The Lower Paleolithic Site at Hoxne, England. Chicago: University of Chicago Press. p 203–205.

Schwarcz HP, Grün R, Vandermeersch B, Bar-Yosef O, Valladas H, Tchernov E. 1988. ESR dates for the hominid burial site of Qafzeh in Israel. J Hum Evol 17:733–737.

Schwarcz HP, Simpson JJ, Stringer CB. 1998. Neanderthal skeleton from Tabun: U-series data by γ-ray spectrometry. J Hum Evol 35:635–645.

Shackleton NJ, Fairbanks RG, Chiu T, Parrenin F. 2004. Absolute calibration of the Greenland time scale: Implications for Antarctic time scales and for $\Delta^{14}C$. Quaternary Sci Rev 23:1513–1522.

Shen G, Wang W, Wang Q, Zhao J, Collerson K, Zhou C, Tobias PV. 2002. U-Series dating of Liujiang hominid site in Guangxi, Southern China. J Hum Evol 43:817–829.

Shen G, Yokoyama Y. 1984. Th-230/U-234 dating of Petralona speleothems. Anthropos (Athens) 11:23–32.

Sillen A, Morris AG. 1996. Diagenesis of bone from Border Cave: Implications for the age of the Border Cave hominids. J Hum Evol 31:499–506.

Simpson JJ, Grün R. 1998. Non-destructive γ spectrometric U-series dating. Quaternary Sci Rev 18:1009–1022.

Singer R, Gladfelder BG, Wymer JJ. 1993. The Lower Paleolithic Site at Hoxne, England. Chicago: University of Chicago Press.

Smith FH, Trinkaus E, Pettitt PB, Karavanic I, Paunovic M. 1999. Direct radiocarbon dates for Vindija G(1) and Velika Pecina Late Pleistocene hominid remains. Proc Natl Acad Sci USA 96:12281–12286.

Stafford TW Jr, Hare PE, Currie L, Jull AJT, Donahue DJ. 1990. Accuracy of North American human skeleton ages. Quaternary Res 34:111–120.

Stafford TW Jr, Jull AJT, Zabel TH, Donahue DJ, Duhamel RC, Brendel K, Haynes CV Jr, Bischoff JL, Payen LA, Taylor RE. 1984. Holocene age of the Yuha burial: Direct radiocarbon determinations by accelerator mass spectrometry. Nature 308: 446–447.

Straus LG. 1999. The Neanderthal problem continued. Curr Anthropol 40:352–355.

Strauss LG, Bischoff JL, Carbonell E. 1993. A review of the Middle to Upper Paleolithic transition in Iberia. Préhistoire Européenne 3:11–27.

Stringer CB, Grün R, Schwarcz HP, Goldberg P. 1989. ESR dates for the hominid burial site of Es Skhul in Israel. Nature 338:756–758.

Stringer CB, Hublin JJ, Vandermeersch B. 1984. The origin of anatomically modern humans in Western Europe. In: Smith FH, Spencer F, editors. The origin of Modern Humans: A world survey of the fossil evidence. New York: Liss. p 51–135.

Stuiver M, Polach HA. 1977. Reporting of ^{14}C data. Radiocarbon 19:355–363.

Stuiver M, Reimer PJ, Bard E, Beck JW, Burr GS, Hughen KA, Kromer B, McCormac G, van der Plicht J, Spurk M. 1998. INTCAL 98 radiocarbon age calibration, 24,000-0 cal BP. Radiocarbon 40:1041–1084.

Suess HE. 1955. Radiocarbon concentration in modern wood. Science 122:415–417.

Tandon L, Iyengar GV, Parr RM. 1998. A review of radiologically important trace elements in human bones. Appl Radiat Isot 49:903–910.

Tattersall I, Schwartz JH. 1999. Hominids and hybrids: The place of Neanderthals in human evolution. Proc Natl Acad Sci USA 96:7117–7119.

Taylor RE. 1983. Non-concordance of radiocarbon and amino acid racemization deducted age estimates on human bone. Radiocarbon 25:647–654.

Taylor RE. 1997. Radiocarbon dating. In: Taylor RE, Aitken MJ, editors. Chronometric dating in archaeology. New York: Plenum. p 65–96.

Taylor RE. 2001. Radiocarbon dating. In: Brothwell DR and Pollard AM, editors. Handbook of archaeological sciences. Chichester: Wiley. p 23–46.

Taylor RE, Payen LA, Gerow B, Donahue DJ, Zabel TH, Jull AJT, Damon PE. 1983. Middle Holocene age of the Sunnyvale human skeleton. Science 220:1271–1273.

Taylor RE, Payen LA, Prior CA, Slota PJ, Gillespie R, Gowlett JAJ, Hedges REM, Jull AJT, Zabel TH, Donahue DJ, Berger R. 1985. Major revision in the Pleistocene age assignment for North American human skeletons by ^{14}C accelerator mass spectrometry: none older than 11,000 ^{14}C years B.P. Am Antiq 50:135–140.

Theodorsson P. 1996. Measurement of weak radioactivity. Singapore: World Scientific. 333 p.

Thorne AG. 1980. The longest link: human evolution in Southeast Asia and the settlement of Australia. In: Fox JJ, Garnaut AG, McCawley PT, Maukie JAC, editors. Indonesia: Australian Perspectives. Canberra: Australian National University. p 35–43.

Thorne A, Grün R, Mortimer G, Spooner NA, Simpson JJ, McCulloch MT, Taylor L, Curnoe D. 1999. Australia's oldest human remains: age of the Lake Mungo 3 skeleton. J Hum Evol 36:591–612.

Torres T, Llamas FJ, Canoira L, Garcia-Alonso P, Ortiz JE. 1999. Estratigrafia bimolecular. La racemizacion/epimerizacion de aminoacidos como herramineta geocronologica y paleotermometrica. ENRESA Publication Tecnica 09/99.

Torres T, Ortiz JE, Llamas FJ, Canoira L, Julia R, Garcia-Martinez MJ. 2002. Bear dentine aspartic acid racemization analysis: a proxy for the dating of Pleistocene cave infills. Archaeometry 44:417–426.

Trinkaus E. 2005. Early modern humans. Annu Rev Anthropol 34:207–230.

Trumbore SE. 2000. Radiocarbon geochronology. In: Noller JS, Sowers JM, Lettis WR, editors. Quaternary geochronology methods and applications. Washington DC: American Geophysical Union. p 41–60.

Tuniz C, Bird JR, Fink D, Herzog GF. 1998. Accelerator mass spectrometry. Boca Raton: CRC Press. 371 p.

Turney CSM, Bird MI, Fifield LK, Roberts RG, Smith MA, Dortch CE, Grün R, Lawson E, Miller GH, Dortch J, Cresswell RG, Ayliffe LK. 2001a. Breaking the radiocarbon barrier and early human occupation at Devil's Lair, southwestern Australia. Quaternary Res 55:3–13.

Tuross N, Behrensmeyer AK, Eanes ED, Fisher LW, Hare PE. 1989. Molecular preservation and crystallographic alterations in a weathering sequence of wildebeest bones. Appl Geochem 4:261–270.

Valladas H, Reyss JL, Joron JL, Valladas G, Bar-Yosef O, Vandermeersch B. 1988. Thermoluminescence dating of Mousterian 'Proto-Cro-Magnon' remains from Israel and the origin of modern man. Nature 331:614–616.

Vandermeersch B. 1981. Les hommes fossiles de Qafzeh (Israel). Paris: CNRS.

Van der Plicht J. 2000. The 2000 radiocarbon varve/comparison issue. Radiocarbon 42:313–322.

Van der Plicht J, Beck JW, Bard E, Baillie MGL, Blackwell PG, Buck CE, Friedrich M, Guilderson TP, Hughen KA, Kromer B, McCormac FG, Ramsey CB, Reimer PJ, Reimer RW, Remmele S, Richards DA, Southon JR, Stuiver M, Weyhenmeyer CE. 2004. NotCal04—Comparison/calibration C-14 records 26-50 cal kyr BP. Radiocarbon 46:1225–1238.

Vanhaelewyn G, Callens F, Grün R. 2000. EPR spectrum deconvolution and dose assessment of fossil tooth enamel using maximum likelihood common factor analysis. Appl Radiat Isot 52:1317–1326.

Vanhaelewyn GCAM, Sadlo J, Matthys PFAE, Callens F. 2002. Comparative X- and Q-band EPR study of radiation-induced radicals in tooth enamel. Radiat Res 158:615–625.

Van Klinken GJ, Mook WG. 1990. Preparative high-performance liquid chromatographic separation of individual amino acids derived from fossil bone collagen. Radiocarbon 32:155–164.

Van Riet Lowe C. 1929. Notes on some stone implements from Tuinplaas, Spingbok Flats. S Afr J Sci 26:623–630.

Voelker AHL, Grootes PM, Nadeau MJ, Sarnthein M. 2000. Radiocarbon levels in the Iceland Sea from 25-53 kyr and their link to the Earth's magnetic field intensity. Radiocarbon 42:437–452.

Voelker AHL, Sarnthein M, Grootes PM, Erlenkeuser H, Laj C, Mazaud C, Nadeau MJ, Schleicher M. 1998. Correlation of marine ^{14}C ages form the Nordic Seas with the GISP2 isotopes record: implications for ^{14}C calibration beyond 25 ka BP. Radiocarbon 40:517–534.

Vogel JC, Kronfeld J. 1997. Calibration of radiocarbon dates for the Late Pleistocene using U/Th dates on stalagmites. Radiocarbon 39:27–32.

Vogel JC, Marais M. 1971. Pretoria radiocarbon dates I. Radiocarbon 13:378–394.

Wadley L, Jacobs Z. 2004. Sibudu Cave, KwaZulu-Natal: Background to the excavations of middle stone age and iron age occupations. S Afr J Sci 100:145–151.

Wagner GA. 1998. Age determination of young rocks and artifacts—Physical and chemical clocks in Quaternary geology and archaeology. Berlin: Springer.

Webb GS, Cupper ML, Robins R. 2006. Pleistocene human footprints from the Willandra Lakes, southeastern Australia. J Hum Evol 50:405–413.

Webb G. 1989. The Willandra Lakes Hominids. Department of Prehistory, Research School of Pacific Studies, Australian National University, Canberra.

Weber J, Czarnetzki A, Pusch CM. 2005. Comment on "The Brain of LB1, *Homo floresiensis*". Science 310, 236b.

Wehmiller JF, Miller GH. 2000. Aminostratigraphic dating methods in Quaternary geology. In: Noller JS, Sowers JM, Lettis WR, editors. Quaternary geochronology methods and applications. Washington, DC: American Geophysical Union. p 115–120.

Weninger B, Jöris O, Danzeglocke U. 2002. Cologne radiocarbon calibration and paleoclimate research package. Available at http://www.calpal.de/calpal/index.htm (updated May 2006).

White TD, Asfaw B, DeGusta D, Gilbert H, Richards GD, Suwa G, Howell FC. 2003. Pleistocene *Homo sapiens* from Middle Awash, Ethiopia. Nature 423:742–747.

Wieser A, Debuyst R, Fattibene P, Meghzifene A, Onori S, Bayankin SN, Blackwell B, Brik A, Bugay A, Chumak V, Ciesielski B, Hoshi M, Imata H, Ivannikov A, Ivanov D, Junczewska M, Miyazawa C, Pass B, Penkowski M, Pivovarov S, Romanyukha A, Romanyukha L, Schauer D, Scherbina O, Schultka K, Shames A, Sholom S, Skinner A, Skvortsov V, Stepanenko V, Tielewuhan E, Toyoda S, Trompier F. 2005. The 3rd international intercomparison on EPR tooth dosimetry, Part 1: General analysis. Appl Rad Isot 62:163–171.

Wieser A, Mehta K, Amira S, Aragno D, Bercea S, Brik A, Bugai A, Callens F, Chumak V, Ciesielski B, Debuyst R, Dubovsky S, Duliu OG, Fattibene P, Haskell EH, Hayes RB, Ignatiev EA, Ivannikov A, Kirillov V, Kleschenko E, Nakamura N, Nather M, Nowak J, Onori S, Pass B, Pivovarov S, Romanyukha A, Scherbina O, Shames AI, Sholom S, Skvortsov V, Stepanenko V, Tikounov DD, Toyoda S. 2000. The second international intercomparison on EPR tooth dosimetry. Radiat Meas 32:549–557.

Yokoyama Y, Falgueres C, Bibron R. 1988. Direct dating of Neanderthalian remains and animal bones by the non-destructive γ-ray spectrometry: Comparison with other methods. L'Homme de Néandertal 1:135–141.

Yokoyama Y, Falgueres C, de Lumley MA. 1997. Datation directe d 'un crane Proto-Cro-Magnon de Qafzeh par la spectrometrie gamma non destructive. CR Acad Sci Paris Serie II 324:773–779.

Yokoyama Y, Nguyen HV. 1980. Direct and non-destructive dating of marine sediments, manganese nodules, and corals by high resolution γ Ray Spectrometry. In: Goldberg E, Horibe Y, Saruhashi K, editors. Isotope marine chemistry. Tokyo: Rokakuho University. p 259–289.

Yokoyama Y, Nguyen HV. 1981. Direct dating by non-destructive γ-ray spectrometry of fossil human skull Arago XXI, fossil animal bones and stalagmites of the Caune de l'Arago at Tautavel. In: DeLumley H, Labeyrie J, editors. Absolute dating and isotope analysis in prehistory—Methods and limits. Proceedings Pretirage. p 355–375.

Zilhao J, d'Errico F. 1999. The Neanderthal problem continued. Curr Anthropol 40, 355–364.